ADVANCES IN ATOMIC, MOLECULAR AND OPTICAL PHYSICS, VOL. 54

CONTROLLING OPTICAL CHAOS, SPATIO-TEMPORAL DYNAMICS, AND PATTERNS

LUCAS ILLING[1], *DANIEL J. GAUTHIER*[1] *and RAJARSHI ROY*[2]

[1]*Department of Physics and Center for Nonlinear and Complex Systems, Duke University, Durham, NC 27708, USA*

[2]*Department of Physics and Institute for Physical Science and Technology, University of Maryland, College Park, MD 20742, USA*

ISSN 1049-250X
DOI: 10.1016/S1049-250X(06)54010-8

Abstract
We describe how small perturbations applied to optical systems can be used to suppress or control optical chaos, spatio-temporal dynamics, and patterns. This research highlights the fact that complex behavior, such as chaos, has a beautiful and orderly underlying structure. We demonstrate that this orderly structure can be exploited for a variety of applications, such as stabilizing laser behavior in a regime where the device would normally produce erratic behavior, communicating information masked in a seemingly noise-like chaotic carrier, and improving the sensitivity of ultra-low-light level optical switches.

Keywords: chaos, synchronization, spatio-temporal chaos, transverse patterns, controlling chaos

1. Introduction

Why do some lasers produce noise-like intensity spikes? What is the optimum implementation of an optical switch? Such questions have motivated scientists over the last four decades to uncover the sources of instability in nonlinear optical systems. Recently, there has been a surge in the number of researchers investigating the dynamics of optical systems because it now seems possible to tackle problems that seemed intractable two decades ago, such as the origin of optical 'turbulence' and controlling optical chaos. This renaissance has been spurred by our understanding of relatively simple optical systems and by advances in nonlinear dynamics, mathematics, computational physics and experimental techniques.

Many laser users have been confronted by the appearance of 'noise-like' intensity fluctuations or 'turbulent' spatial patterns in the beam emitted from the laser. This type of behavior was clearly evident even during the earliest investigations of lasers in the 1960's (Collins et al., 1960; Nelson and Boyle, 1962) where it was found that the intensity of the light generated by the ruby laser displayed irregular spiking, as shown in Fig. 1. Was the spiking due to inadequate shielding of the laser from the environment or was is it due to some intrinsic property of the laser?

After many years of research on nonlinear optical systems, we now understand that the instabilities can arise from deterministic and stochastic effects that govern the interplay between the radiation field and matter. The path to this realization was rather long because it took considerable effort to uncover and model with precision the origin of the instabilities. Then, it took several years to place the research in the framework of universal behavior of dynamical systems.

From the general perspective of the field of nonlinear dynamics, optical devices are fascinating because seemingly simple textbook devices, such as a single mode laser, can show exceedingly erratic, noise-like behavior that is a manifestation of

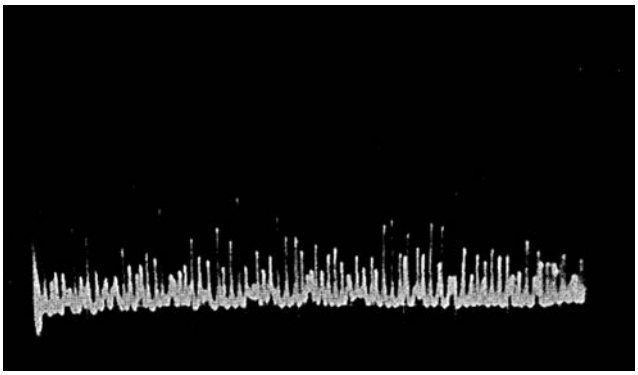

FIG. 1. Temporal evolution of the intensity of the beam emitted by a ruby laser. From Nelson and Boyle (1962).

deterministic chaos. Deterministic refers to the idea that the future behavior of the system can be predicted using a mathematical model that does not include random or stochastic influences. Chaos refers to the idea that the system displays extreme sensitivity to initial conditions so that arbitrarily small errors in measuring the initial state of the system grow large exponentially and hence practical, long-term predictability of the future state of the system is lost.

Although mathematicians have studied chaotic solutions of dynamical systems since the works of Henri Poincaré at the turn of the 20th century, the possibility of chaos in real physical systems was not widely appreciated until relatively recently. A major turning point was the seminal paper by the meteorologist Edward Lorenz (Lorenz, 1963), in which he studied the problem of convection of a fluid heated from below (a highly simplified model of the Earth's atmosphere). Lorenz's numerical computations revealed a totally new aspect of the behavior of this dynamical system: large, irregular fluctuations appeared to originate from an innocuous looking set of three-coupled, nonlinear ordinary differential equations without any sources of noise or fluctuations included in them. Even more surprising was the incredible sensitivity of solutions of these equations to a small difference in initial conditions. Lorenz engraved this aspect of chaotic dynamics in our minds through the title of his talk to the American Association for the Advancement of Science in 1972, "Does the Flap of a Butterfly's Wings in Brazil Set off a Tornado in Texas?" (Lorenz, 1993).

The connection between chaotic dynamics and laser instabilities was made by Hermann Haken, who, in a short paper (Haken, 1975), remarked on a beautiful similarity that he had discovered between the chaotic equations for a fluid studied by Lorenz a dozen years earlier (Lorenz, 1963), and the semi-classical equations that describe the operation of a single-mode laser.

In the decades following the works of Lorenz and Haken, most scientists and engineers have begun to recognize that chaotic behavior is commonplace in physical, chemical, and biological systems.

Early nonlinear dynamics research in the 1980s focused on identifying systems that display chaos, developing mathematical models to describe them, developing new nonlinear statistical methods for characterizing chaos, and identifying the way in which a nonlinear system goes from simple to chaotic behavior as a parameter is varied (the so-called route to chaos). One outcome of this research was the understanding that the behavior of nonlinear systems falls into just a few universal categories. For example, the route to chaos for a pendulum, a nonlinear electronic circuit, and a piece of paced heart tissue are all identical under appropriate conditions.

This observation is very exciting because experiments conducted with an optical device can be used to understand some aspects of the behavior of a fibrillating heart, for example. Such universality has fueled a large increase in research on nonlinear systems that transcends disciplinary boundaries and often involves interdisciplinary or multidisciplinary research teams.

In the 1990s, the focus of research shifted toward the possibility of controlling chaotic systems. The main idea behind the research on controlling chaos (Ott et al., 1990; Shinbrot et al., 1993; Gauthier, 2003) is to stabilize the unstable periodic orbits that are contained within the chaotic dynamics of a nonlinear system, or to stabilize the unstable steady state of the system. The most amazing aspect of these novel schemes to control chaotic systems is that the perturbations necessary are vanishingly small as the system approaches the dynamical state that is desired, whether it is periodic or steady. It is the very sensitivity of chaotic systems to perturbations that allows one to control them with tiny perturbations.

A second topic that evolved through the 1990s is the problem of synchronization of chaotic systems. Though the synchronization of clocks (periodic systems) has been studied with great care over centuries, it was the surprising discovery of temporal synchronization between two chaotic systems that initiated the field of chaotic communications. At first, even the notion of synchronization of chaotic systems appears self-contradictory. How can two chaotic systems that inevitably start from slightly different initial conditions ever be synchronized? After all, the exponentially fast divergence of state-space trajectories from ever so slightly different initial conditions is one of the hallmarks of chaos. The crucial realization was that, when two chaotic systems are coupled to each other in a suitable way, they exert a form of control on each other, and it is possible for both systems to synchronize their dynamics, even when they start from very different initial conditions (Fujisaka and Yamada, 1983; Afraimovich et al., 1986; Pecora and Carroll, 1990). The first experimental demonstrations of synchronization of chaotic systems were done on electronic circuits (Pecora and Carroll,

1990), and soon lead to the question: Can the chaotic dynamics of these systems be used for something practical?

The possibility that chaotic lasers could be synchronized was examined very shortly after the appearance of Pecora and Carroll's work, in an important numerical study by Winful and Rahman (1990) on a linear array of coupled semiconductor lasers. They showed that synchronization can be achieved by mutually coupling nearest-neighbor lasers through injection of their optical fields. Their work stimulated experiments a few years later on mutually coupled solid state lasers (Roy and Thornburg, 1994), as described in Section 4. Independently, Sugawara et al. (1994) studied synchronization of one-way coupled CO_2 lasers. These early studies demonstrated that synchronization of chaotic optical systems could provide a means for communications through free space or optical fibers, and motivated much of the research on chaos synchronization and chaos communication.

Instabilities of physical systems are not confined to the temporal domain but also arise in the spatial domain leading to such phenomena as pattern formation, spatio-temporal chaos, and turbulence. Optics addressed the issue of spatio-temporal effects much later than the more traditional fields of nonlinear chemical reactions and, especially, hydrodynamics. This is despite the fact that it was well known that optical systems exhibit spatio-temporal effects such as spontaneous pattern formation in the structure of the electromagnetic field in the planes orthogonal to the propagation direction. However, these phenomena were mostly considered undesirable and difficult to understand and control. This view changed in the 1980's when pattern formation in laser beams became a major topic of the newly born field of transverse nonlinear optics. During this period, many different spatio-temporal phenomena were revealed and explained (Lugiato, 1994). It is the greater understanding of these intriguing phenomena that allowed recent progress in manipulating the transverse optical patterns for practical applications, such as all-optical switches. It also lead, in combination with the experience gained from temporal chaos, to recent efforts to synchronize and control spatio-temporal chaos, as discussed in Section 6.

The purpose of this chapter is to review important aspects of controlling optical chaos, spatio-temporal dynamics and patterns. In this review we discuss mainly facets of our own research, but start off by briefly highlighting a few fascinating results by other groups on chaos control and synchronization that have been published recently. Subsequently, chaos control is discussed in Section 3, whereas a review of chaos synchronization is given in Section 4, and its uses for chaos communication are described in Section 5. Spatio-temporal optical systems are the focus of Section 6 and we conclude with an outlook in Section 7.

2. Recent Examples

In this section, we summarize a few recent advances on controlling optical chaos, turbulence, and patterns to demonstrate the vibrancy of the field. A quick search on a publication database using the keywords 'optical' and 'chaos' reveals that the field began around 1981 and has grown steadily; there have been consistently greater than 200 papers published per year since 1994. Unfortunately, it is not possible to describe each of these studies in this review; we only highlight a few examples to whet the reader's appetite.

2.1. The 'Green Problem'

Green and blue lasers are very important light sources for CD players and information processing applications, as well as pump sources for other lasers. Since 1986, it has been know that a 532-nm (green color) Nd:YAG laser with an intercavity frequency-doubling crystal displays complex dynamics when operated at moderate to high pump rates, known familiarly as the 'green problem'. Given the technical importance of these lasers and that many users require a steady beam, it is important to identify methods of suppressing the instability. In Section 3.2.1, we describe some of the early research that used closed-loop feedback methods for controlling the laser behavior at moderate pump rates. At higher pump rates, more complex 'type-II' chaos occurs where modes in two perpendicular polarization directions are active; this type of behavior has been difficult to suppress using standard chaos-control methods.

Recently, Ahlborn and Parlitz (2004) have devised a new method, known as multiple delayed feedback control, that is effective in suppressing type-II chaos. In their setup (see Fig. 2(a)), they measure the intensity of the light emitted by a frequency-doubled Nd:YAG laser in two orthogonal linear polarization components. They generate a feedback error signal by comparing the intensity in each state of polarization with the intensities measured at a previous (or delayed) time. This error signal is applied to the laser through the injection current of the diode laser that serves as the pump of the Nd:YAG crystal. By appropriate adjustment of the feedback parameters (six total), they are able to obtain robust suppression of the chaotic intensity and polarization fluctuations, as shown in Fig. 2(b), where control is switched on at $t = 0$. Using this method, they were able to run the laser up to three times above the lasing threshold with stable behavior. The controller can be made compact so that it should be possible to integrate it in existing commercial products at low cost.

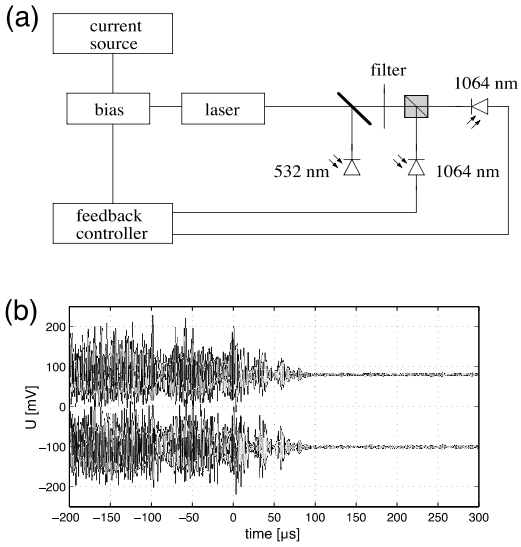

FIG. 2. Controlling the "green problem". (a) Experimental setup using modified delayed feedback control to suppress chaotic intensity fluctuations in a frequency-doubled Nd:YAG laser. (b) Suppression of chaos using chaos control. Temporal evolution of both linear polarization components of the beam emitted by the laser. Reprinted with permission from A. Ahlborn and U. Parlitz, *Phys. Rev. Lett.* **93**, 264101 (2004). © 2004 American Physical Society

2.2. SYNCHRONIZING LASER CHAOS

While many laser users desire stable behavior, there are some potential applications of optical chaos. One is communicating information that is 'hidden' in a chaotic carrier, which requires synchronization of the chaos produced by two lasers (one in the transmitter and one in the receiver). There have been several demonstrations of synchronizing optical chaos (see Section 4); the current push is to obtain synchronization in devices that match with current telecommunication technologies or to investigate the case when there is a large distance between transmitter and receiver.

Hong et al. (2004) have investigated synchronized chaos in vertical-cavity surface-emitting semiconductor lasers (VCSELs) using the setup shown in Fig. 3(a). VCSELs have many technologically important characteristics, such as low threshold current, single-longitudinal-mode operation, circular output beam profiles, and wafer-scale integration. On the other hand, the lasers tend to exhibit changes in the emission polarization and hence polarization effects need to be considered when attempting to synchronize their behavior.

In their setup, chaos is induced in one laser (VCSEL1) by retro-reflecting about 20% of the beam emitted by the laser using mirror M1. By unidirectional coupling of some of the light emitted by VCSEL1 in one linear polarization component

into the other laser (VCSEL2) and properly adjusting the state of polarization of the light, they obtain high-quality chaos synchronization. Figure 3(b) shows the temporal evolution of the light injected into VCSEL2 in the y-polarization component and the resulting light emitted by the laser in this component. It is seen that the two traces are highly correlated, indicating synchronization. Surprisingly, they find that the light emitted in the x-polarization component is anti-correlated (so-called anti-synchronization), as shown in Fig. 3(c). Note that the time scale of the chaotic fluctuations is nanoseconds and hence these devices could be used for transmitting information at data rates that are compatible with existing commercial optical telecommunication systems.

Using a similar experimental system, but with bidirectional rather than unidirectional coupling, Mulet et al. (2004) have investigated what happens when the distance between the two lasers is so large that the transit time of light propagating from one laser to the other is comparable to or longer than the time scale of the chaotic fluctuations. They observe achronal synchronization (e.g., high correlation between the signals at a non-zero time lag) between the lasers once the coupling strength is greater than a critical value. The role of 'leader' and 'follower' can be switched depending on the initial conditions, even under symmetric coupling conditions.

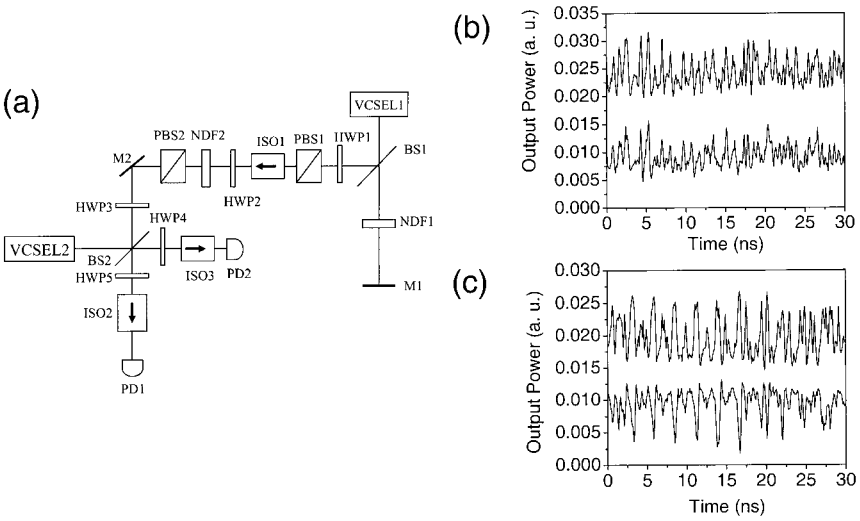

FIG. 3. Chaos synchronization in coupled vertical-cavity surface-emitting semiconductor lasers. (a) Experimental setup. Temporal evolution of (b) the injected beam (top trace) and the receiver output (bottom trace) in one linear polarization component, and (c) the injected beam (top trace) and the receiver output (bottom trace) in the opposite linear polarization component. From Hong et al. (2004).

These results demonstrate that it is possible to achieve synchronization of sub-nanosecond optical chaos, paving the way for development of high-bit-rate communication systems based on chaotic waveforms.

2.3. Optical Chaos Communication

The primary schemes being considered for practical chaos communication systems are based on chaotic waveforms generated by lasers with external cavity feedback (the systems described in the previous subsection), opto-electronic feedback (Goedgebuer et al., 1998; Blakely et al., 2004b), and electro-optic feedback (Goedgebuer et al., 2002). To date, the electro-optic feedback methods have progressed most rapidly toward deployment and we briefly mention some of the most recent achievements.

The electro-optic feedback devices described by Gastaud et al. (2004) consists of a 1.55-μm telecommunications laser whose output beam passes through a Mach–Zehnder electro-optic modulator, a long length of standard telecommunication fiber, and is converted to a voltage via a photoreceiver, as shown in Fig. 4(a). The voltage is amplified and is used to drive the Mach–Zehnder modulator. The source of nonlinearity is the modulator, whose intensity transmission is proportional to the sine squared of the drive voltage; the laser is merely a passive source of high-power optical radiation. The system is known as a delay dynamical system because the delay in the optical fiber is long in comparison to the response time of the modulator. What is impressive about this system is that it uses off-the-shelf optical telecommunication components, can operate at data rates exceeding 1 Gbit/s, and can be readily integrated into existing underground systems.

To mask information within the chaotic waveform produced by the electro-optic feedback loop, a binary message is encoded on the beam produced by an auxiliary laser using a standard telecommunication modulation protocol, where an eye-diagram for the message is shown in the top trace of Fig. 4(b). The message beam is 'folded' into the electro-optic chaos device using a 2×2 fiber coupler. Specifically, half of the message beam is coupled directly into the electro-optic feedback loop, while half of it is sent to the receiver side of the communication system. Simultaneously, half of the beam circulating in the electro-optic feedback loop is coupled out of the loop and sent to the receiver side of the system, while the other half is combined with the message and circulated around the feedback loop. The resulting masked signal that propagates over the communication channel is shown in the middle trace of Fig. 4(b), where it is seen that signal has little resemblance to the data waveform and the eye-diagram is completely closed.

The receiver side of the communication system consists of an identical electro-optic feedback loop that has been split apart, as shown in the right-hand side of Fig. 4(a). A fraction of the incoming signal is sent to a photoreceiver and converted to a voltage. The rest of the signal propagates through an optical fiber,

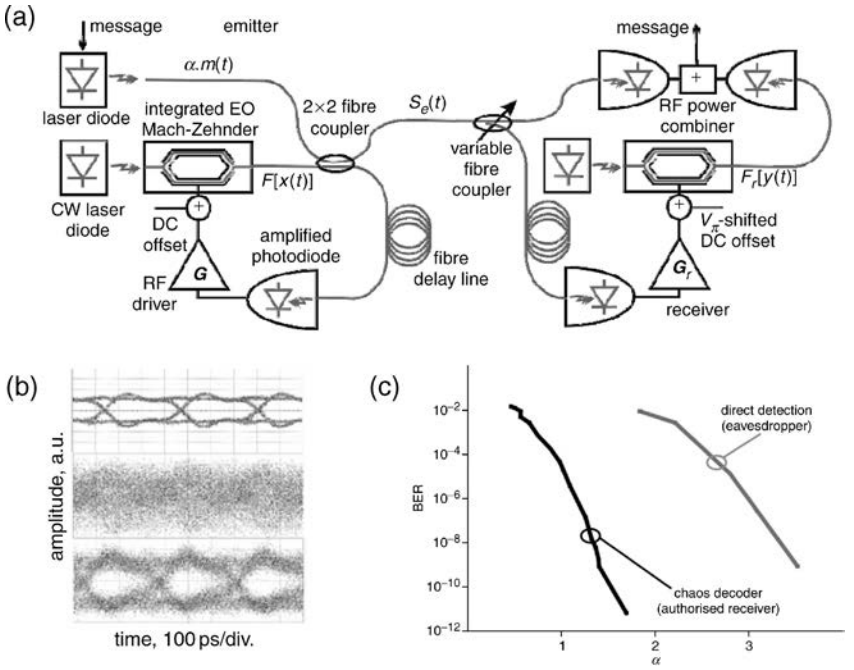

FIG. 4. Chaos communication using synchronized electro-optic feedback devices. (a) Experimental system setup. (b) Eye diagrams for a 3 Gbit/s pseudo-random bit sequence (upper: original; middle: encoded; lower: decoded). (c) Bit error rate versus the masking coefficient α. Reprinted with permission from N. Gastaud, S. Poinsot, L. Larger, J.-M. Merolla, M. Hana, J.-P. Goedgebuer, and F. Malassenet, *Electron. Lett.* **40**, 898 (2004). © 2004 Institute of Engineering & Technology

which delays the signal by an amount that is identical to the delay produced by the long fiber in the transmitter, and the resulting signal is used to drive an identical Mach–Zehnder modulator. An auxiliary laser beam passes through this modulator and is converted to a voltage via a photoreceiver. This voltage is subtracted from the voltage proportional to the incoming signal. The resulting difference signal contains the original message; the chaos part of the signal is removed from the waveform with high rejection, as shown in the bottom trace of Fig. 4(b). The re-opened eye-diagram is clearly evident, indicating high quality message recovery. This type of receiver is known as an open-loop device and does not display chaos in the absence of an input signal. Gastaud et al. (2004) have also demonstrated that the bit error rate (BER) is orders-of-magnitude smaller using the chaos-based receiver versus direct detection of the masked signal, as shown in Fig. 4(c), demonstrating that a high level of signal privacy is possible using this approach.

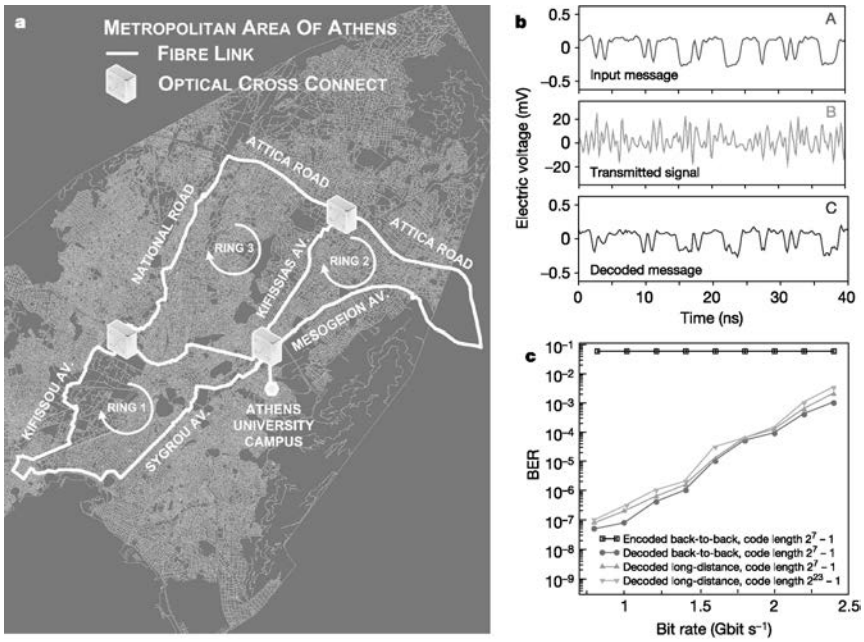

FIG. 5. Practical implementation of chaos-based optical communication. (a) Network topology in Athens, Greece. (b) Temporal sequence of 1 Gbit/s data (upper trace), message masked in the chaotic waveform (middle trace) and decoded message (lower trace). (c) The bit-error-rate of the encoded signal (squares), back-to-back decoded messages (circles) and decoded message after transmission through the network for two different code lengths (triangles). Reprinted with permission from Macmillan Publishers Ltd: *Nature* (A. Argyris, D. Syvridis, L. Larger, V. Annovazzi-Lodi, P. Colet, I. Fischer, J. García-Ojalvo, C.R. Mirasso, L. Pesquera, and K.A. Shore, *Nature* **437**, 343 (2005)). © 2004

Very recently, Argyris et al. (2005) have used two different time-delay chaotic devices to communicate high-speed digital data over 120 km of optical fiber in the metropolitan area network of Athens, Greece (a schematic of the network topology is shown in Fig. 5(a)). They independently investigated the use of an electro-optic feedback device similar to the system described by Gastaud et al. (2004) and a device based on laser external cavity feedback similar to the systems described by Hong et al. (2004) and Mulet et al. (2004).

The optical fiber used for the experiments in Athens was temporarily free of network traffic, but was still installed and connected to the switches of the network nodes. The authors measured the characteristics of the fiber, such as its attenuation and chromatic dispersion, before the experiment. This allowed them, for example, to exactly counter the effects of dispersion by inserting an appropriate length of dispersion-compensating fiber at the beginning of the link. Three amplifiers were

used, one at the transmitter, one 50 kilometers from the transmitter and one at the receiver, followed by optical filters with bandwidths of around 1 nanometer—this compensated for optical losses and removed spontaneous noise, respectively. Figures 5(b) and (c) show the message, masked message, and decoded message, and the corresponding bit-error-rate as a function of transmission data rate, respectively. These results demonstrate that chaos-based communication methods can be integrated into a real-world system and operate at high data rates with reasonably low errors. Whether this technology will be adopted depends, in part, on whether commercial vendors will be willing to incorporate 'non-standard' transmitters and receivers in their devices.

2.4. Spatio-Temporal Chaos

In all the previous examples described above, complexity appeared in the temporal behavior of the device. Here, we discuss recent investigations of systems that display complexity in both space and time. In optical devices, the spatial dimensions displaying complexity are usually the coordinates transverse to the propagation vector of a beam of light and hence they are sometimes referred to as arising from transverse-beam instabilities.

Pastur et al. (2004) have recently investigated spatio-temporal instabilities occurring in a nonlinear optical system containing a liquid crystal light valve (LCLV). The LCLV consists of an absorptive photoconductor on one side and a mirror coated with a thin layer of liquid crystal on the other side. Light falling on the photoconductor at one spatial location changes an electric field on the opposite side of the device at the same spatial (transverse) location, thereby changing the orientation of the liquid crystal. The device, when illuminated from either side, behaves approximately as a material described by an extremely large third-order nonlinear optical susceptibility—a sensitive Kerr medium. Figure 6(a) shows the experimental setup of their oscillator, where a laser beam is split, part reflects off the reflective side of the LCLV and is redirected to the photoconductive side. Under appropriate conditions, the oscillator can display complex spatio-temporal patterns such as those shown in Figs. 6(b) and (c). The time scale of the changes in the observed pattern dynamics is of the order of one second.

Using small perturbations via optical feedback, they are able to suppress spatio-temporal complexity and control the system to various regular patterns (Figs. 6(d) and (e)) or they can target a specific complex spatio-temporal pattern (Fig. 6(f)). To control the device, they measure in real time the pattern emanating from the oscillator using a video camera, compare this image to a known target pattern that is stored in a computer, and use this difference signal to drive a liquid crystal display. A portion of the laser beam passes through the liquid crystal display and is injected into the optical resonator. The observed controlled or targeted pattern

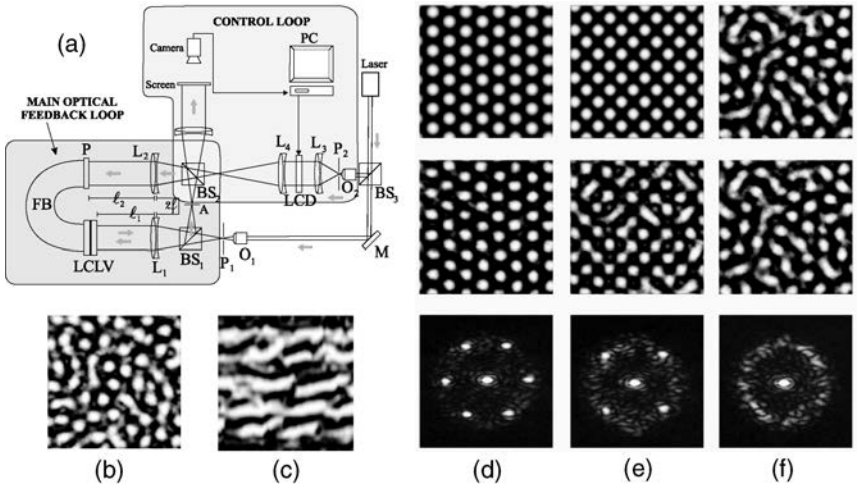

FIG. 6. Targeting and control of spatio-temporal chaos. (a) Experimental setup. (b) Snapshot of the uncontrolled spatio-temporally complex state. (c) Space- (vertical) time (horizontal) dynamical evolution of the central vertical line of pixels from (b). (d)–(f) Examples of target patterns (top row), controlled pattern (center row), and corresponding far-field images (bottom row) for the control trials of (d) hexagonal pattern, (e) square pattern, and (f) a snapshot of the uncontrolled dynamics. Reprinted with permission from L. Pastur, L. Gostiaux, U. Bortolozzo, S. Boccaletti, and P.L. Ramazza, *Phys. Rev. Lett.* **93**, 063902 (2004). © 2004 American Physical Society

is highly correlated with the desired pattern, with a normalized correlation coefficient exceeding 0.6 for all conditions shown in the middle panels of Figs. 6(d)–(f).

Another type of spatio-temporal behavior displayed by a cavity containing a nonlinear optical material driven by a coherent field (holding beam) is known as a cavity soliton. Cavity solitons are localized intensity peaks that can form in a homogeneous background of light arising from the holding beam and are formed when focused laser pulses are injected into the cavity. The ability to turn them on and off and to control their location suggests that they can be used as 'pixels' for reconfigurable arrays or all-optical processing units.

Recently, Barland et al. (2002) used a VCSEL that was pumped electrically to just below the laser threshold and illuminated by a holding beam. The ability to create a cavity soliton is very sensitive to the precise resonance frequency of the VCSEL. Slight manufacturing imperfections allow only the creation of cavity solitons in a narrow vertical stripe shown in Fig. 7(a) bounded by the complex intensity pattern to the left and the uniform field to the right. When a focused beam is injected into this region, a high-intensity spot is created (the dark spot in Fig. 7(b)). After the injected beam is removed, the spot reshapes slightly but remains in the same spatial location (Fig. 7(c)). They also find that additional cavity solitons can be written in the device and that the cavity solitons can be

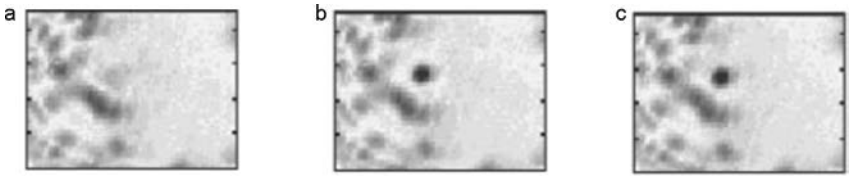

FIG. 7. Experimental demonstration of independent writing of a cavity soliton. The intensity distribution of the output field is shown over a 60 μm × 60 μm region in the sample center. (a) The underlying pattern when the writing beam is blocked. (b) The 15-μm-diameter writing beam (single dark high-intensity spot) is directed to the edge of the homogeneous region. The writing beam is blocked and a 10-μm-diameter spot remains stable (the cavity soliton). Reprinted with permission from Macmillan Publishers Ltd: *Nature* (S. Barland, J. Tredicce, M. Brambilla, L. Lugiato, S. Balle, M. Giudicl, T. Maggipinto, L. Spinelli, G. Tissoni, T. Knodl, M. Miller, and R. Jager, *Nature* **419**, 699 (2002)). © 2002

erased using a writing beam that has its phase shifted by π with respect to the beam that originally wrote the cavity soliton. Future work will require a method for writing and manipulating a large number of cavity solitons in a single device.

This completes our brief overview of recent research. We now turn to the more detailed discussion of controlling optical chaos, spatio-temporal dynamics, and patterns.

3. Control

3.1. INTRODUCTION

As mentioned at the beginning of Section 1, chaos arising in a dynamical system can be controlled by applying appropriately designed minute perturbations to an accessible system parameter (a 'knob' that affects the state of the system) that forces it to follow a desired behavior rather than the erratic, noise-like behavior indicative of chaos. In greater detail, the key idea underlying most controlling-chaos schemes is to take advantage of the unstable steady states (USSs) and unstable periodic orbits (UPOs) of the system (infinite in number) that are embedded in the chaotic attractor characterizing the dynamics in state space. Figure 8(a) shows an example of chaotic oscillations in which the presence of UPOs is clearly evident with the appearance of nearly periodic oscillations during short intervals. (This figure illustrates the dynamical evolution of current flowing through an electronic diode resonator circuit described in Sukow et al., 1997.) Many of the control protocols attempt to stabilize one such UPO by making small adjustments to an accessible parameter when the system is close to the targeted UPO.

Techniques for stabilizing unstable states in nonlinear dynamical systems using small perturbations fall into three general categories: feedback, non-feedback schemes, and a combination of feedback and non-feedback. In non-feedback

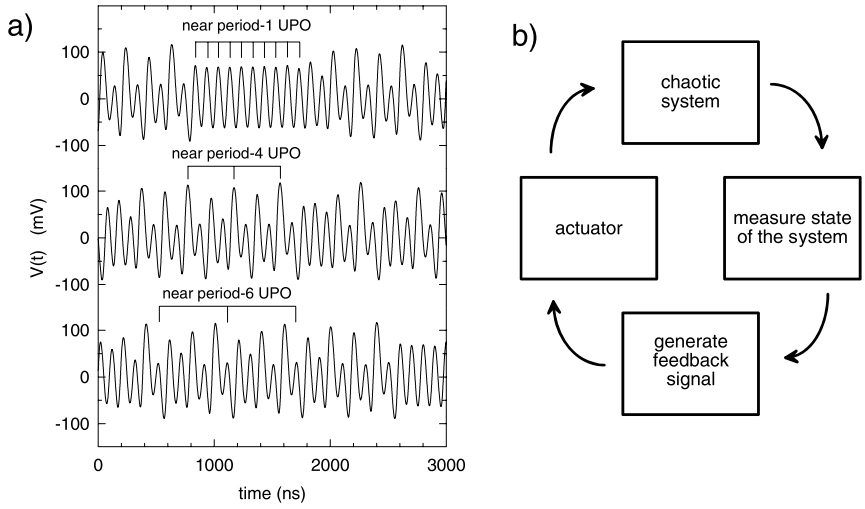

FIG. 8. (a) Chaotic behavior observed in a nonlinear electronic circuit. The system naturally visits the unstable period orbits embedded in the strange attractor, three of which are indicated. (b) Closed-loop feedback scheme for controlling a chaotic system. From Sukow et al. (1997).

(open-loop) schemes, an orbit similar to the desired unstable state is entrained by adjusting an accessible system parameter about its nominal value by a weak periodic signal, usually in the form of a continuous sinusoidal modulation. This is somewhat simpler than feedback schemes because it does not require real-time measurement of the state of the system and processing of a feedback signal. Unfortunately, periodic modulation fails in many cases to entrain the UPO (its success or failure is highly dependent on the specific form of the dynamical system).

The possibility that chaos and instabilities can be controlled efficiently using feedback (closed-loop) schemes to stabilize UPOs was described by Ott et al. (1990) (OGY). The basic building blocks of a generic feedback scheme consist of the chaotic system that is to be controlled, a device to sense the dynamical state of the system, a processor to generate the feedback signal, and an actuator that adjusts the accessible system parameter, as shown schematically in Fig. 8(b).

In concept, closed-loop feedback works because, by observing the dynamics of the system in the neighborhood of a fixed point or periodic state, one can find the direction and amount of instability. One can then use that information to keep the system near the fixed point or periodic orbit. A (non-chaotic) example may serve to make this point clear. Imagine trying to balance a ball at the center of a saddle. The saddle surface is unstable in the direction of convexity; the ball will fall off along the sides of the saddle. The amount of instability, or how fast the ball falls off, is determined by the curvature of the saddle. In the other direction, the saddle

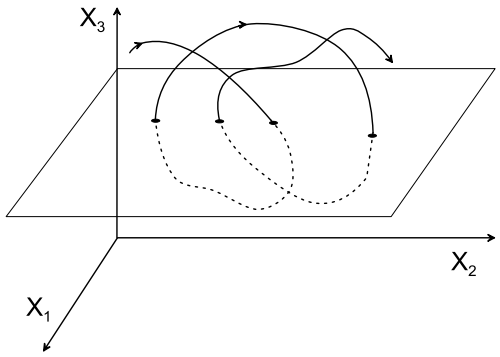

FIG. 9. A segment of a trajectory in a three-dimensional state space and a possible surface-of-section through which the trajectory passes. Some control algorithms require only knowledge of the coordinates where the trajectory pierces the surface, indicated by the dots. From Gauthier (2003).

is stable; the ball returns towards the center if displaced along the ridge of the saddle. Feedback control schemes, such as the OGY algorithm, tell us essentially how to move a saddle under the ball so as to keep it balanced at the center. Once the curvature of the saddle in the unstable direction is known, one can balance the ball at the center by making observations of the position of the ball from time to time. If control is initiated when the ball is sufficiently close to the center, control can be maintained in a small neighborhood of the center with only small corrective motions.

In their original conceptualization of the control scheme, OGY suggested the use of discrete proportional feedback because of its simplicity and because the control parameters can be determined straightforwardly from experimental observations. In this particular form of feedback control, the state of the system is sensed and adjustments are made to the accessible system parameter as the system passes through a surface-of-section. Figure 9 illustrates a portion of a trajectory in a three-dimensional state space and one possible surface-of-section that is oriented so that all trajectories pass through it. The dots on the plane indicate the locations where the trajectory pierces the surface.

In the OGY control algorithm, the size of the adjustments is proportional to the difference between the current and desired states of the system. Specifically, consider a system whose dynamics on a surface-of-section is governed by the m-dimensional map

$$\mathbf{z}_{i+1} = \mathbf{F}(\mathbf{z}_i, p_i), \tag{1}$$

where $\mathbf{z}_i$ is its location on the ith piercing of the surface and p_i is the value of an externally accessible control parameter that can be adjusted about a nominal value $\bar{p}$. The map $\mathbf{F}$ is a nonlinear vector function that transforms a point

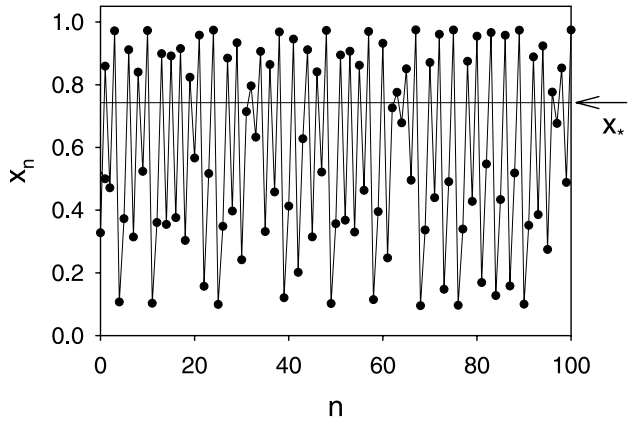

FIG. 10. Chaotic evolution of the logistic map for $r = 53.9$. The circles denote the value of x_n on each iterate of the map. The solid line connecting the circles is a guide to the eye. The horizontal line indicates the location of the period-1 fixed point. From Gauthier (2003).

on the plane with position vector $\mathbf{z}_i$ to a new point with position vector $\mathbf{z}_{i+1}$. Feedback control of the desired UPO (characterized by the location $\mathbf{z}_*(\bar{p})$ of its piercing through the section) is achieved by adjusting the accessible parameter by an amount

$$\epsilon_i = p_i - \bar{p} = -\gamma \mathbf{n} \cdot \left[\mathbf{z}_i - \mathbf{z}_*(\bar{p})\right] \tag{2}$$

on each piercing of the section when $\mathbf{z}_i$ is in a small neighborhood of $\mathbf{z}_*(\bar{p})$, where γ is the feedback gain and $\mathbf{n}$ is an m-dimensional unit vector that is directed along the measurement direction. The location of the unstable fixed-point $\mathbf{z}_*(\bar{p})$ must be determined before control is initiated; fortunately, it can be determined from experimental observations of $\mathbf{z}_i$ in the absence of control (a learning phase). The feedback gain γ and the measurement direction $\mathbf{n}$ necessary to obtain control are determined from the local linear dynamics of the system about $\mathbf{z}_*(\bar{p})$ using standard techniques of modern control engineering (see, for example, Ogata, 1990 and Romeiras et al., 1992), and they are chosen so that the adjustments ϵ_i force the system onto the local stable manifold of the fixed point on the next piercing of the section. Successive iterations of the map in the presence of control direct the system to $\mathbf{z}_*(p_o)$. It is important to note that ϵ_i vanishes when the system is stabilized; the control only has to counteract the destabilizing effects of noise.

As a simple example, consider control of the one-dimensional logistic map defined as

$$x_{n+1} = f(x_n, r) = r x_n (1 - x_n). \tag{3}$$

This map can display chaotic behavior when the 'bifurcation parameter' r is greater than $\sim$3.57. Figure 10 shows x_n (closed circles) as a function of the it-

erate number n for $r = 3.9$. The non-trivial period-1 fixed point of the map, denoted by x_*, satisfies the condition $x_{n+1} = x_n = x_*$ and hence can be determined through the relation

$$x_* = f(x_*, r). \tag{4}$$

Using the function given in Eq. (3), it can be shown that

$$x_* = 1 - 1/r. \tag{5}$$

A linear stability analysis reveals that the fixed point is unstable when $r > 3$. For $\bar{r} = 3.9$, $x_* = 0.744$, which is indicated by the thin horizontal line in Fig. 10. It is seen that the trajectory naturally visits a neighborhood of this point when $n \sim 32$, $n \sim 64$, and again when $n \sim 98$ as it explores state space in a chaotic fashion.

Surprisingly, it is possible to stabilize this unstable fixed point by making only slight adjustments to the bifurcation parameter of the form

$$r_n = \bar{r} + \epsilon_n, \tag{6}$$

where

$$\epsilon_n = -\gamma(x_n - x_*). \tag{7}$$

When the system is in a neighborhood of the fixed point (i.e., when x_n is close to x_*), the dynamics can be approximated by a locally linear map given by

$$x_{n+1} = x_* + \alpha(x_n - x_*) + \beta\epsilon_n. \tag{8}$$

The Floquet multiplier of the uncontrolled map is given by

$$\alpha = \left.\frac{\partial f(x, r)}{\partial x}\right|_{x=x_*, r=\bar{r}} = \bar{r}(1 - 2x_*), \tag{9}$$

and the perturbation sensitivity by

$$\beta = \left.\frac{\partial f(x, r)}{\partial r}\right|_{x=x_*, r=\bar{r}} = x_*(1 - x_*), \tag{10}$$

where that fact that $\epsilon_n = 0$ when $x = x_*$ and $r = \bar{r}$ has been used to obtain these results. For future reference, $\alpha = -1.9$ and $\beta = 0.191$ when $\bar{r} = 3.9$ (the value used to generate Fig. 10). Defining the deviation from the fixed point as

$$y_n = x_n - x_*, \tag{11}$$

one finds that the behavior of the controlled system in a neighborhood of the fixed point is governed by

$$y_{n+1} = (\alpha + \beta\gamma)y_n, \tag{12}$$

where the size of the perturbations is given by

$$\epsilon_n = \beta\gamma y_n. \tag{13}$$

In the absence of control ($\gamma = 0$), $y_{n+1} = \alpha y_n$ so that a perturbation to the system grows (i.e., the fixed point is unstable) when $|\alpha| \geqslant 1$.

With control, it is seen from Eq. (12) that an initial perturbation shrinks when

$$|\alpha + \beta\gamma| < 0, \tag{14}$$

and hence control stabilizes successfully the fixed point when condition (14) is satisfied. Any value of γ satisfying condition (14) will control chaos, but the time to achieve control and the sensitivity of the system to noise is affected by the specific choice. For the proportional feedback scheme (7) considered in this simple example, the optimum choice for the control gain occurs when $\gamma = -\alpha/\beta$. In this situation, a single control perturbation is sufficient to direct the trajectory to the fixed point and no other control perturbations are required if control is applied when the trajectory is close to the fixed point and there is no noise in the system. If control is applied when the y_n is large, nonlinear effects become important and additional control perturbations are required to stabilize the fixed point.

Figure 11 shows the behavior of the controlled logistic map for $\bar{r} = 3.9$ and the same initial condition used to generate Fig. 10. Control is turned on suddenly as soon as the trajectory is somewhat close to the fixed point near $n \sim 32$ with the control gain set to $\gamma = -\alpha/\beta = 9.965$. It is seen in Figs. 11(a) and (b) that only a few control perturbations are required to drive the system to the fixed point. Also, the size of the perturbations vanish as n becomes large since they are proportional to y_n (see Eq. (13)). When random noise is added to the map on each iterate, the control perturbations remain finite to counteract the effects of noise, as shown in Figs. 11(c) and (d).

This simple example illustrates the basic features of control of an unstable fixed point in a nonlinear discrete-time dynamical system using small perturbations. It also demonstrates the control of unstable periodic orbits since periodic orbits correspond to fixed points of the map describing the dynamics on the surface-of-section. Over the past decade, since the early work on controlling chaos, researchers have devised many techniques for controlling chaos that go beyond the closed-loop proportional method described above. Below, we describe some of our own work on advancing the control of chaos in optical systems.

3.2. Controlling Unstable Periodic Orbits

In this section, we focus on closed-loop feedback methods we have investigated for controlling UPOs in optical systems. This problem is very rich because there are a very large (probably infinite) number of UPOs embedded in a chaotic attractor, as mentioned in Section 3 and seen in Fig. 8(a). Thus, it should be possible

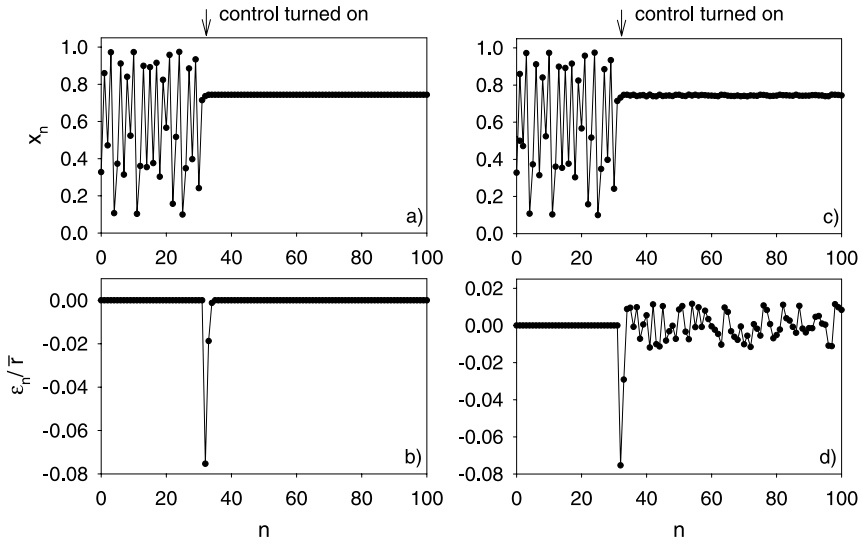

FIG. 11. Controlling chaos in the logistic map. (a) Proportional control is turned on when the trajectory approaches the fixed point. (b) The perturbations ϵ_n vanish once the system is controlled in this example where there is no noise in the system. (c) Uniformly distributed random numbers between ± 0.1 are added to the logistic map on each iterate. (d) The perturbations ϵ_n remain finite to counteract the effects of the noise. From Gauthier (2003).

to switch between the various orbits just by changing the settings of the feedback loop, while always using tiny perturbations. Such control might have applications as an agile waveform generator or for transmitting information by symbolic dynamics, where each orbit corresponds to a different letter in the communication alphabet.

For convenience, we define here a notation that is used in the remaining sections on chaos control. We denote the continuous-time state of the system by the m-dimensional state-vector $\mathbf{z}(t)$, the measured dynamical state of the system by $\xi(t) = \mathbf{n} \cdot \mathbf{z}(t)$, where $\mathbf{n}$ is an m-dimensional unit vector along the measurement direction, the nominal value of the accessible system parameter by $\bar{p}$ and the closed-loop feedback perturbations by $\epsilon(t)$. The key to the problem of controlling chaos is to devise an algorithm that relates the perturbations $\epsilon(t)$ to the measured state of the system $\xi(t)$ so that the system is directed to the desired state.

3.2.1. Applying Occasional Proportional Feedback Control to the 'Green Problem'

Baer (1986) studied the generation of green light from a diode laser pumped Nd:YAG laser with an intracavity KTP crystal. He found that though the Nd:YAG laser operated in a stable steady state without the intracavity crystal, large irreg-

ular intensity fluctuations were sometimes observed when the intracavity KTP crystal was used to generate green light from the system. Baer noted that this behavior occurred when the laser operated in three or more longitudinal modes and hypothesized that sum-frequency generation in the KTP crystal could provide mode-mode coupling that would destabilize the laser. This was not a desirable situation for proposed practical applications of the system, in optical disk readers, for example. The unstable behavior of this system soon came to be known as the "green problem." The chaotic nature of the green laser was investigated in some detail and connected to the destabilization of relaxation oscillations (Bracikowski and Roy, 1991). Relaxation oscillations are always present in a laser; they are the result of power exchange between the atoms of the active medium and the electric field in the cavity and are normally very small in amplitude. It was found that the nonlinear coupling of the modes through sum-frequency generation resulted in the destabilization of relaxation oscillations in the green laser system. A reasonably accurate model was developed for the system, predicting many aspects of system behavior, both chaotic and non-chaotic.

As may be expected, several methods were proposed and implemented to get rid of the fluctuations. These methods consisted of system modifications such as restricting the laser to operate in two orthogonally polarized modes by adding wave plates to the laser cavity (Oka and Kubota, 1988; Anthon et al., 1992) or proper orientation of the YAG and KTP crystals (James et al., 1990). These are typical examples of what has been the traditional reaction of scientists and engineers when faced with irregular fluctuations in a laser system—redesign the system so that it is inherently stable or try to find a parameter regime where chaos does not exist. A departure from this traditional mindset required a new perspective and approach towards working with chaotic systems.

It was clear, soon after publication of the OGY paper (Ott et al., 1990), that it would be of great interest to try and apply these new chaos control techniques to the chaotic green laser. There was the purely scientific motivation—could one demonstrate control of a chaotic laser in an experiment and stabilize several different periodic waveforms for the same laser parameters? There was also the practical motivation—could such control techniques be used to stabilize chaotic lasers without having to redesign the system?

It was at this point that one of the authors (R.R.) fortuitously happened to learn that Earle Hunt (of Ohio University) had developed an analog circuit to stabilize periodic waveforms generated by a chaotic diode resonator circuit through implementation of a variant of the OGY approach which he called Occasional Proportional Feedback (OPF) (Hunt, 1991; Hunt and Johnson, 1993). The name arose from the fact that the feedback consisted of a series of perturbations of limited duration δt ("kicks") delivered to the input drive signal at periodic intervals (T) in proportion to the difference of the chaotic output signal from a reference value. The OPF algorithm is shown schematically in Fig. 12.

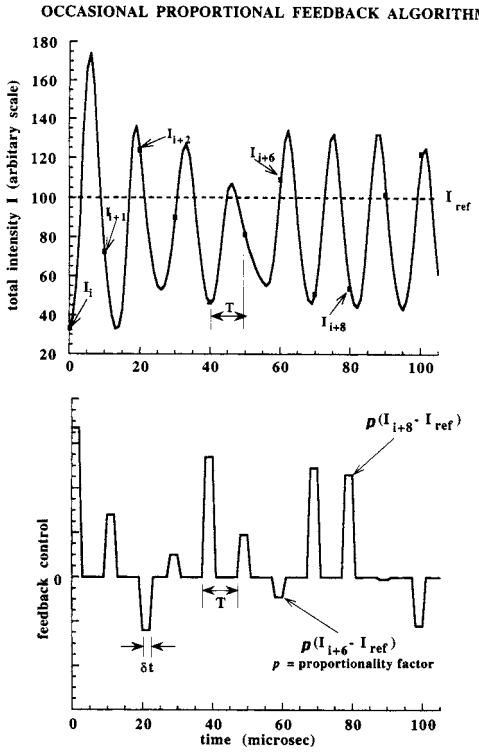

FIG. 12. The Occasional Proportional Feedback (OPF) algorithm used for control of the chaotic laser. The four parameters of the control circuit, T, δt, p and I_{ref} are shown. From Roy et al. (1994).

The OPF technique appeared to be perfectly suited for an attempt to stabilize periodic orbits of the green laser, because the operation of the circuit could easily be speeded up to the microsecond time scale required for the laser. The laser intensity was detected with a fast photodiode and this signal provided the input for the control circuit. The output of the control circuit modified the injection current-of the diode laser used to pump the Nd:YAG crystal. This seemed to be the most natural and convenient choice of control parameter. To adapt Hunt's circuit for control of the autonomously chaotic laser, Roy et al. (1992) had to supply an external timing signal from a function generator. This determined the interval T between "kicks" applied to the pump laser injection current. Even though there was no external periodic modulation responsible for the chaotic dynamics, the relaxation oscillations of the laser intensity provided a natural time scale for perturbative corrections. The interval between kicks was thus adjusted to be roughly at the relaxation oscillation period (approximately 100 kHz), or a fractional multiple of it. The period T, duration of the kicks δt, reference level I_{ref} with respect to

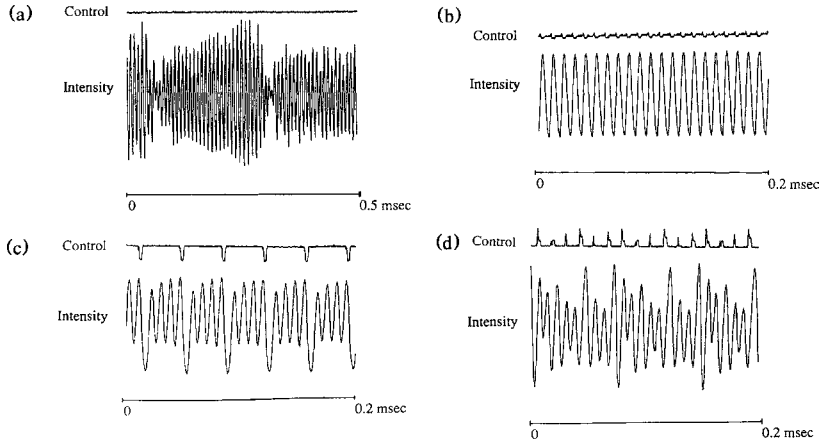

FIG. 13. Control signal and time traces of the Nd:YAG laser intensity. (a) The chaotic intensity fluctuations of the laser output without any applied control signal. (b) A period-1 orbit obtained by adjusting the interval T between "kicks" to approximately the relaxation oscillation frequency. (c) A period-4 orbit obtained by adjusting T to approximately $1/4$ the relaxation oscillation frequency. (d) A period-9 orbit obtained by adjusting the interval T to approximately $6/9$ of the relaxation oscillation frequency. The complex nature of the control signal is clearly visible. From Roy et al. (1992).

which the deviation of the signal is measured and the proportionality factor p to determine the amplitude of the kicks are the four parameters of the control circuit.

The results of application of OPF to the laser were quite remarkable. Roy et al. (1992) were able to demonstrate stabilization of a large variety of periodic waveforms with perturbations of a few percent applied to the pump laser injection current. A typical chaotic waveform, together with several periodic waveforms stabilized in this way are shown in Fig. 13. The control signal fluctuations are shown above the intensity waveforms. The particular waveforms stabilized can be selected by changes of control circuit parameters, mainly the time period T and the reference level I_{ref}.

We note here that the laser had to be operated so as to generate very little green light for the control circuit to work successfully. The laser is "weakly" chaotic in this regime; the rate of separation of initially close trajectories in phase space is small, and there is only one direction of instability. If a significant amount of green light was generated, and the laser was highly chaotic (particularly if the laser has more than one direction of instability in phase space), the circuit was unable to stabilize the laser.

3.2.2. Extended Time-Delay Autosynchronization

Occasional proportional feedback and related approaches have been very successful in controlling chaos in slow systems (characteristic time scale <1 μs), but

scaling these schemes to significantly higher frequencies, such as those encountered in high-speed electronic or optical systems, for example, is challenging for several reasons. One important issue in high-speed feedback control of chaotic systems is the latency through the control loop, that is, the time τ_ℓ between the sensing of the state of the system and the application of the control signal. The latency of the control loop is affected by the propagation speed of the signals through the components of the loop and the processing time of the feedback signal. An additional important issue is that it is difficult to accurately sample the state of the system at discrete times in order to compare it with the reference value and to rapidly adjust the control parameter on a time-scale comparable to the response time of the system.

Continuous feedback schemes avoid or reduce many of these problems and hence may be useful for controlling high-speed chaos. An obvious extension of the original OGY suggestion for controlling UPOs is to use continuous adjustment of the accessible system parameter by an amount

$$\epsilon(t) = -\gamma \mathbf{n} \cdot \big[\mathbf{z}(t) - \mathbf{z}_*(t)\big], \tag{15}$$

where γ is a constant feedback gain (Pyragas, 1992; Qu et al., 1993). This scheme is not amenable for controlling the dynamics of high-speed systems, however, because it is difficult to accurately determine, store, and regenerate $\mathbf{z}_*(t)$.

As first suggested by Pyragas (1992), the UPOs of a dynamical system can be controlled using continuous feedback that does not require knowledge of $\mathbf{z}_*(t)$. In this scheme, which we refer to as 'time-delay autosynchronization' (TDAS), the control perturbations are designed to synchronize the current state of the system and a time-delayed version of itself, with the time delay equal to one period of the desired orbit. Specifically, UPOs of period τ can be stabilized by continuous adjustment of the accessible parameter by an amount

$$\epsilon(t) = -\gamma\big[\xi(t) - \xi(t-\tau)\big], \tag{16}$$

where γ is the feedback gain. Note that $\epsilon(t)$ vanishes when the system is on the UPO since $\xi(t) = \xi(t-\tau)$ for all t. This control scheme has been demonstrated experimentally in electronic circuits (Pyragas and Tamasevicius, 1993; Gauthier et al., 1994) operating at frequencies of 10 MHz, corresponding to $\tau \sim 100$ ns. The main drawback to TDAS is that it is not effective at controlling highly unstable orbits.

Socolar et al. (1994) introduced a generalization of TDAS that is capable of extending the domain of effective control significantly (Pyragas, 1995; Sukow et al., 1997) and is easy to implement in high-speed systems. Stabilizing UPOs is achieved by feedback of an error signal that is proportional to the difference between the value of a state variable and an infinite series of values of the state variable delayed in time by integral multiples of τ. Specifically, ETDAS

prescribes the continuous adjustment of the system parameter by

$$\epsilon(t) = -\gamma\left[\xi(t) - (1-R)\sum_{k=1}^{\infty} R^{k-1}\xi(t-k\tau)\right], \tag{17}$$

where $-1 \leqslant R < 1$ regulates the weight of information from the past. As we discuss below, highly unstable orbits can be stabilized as $R \to 1$. The case $R = 0$ corresponds to TDAS, the scheme introduced by Pyragas (1992). We emphasize that, for any R, $\epsilon(t)$ vanishes when the UPO is stabilized since $\xi(t - k\tau) = \xi(t)$ for all t and k, so there is no power dissipated in the feedback loop whenever ETDAS is successful. Note that no property of the UPO must be known in advance except its period. In periodically driven systems, where the period of the orbit is determined from the driving, no features of the UPO need ever be determined explicitly. The control parameters γ and R can be determined empirically in an experiment or by performing a linear stability analysis of the system in the presence of ETDAS feedback control for fixed $\mathbf{n}$ and $\bar{p}$ (Bleich and Socolar, 1996; Just et al., 1997).

Some insight into the underlying reasons for effectiveness of ETDAS in stabilizing highly unstable orbits as $R \to 1$ can be gained using a frequency-domain analysis. To begin, note that the ETDAS feedback signal given by Eq. (17) linearly relates the input signal $\xi(t)$ with the output signal $\epsilon(t)$; hence $\epsilon(\omega) = -\gamma T(\omega)\xi(\omega)$, where $\xi(\omega)$ and $\epsilon(\omega)$ are the Fourier amplitudes of the input and output signals, respectively, and

$$T(\omega) = \frac{1 - \exp(i\omega\tau)}{1 - R\exp(i\omega\tau)} \tag{18}$$

is the transfer function for ETDAS feedback. The transfer function 'filters' the observed state of the dynamical system, characterized by $\xi(f)$, to produce the necessary feedback signal.

Figure 14 shows the frequency dependence of $|T(\omega)|$ for $R = 0$ (TDAS) and $R = 0.65$ (ETDAS) where it is seen that there is a series of notches that drop to zero at multiples of the characteristic frequency of the orbit $\omega_* = 2\pi/\tau$ and that the notches become narrower for larger R. The existence of the notches in the transfer function can be understood easily by considering that $\epsilon(t)$, and hence $\epsilon(\omega)$ must vanish when the UPO is stabilized. Recall that the spectrum $\xi(\omega)$ of the system when it is on the UPO consists, in general, of a series of δ-functions at multiples of the characteristic frequency of the orbit $\omega_* = 2\pi/\tau$; therefore, the filter must remove these frequencies (via the notches) so that $\epsilon(\omega) = 0$. The ETDAS feedback is more effective in stabilizing UPOs for larger R partly because it is more sensitive to frequencies that could potentially destabilize the UPO. The narrower notches imply that more feedback is generated for signals with frequency components slightly different from the desired set. In addition, $|T(\omega)|$ is flatter

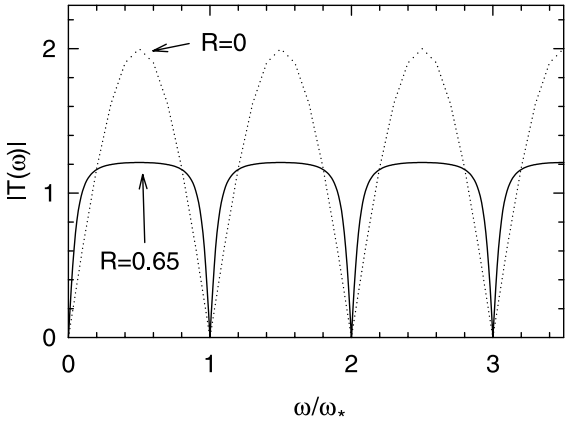

FIG. 14. Transfer function $|T(\omega)|$ of ETDAS feedback. The dashed line is for $R = 0$ and the solid line is for $R = 0.65$. Note that notches at $\omega/\omega_* = q$ ($q = 0, 1, 2, \ldots$) are narrower for $R = 0.65$. From Sukow et al. (1997).

and remains near one between the notches for larger R, so the system is less likely to be destabilized by a large feedback response at these intermediate frequencies.

We note that other transfer functions that possess notches at multiples of ω_* could stabilize the dynamics of the UPO; however, Eq. (18) is easy to implement experimentally. For example, Sukow et al. (1997) constructed an analog circuit, consisting of high-speed video amplifiers and coaxial-cable delay lines, that implements ETDAS feedback. They were able to stabilize highly unstable UPOs in a chaotic electronic circuit, known as a diode resonator, which consists of a sinusoidally-driven series-connected switching diode, inductor, and resistor. The measured system variable was a voltage drop $V(t)$ across the resistor and the system was driven into the chaotic regime by increasing the amplitude of the sinusoidal drive voltage beyond a critical value.

Figures 15(a) and (b) show the temporal evolution of $V(t)$ when the ETDAS feedback circuitry is adjusted to stabilize the period-1 and period-4 UPOs, respectively. It is seen that the feedback signal $V_\epsilon(t)$ is a small fraction of the drive amplitude ($<2\times10^{-3}$ for both cases). The slight increase in $V_\epsilon(t)$ for the period-4 orbit was due mainly to imperfect reproduction of the form of the ETDAS feedback signal by the analog circuitry. This effect is more prevalent for the period-4 setup because the delay line is longer and hence causes more distortion of the signals due to the dispersion and frequency-dependent loss of the coaxial cable.

Figures 15(c) and (d) presents further evidence that the ETDAS feedback indeed stabilizes the UPOs embedded within the strange attractor of the diode resonator. Shown are the return maps for the uncontrolled system (light dots) and the controlled system (dark dots indicated by arrows) for the stabilized period-1

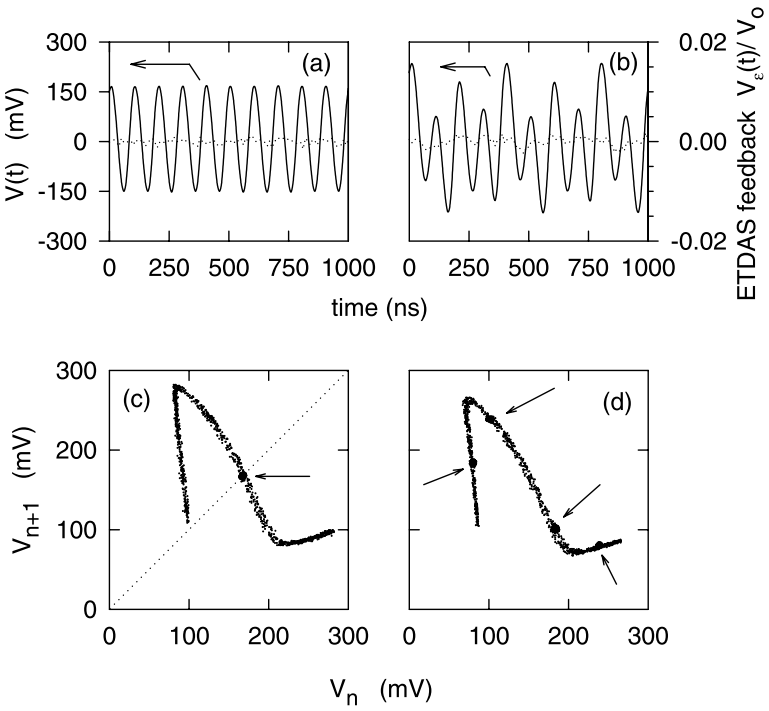

FIG. 15. Time series data and first return maps illustrating successful ETDAS control. Temporal evolution (solid lines, scale on left) of the stabilized (a) period-1 UPO ($\gamma = 6.2$, $R = 0.28$) and (b) period-4 UPO ($\gamma = 4.2$, $R = 0.26$) along with their associated ETDAS error signals $V_\epsilon(t)$ (dashed lines, scale on right), expressed as a fraction of the drive amplitude. Similar data in the form of a first return map for the controlled (c) period-1 ($\gamma = 4.4$, $R = 0$) and (d) period-4 ($\gamma = 3.1$, $R = 0.26$) trajectories are highlighted by the dark concentrations of points indicated by arrows. These maps are superimposed on maps of the uncontrolled chaotic resonator. From Sukow et al. (1997).

orbit (Fig. 15(c)) and the period-4 orbit (Fig. 15(d)). It is clear that the stabilized orbits lie on the unperturbed map, indicating that they are periodic orbits internal to the dynamics of the uncontrolled system.

Finally, we note that a useful feature of ETDAS feedback is the ability to generate the error signal using an all-optical technique. Specifically, the form of the ETDAS error signal given by Eq. (17) is identical to an equation that describes the reflection of light from a Fabry–Perot interferometer consisting of two equal-reflectivity mirrors, where $R = r^2$ corresponds to the square of amplitude-reflection-coefficient r of the mirrors, and τ corresponds to the round-trip transit-time of light in the cavity. In one possible scenario, a transducer converts the measured dynamical state of the system $\xi(t)$ into a laser beam of field strength $E_{\text{inc}}(t)$ that is directed toward an optical attenuator or amplifier (adjusting γ) and

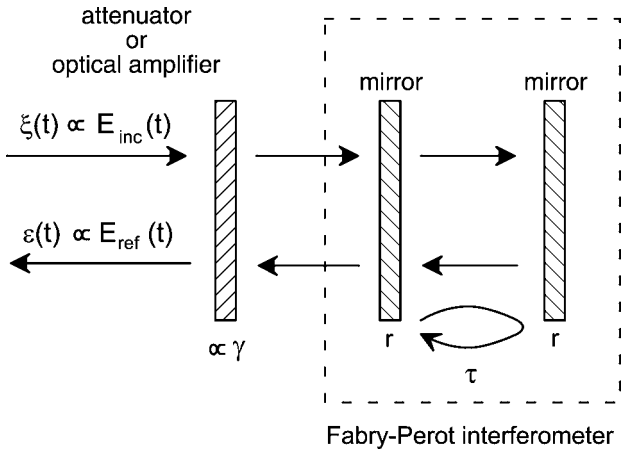

FIG. 16. All-optical implementation of ETDAS feedback using a Fabry–Perot interferometer consisting of two mirrors with amplitude reflection coefficient r separated by a distance such that the round-trip-time of light in the cavity is equal to the period τ of the desired UPO. An optical attenuator or amplifier adjusted the feedback gain γ. From Sukow et al. (1997).

a Fabry–Perot interferometer, as shown in Fig. 16. The field $E_{\text{ref}}(t)$ reflected by the interferometer passes through the attenuator/amplifier and is converted to the ETDAS error signal $\epsilon(t)$ by an output transducer. It may be possible to control fast dynamics of optical systems that generate a laser beam directly, such as semiconductor lasers, using the field generated by the laser as the measured system parameter $\xi(t)$ *and* as the accessible system parameter $\epsilon(t)$; no transducers are required.

3.2.3. Controlling UPOs with Large Control-Loop Latency

In some situations it may be impossible to produce a feedback signal that faithfully reproduces the form of Eq. (17) due to the latency of the control loop. Latency is the time τ_ℓ that it takes to measure the state of the system, determine the feedback signal, and apply the perturbation to the system. As a rough guideline, the latency becomes an issue when τ_ℓ is comparable to or larger than the correlation time of the chaotic system, which is approximately equal to λ^{-1}, where λ is the largest (local) positive Lyapunov exponent of the desired UPO in the absence of control. (A positive Lyapunov exponent is a measure of the exponential divergence of nearby initial points in state space.)

Another issue that arises in fast dynamical systems is that the time it takes for signals to propagate through the device components is comparable to the time scale of the fluctuations and hence many fast systems are most accurately described by time-delay differential equations (Ikeda et al., 1982; VanWiggeren and

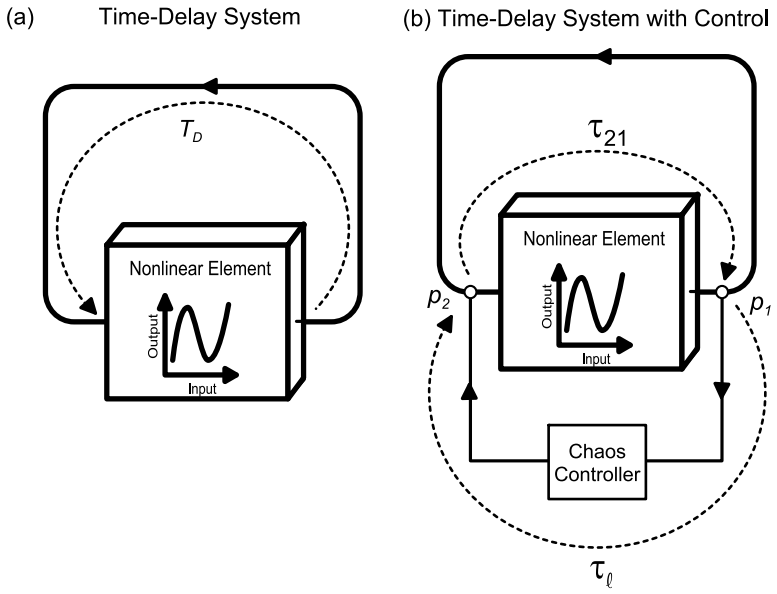

FIG. 17. (a) Schematic of a typical topology of a time-delay system consisting of a nonlinear element and a long loop connecting the output to the input of the element, introducing a total time-delay T_D. (b) Schematic of feedback control that measures the state at point p_1 and perturbs the system at p_2. The propagation time through the controller (control loop latency) is denoted by τ_ℓ, and τ_{21} is the propagation time from p_2 to p_1 (along the path through the nonlinear element). Note that the signal takes a time $T_D - \tau_{21}$ to get from p_1 to p_2. From Blakely et al. (2004a).

Roy, 1998a). An advantageous feature of these time-delay devices is that the complexity of the dynamics can be tuned by adjusting the delay.

The control of very fast chaotic systems with time scales <10 ns is difficult because of these two challenges: control-loop latencies are unavoidable, and complex high-dimensional behavior of systems is common due to inherent time-delays. Recently, Blakely et al. (2004b) described a novel approach for controlling time-delay systems even in the presence of substantial control-loop latency. This is a general approach that can be applied to any fast systems describable with time-delay differential equations. As a specific example, they demonstrated this general approach by using TDAS to stabilize fast periodic oscillations ($\tau \sim 12$ ns) in a photonic device, the fastest controlled chaotic system at that time. In principle, much faster oscillations can be controlled using, for example, high speed electronic or all-optical control components, paving the way to using controlled chaotic devices in high-bandwidth applications.

Blakely et al. (2004a) discovered that the effects of control-loop latency can be mitigated when controlling chaotic systems consisting of a nonlinear element and an inherent time-delay T_D, as shown schematically in Fig. 17(a). Chaos can

be controlled in time-delay systems by taking advantage of the fact that it is often possible to measure the state of the system at one point in the time-delay loop (p_1) and to apply perturbations at a different point (p_2), as shown in Fig. 17(b). Such distributed feedback is effective because the state of the system at p_2 is just equal to its state p_1 delayed by the propagation time $T_D - \tau_{21}$ through the loop between the points. The arrival of the control perturbations at p_2 is timed correctly if

$$\tau_\ell + \tau_{21} = T_D. \tag{19}$$

Hence, it is possible to compensate for a reasonable amount of control loop latency τ_ℓ by appropriate choice of p_1 and p_2. The advantage of this approach is that the propagation time through the controller does not have to be faster than the controlled dynamics. In contrast, the conventional approach for controlling chaos is to perform the measurement and apply the perturbations instantaneously ($\tau_\ell \to 0$), which requires controller components that are much faster than the components of the chaotic device to approximate instantaneous feedback. Note that the method of computing the control perturbations has not been specified. In principle, any existing method may be used as long as they can be implemented with latency satisfying Eq. (19).

To demonstrate the feasibility of controlling fast chaos using this general concept, Blakely et al. (2004a) applied it to a chaotic photonic device shown schematically in Fig. 18(a). The device consists of commercially-available components including a semiconductor laser, a Mach–Zehnder interferometer, and an electronic time-delay feedback, and can display nanosecond-scale chaotic fluctuations (Blakely et al., 2004b). The semiconductor laser acts as a simple current-controlled source that converts current oscillations into oscillations of the optical frequency and, to a lesser extent, into amplitude oscillations. Light generated by the laser traverses an unequal-path Mach–Zehnder interferometer whose output is a nonlinear function of the optical frequency. The light exiting the interferometer is converted to a voltage using a fast silicon photodiode and a resistor. This voltage propagates through a delay line (a short piece of coaxial cable), is amplified and bandpass filtered, and is then used to modulate the laser injection current by combining it with the dc injection current via a bias-T. The system is subject to an external driving force provided by adding an RF voltage to the feedback signal. (The driven system has more prominent bifurcations than the undriven device.) The length of the coaxial cable can be adjusted to obtain values of the time-delay T_D in the range 11–20 ns. This photonic device displays a range of periodic and chaotic behavior that is set by the amplifier gain and the ratio of the time-delay to the characteristic response time of the system (typically set to a large value).

Figure 19(a) shows the chaotic temporal evolution of the voltage measured immediately after the photodiode when the device is operated in the absence of control. The corresponding broadband power spectrum is shown in Fig. 19(b). The behavior of the system is well described by a delay-differential equation,

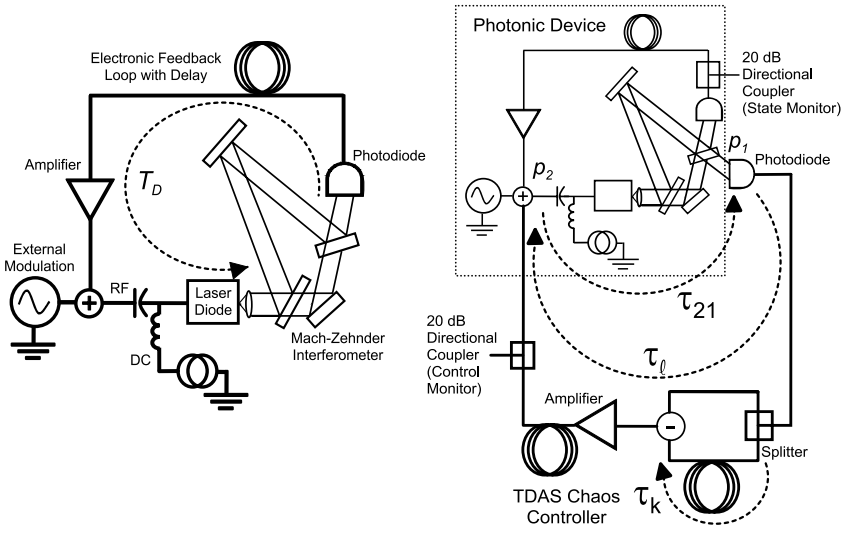

FIG. 18. (a) Experimental setup of a chaotic time-delay device of the type shown in Fig. 17(a). (b) Experimental system with controller. The measurement point p_1 is the second beam splitter of the interferometer. Perturbations are applied at p_2, an RF-power combiner. The time τ_{21} for a signal to propagate from point p_2 to p_1 is $\sim$3 ns. The controller contains two delay lines, the first sets τ_k, the period of the orbit to be controlled, the second is used to adjust the latency τ_ℓ to properly time the arrival of perturbations at p_2. The state of the system is monitored through a directional coupler positioned directly after the photodiode in the delay loop of the photonic device. The control signal is measured through a directional coupler at the output of the controller. From Blakely et al. (2004a).

which they used to investigate numerically the observed dynamics (Blakely et al., 2004b).

Blakely et al. (2004a) applied this control method to the photonic device using the setup shown in Fig. 18(b) by measuring the state of the system at point p_1 and injecting continuously a control signal $\epsilon(t + \tau_\ell)$ at point p_2. For a given device time-delay T_D, coaxial cable was added or removed from the control loop to obtain a value of $\tau_\ell + \tau_{21}$ satisfying Eq. (19). The control perturbations ϵ were computed using the TDAS scheme described in Section 3.2.2. Specifically, $\epsilon(t) = \gamma[\xi(t) - \xi(t - \tau_k)]$ where τ_k is a control-loop delay that is nominally set equal to the period τ of the desired orbit.

Controlling the fast photonic device was initiated by setting the various control-loop time delays ($\tau_\ell + \tau_{21}$ and τ_k) and applying the output of the TDAS controller to point p_2 with γ set to a low value ($\gamma = 0.1$ mV/mW). Upon increasing γ to 10.3 mV/mW, Blakely et al. (2004a) observe that $\epsilon(t)$ decreased, which they

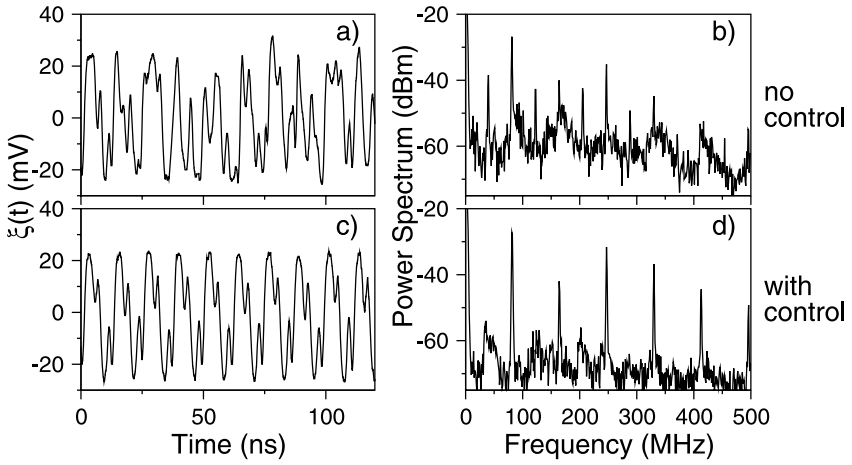

FIG. 19. Experimental data showing control of fast chaos. The state of the system was monitored by measuring the voltage in the delay loop before the amplifier (see Fig. 18(b)). (a) The chaotic time series of the monitored voltage in the absence of control, (b) the corresponding broad power spectrum, (c) the periodic time series of the stabilized orbit with control on, and (d) the corresponding power spectrum. From Blakely et al. (2004a).

further minimized by making fine adjustments to τ_k and $\tau_\ell + \tau_{21}$. Successful control was indicated when $\epsilon(t)$ drops to the noise level of the device. Figure 19(c) shows the periodic temporal evolution of the controlled orbit with a period of $\tau \sim 12$ ns. The corresponding power spectrum, shown in Fig. 19(d), is dominated by a single fundamental frequency of 81 MHz and its harmonics.

The data shown in Fig. 19 demonstrates the feasibility of controlling chaos in high-bandwidth systems even when the latency is comparable to the characteristic time scales of the chaotic device (compare $\tau \sim 12$ ns and $\tau_\ell \sim 8$ ns).

Blakely et al. (2004a) also inferred what would happen if $p_1 = p_2$ (the conventional method of implementing chaos control with nearly instantaneous feedback). In this case, $\tau_{21} = T_D$ and they found that control would be effective only when $\tau_\ell < 0.5$ ns, which was not possible using their implementation of TDAS. Note that the shortest reported control-loop latency of a chaos controller is 4.4 ns (Corron et al., 2003), much too large to control their device.

In principle, faster time-delay chaotic systems can be controlled using this approach as long as the controller uses technology (e.g., integrated circuits, all-optical) that is as fast as the system to be controlled so that τ_ℓ is comparable to T_D. Traditional chaos control schemes require that τ_ℓ be much shorter than T_D, increasing substantially the cost and complexity of the controller.

Note that their control approach is equally useful for non-chaotic fast and ultrafast time-delay devices, where the fast time scale makes the suppression of

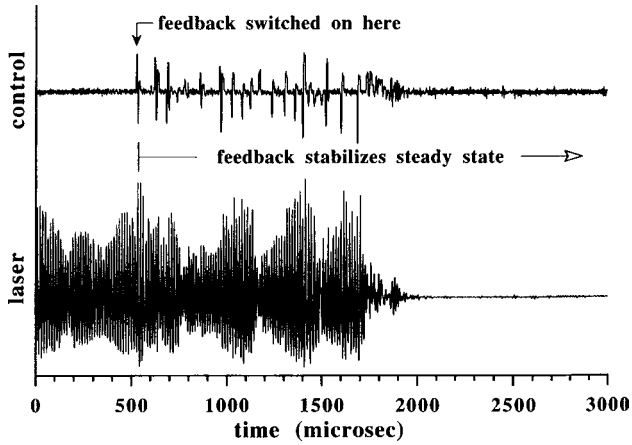

FIG. 20. Stabilization of the steady state of a frequency-doubled Nd:YAG laser. The transition towards the steady state is shown when the control signal is applied to the chaotic laser. From Roy et al. (1994).

undesired instabilities challenging (e.g., the double pulsing instability in femtosecond fiber lasers such as that described by Ilday et al. (2003).)

3.3. CONTROLLING UNSTABLE STEADY STATES

Most research on controlling chaos has focused on stabilizing UPOs. Of course, these experiments beg the question—can the unstable steady state (USS) of a chaotic devices, such as a laser, be stabilized by such control techniques? That is, if the laser is in a chaotic state, can one apply small corrective perturbations to obtain a stable output? This is of course the case of obvious engineering interest and practical application.

3.3.1. Stabilizing USSs Using Occasional Proportional Feedback

Gills et al. (1992) found that one could indeed achieve this result. They used occasional proportional feedback control (described in Section 3.2.1) to stabilize the output of a chaotic multimode Nd:YAG laser with a nonlinear intracavity KTP crystal. Without control the diode laser pumped solid state laser system displays periodic and chaotic fluctuations of the output intensity for certain operating parameter regimes, a feature known as the 'green problem'. Stable laser output was obtained by adjustment of two parameters of the controller: the reference level I_{ref} was set to the mean of the chaotic fluctuations and the period T was chosen to match the relaxation oscillation period. The control voltage fluctuations became extremely small once the steady state was controlled.

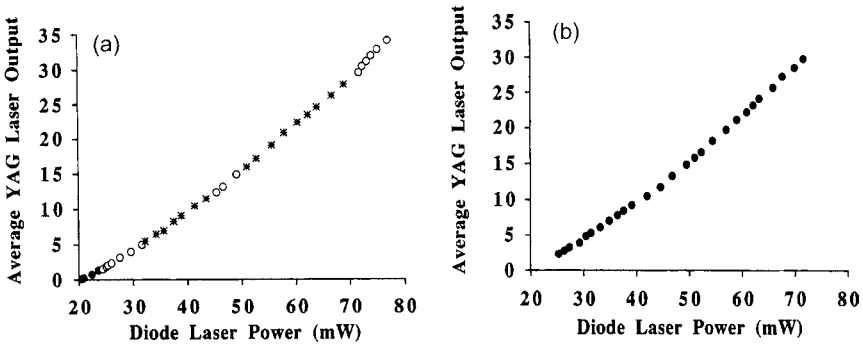

FIG. 21. OPF combined with a tracking algorithm stabilizes the USS of a chaotic Nd:YAG laser. (a) No control: The symbols designate stable steady-state (•), periodic (○), and chaotic (∗) behavior of the laser. Stable operation is obtained only very near to threshold; for higher pump powers, a complex sequence of periodic and chaotic behavior is found. (b) With control: the regime of stable operation was extended from about 20% above threshold to more than 300% above threshold. From Gills et al. (1992).

In Fig. 20 is shown the transient behavior of the laser intensity fluctuations as they are reduced to small fluctuations about the steady state as well as the control signal fluctuations during the stabilization process. If the control parameters are fixed and the pump power of the laser is increased or decreased after the steady state is stabilized, the control signal fluctuations increase rapidly, and control is lost as the laser goes into periodic or chaotic oscillations. Clearly, one needs to change the control circuit parameters as the laser pump power is changed. A procedure called "tracking" accomplishes this change of control parameters in a systematic fashion. Gills et al. (1992) applied such a tracking procedure to the frequency-doubled Nd:YAG laser; the control circuit parameters are varied so as to minimize the control signal fluctuations at each value of the pump power, which is increased in small increments. Their experiment was an illustration of the general algorithms for tracking periodic orbits developed by Schwarz and Triandaf (1992) and Carroll et al. (1992).

Figure 21(a) shows that without the control circuit the laser intensity lost stability at a pump power of about 25 mW, and either periodic or chaotic fluctuations were observed for higher pump powers. Figure 21(b) shows that a combination of stabilization and tracking could maintain a stable steady state as the laser pump power is increased from threshold (21 mW) to more than three times above threshold (about 80 mW). As we noted in Section 3.2.1, the laser is highly chaotic and stabilization of the USS becomes very challenging for even larger pump powers. Stabilization of this highly chaotic regime ('type-II' chaos) was achieve recently by Ahlborn and Parlitz (2004) using a new method, known as multiple delayed feedback control, as discussed in Section 2.1.

3.3.2. Controlling USSs Using Extended Time-Delay Autosynchronization

In a subsequent investigation of the OPF feedback scheme for stabilizing USSs, Johnson and Hunt (1993) determined that the only part of the feedback signal responsible for control was proportional to the *derivative* of $\xi(t)$. In a separate set of experiments, Bielawski et al. (1993) stabilized the dynamics of a fiber laser, and Parmananda et al. (1994) controlled an electrochemical cell using a feedback signal of the form

$$\epsilon(t) = -\gamma \frac{d\xi(t)}{dt}, \tag{20}$$

in which $\xi(t)$ was taken to be the laser intensity. We note that modern control engineers use derivative control to stabilize non-chaotic systems.

Derivative control has several key advantages over previous schemes for controlling USSs: it eliminates the need for a reference state with which to compare the system's current behavior, and it offers the possibility of stabilizing fast systems because it can be generated easily using analog electronics. Despite these advantages, derivative control is not perfect in an experimental setting because it can accentuate fluctuations that are often unrelated to the unstable behavior inherent in the nonlinear system. To understand the origin of the noise sensitivity, it is useful to consider the effects of the controller in the frequency domain. For feedback of the form of Eq. (20), $T(\omega) = i\omega$. It is apparent that derivative control will be very sensitive to high-frequency information contained in $\xi(\omega)$ because $|T(\omega)| \to \infty$ as $\omega \to \infty$. Because the spectrum of the chaotic fluctuations is often band limited, the controller may feedback a high-frequency signal arising from random fluctuations (noise) in the system rather than the chaotic fluctuations. This effect can lead to high-frequency instabilities and large power dissipation in the feedback loop.

Chang et al. (1998) proposed a control scheme that efficiently stabilizes USSs while avoiding the disadvantages of derivative control. It is based on a limiting form of the ETDAS scheme given by Eq. (17), which can be motivated most easily in the frequency domain. The ETDAS transfer function is given by Eq. (18) and shown in Fig. 14 for two different values of the parameter R. Recall, from Section 3.2.2 that the notches in the transfer function correspond to the location of the δ-functions of the UPO spectrum. The filtering action of the ETDAS feedback must remove these frequencies (via the notches) so that $\epsilon(\omega) = 0$.

Based on this reasoning, an appropriate transfer function for stabilizing USSs consists of a notch at $\omega = 0$ because the spectrum of a USS is a single δ-function at $\omega = 0$. All other frequencies are passed by the filter with equal weight, thereby generating a negative feedback signal from this information. We can obtain this transfer function by decreasing the value of τ, thereby increasing the distance between notches, while simultaneously increasing the value of R in order to keep the controller sensitive to frequencies near $\omega = 0$. Placing this discussion on a

rigorous foundation, we rewrite Eq. (17) in an equivalent, recursive form as

$$\epsilon(t) = -\gamma\big[\xi(t) - \xi(t-\tau)\big] + R\epsilon(t-\tau), \tag{21}$$

and perform the limits $\tau \to 0$ and $R \to 1$ with $(1-R)/\tau \equiv \omega_0$ held finite, thereby obtaining a new feedback relation given by

$$\frac{d\epsilon(t)}{dt} = -\omega_0\epsilon(t) - \gamma\frac{d\xi(t)}{dt}, \tag{22}$$

which is effective for stabilizing USSs. The feedback signal prescribed by Eq. (22) is identical to a single-pole high-pass filter familiar from elementary electronics. We note that ETDAS feedback in the form of Eq. (17) with τ small but finite and R near to but less than 1 does not necessarily stabilize USSs (Ahlborn and Parlitz, 2004).

Similar to derivative feedback, the feedback scheme given by Eq. (22) does not require a reference state. This is advantageous in situations where it is difficult to obtain an accurate reference state such as in high-speed dynamical systems, but it may lead to complications when the system possesses more than one USS with similar properties because the controller cannot explicitly select one stable state from the others. Selection of specific states may be possible if the basin of attraction for the states in the presence of control are distinct, or if the domain of feedback parameters that successfully stabilize the USSs are distinct.

A linear stability analysis a dynamical system in the presence of EDTAS control given by Eq. (22) further reveals that it can stabilize only a certain class of USSs. Consider a system whose evolution is governed by

$$\frac{d\mathbf{z}}{dt} = \mathbf{F}(\mathbf{z}, p), \tag{23}$$

possessing an USS $\mathbf{z}_*$. Introduce a new variable $\mathbf{x} \equiv \mathbf{z} - \mathbf{z}_*$ and linearize the dynamics about the USS so that

$$\frac{d\mathbf{x}}{dt} = \mathbf{A}\mathbf{x} + \mathbf{B}\epsilon, \tag{24}$$

where $\mathbf{A} = \partial\mathbf{F}/\partial\mathbf{x}|_{p=\bar{p}}$ is the Jacobian of the system in the absence of control, and $\mathbf{B} = \partial\mathbf{F}/\partial p|_{p=\bar{p}}$ quantifies the manner by which the control signal affects the state of the system. The combined dynamics of the system and the controller can be stated succinctly as

$$\frac{d\mathbf{y}}{dt} = \mathbf{G}\mathbf{y}, \tag{25}$$

where the $(N+1)$-dimensional expanded state vector is given by

$$\mathbf{y} = \begin{bmatrix} \mathbf{x} \\ \epsilon \end{bmatrix}, \tag{26}$$

and the $(N+1) \times (N+1)$ matrix by

$$\mathbf{G} = \begin{bmatrix} \mathbf{A} & \mathbf{B} \\ -\gamma \mathbf{n}^{\mathrm{T}} \mathbf{A} & -(\omega_0 + \gamma \mathbf{n}^{\mathrm{T}} \mathbf{B}) \end{bmatrix}, \tag{27}$$

where $^{\mathrm{T}}$ denotes the transpose of the vector. The system (25) is stable if and only if $\mathbf{G}$ possesses eigenvalues whose real parts are negative. The values of the control parameters γ, ω_0, and $\mathbf{B}$ rendering the system stable can be determined by calculating explicitly the eigenvalues of the matrix or by using the Routh–Hurwitz stability criterion (Ogata, 1990) that does not require an explicit calculation of the eigenvalues of $\mathbf{G}$. Briefly, the Routh–Hurwitz criterion imposes constraints on the values of the characteristic polynomial coefficients of $\mathbf{G}$. Chang et al. (1998) successfully stabilized the USSs of an electronic circuit and found very good agreement between the experimental observations and these theoretical predictions. We also use this approach below when studying the stabilization of USSs in a laser model.

While predictions regarding the stability of a USS under feedback control requires a detailed analysis of the eigenvalues or characteristic polynomial, it is possible to make some general statements regarding the inability of the controller to stabilize certain classes of USSs. First proposed by Ushio (1996), the main idea of this type of argument is to show, by an ingenious application of the intermediate value theorem, that if the Jacobian of the uncontrolled system linearized around the target dynamics (matrix $\mathbf{A}$) has an odd number of positive real eigenvalues, then control is not possible. Ushio (1996) showed this limitation of controllability for the case of stabilizing unstable periodic orbits (UPOs) in discrete-time systems using delayed-feedback controllers (TDAS). Nakajima (1997) extended this type of reasoning to show that the same limitations apply to TDAS-control of UPOs in continuous-time systems (ODEs). Chang et al. (1998) showed that the argument also holds for USS of ODEs, where control using feedback of the form given by Eq. (22) fails for the case when the associated matrix $\mathbf{A}$ has an odd number of positive real eigenvalues.

Finally, Chang et al. (1998) noted that Eq. (25) can be written in a slightly different form in which $\mathbf{G} = \widetilde{\mathbf{A}} + \widetilde{\mathbf{B}}\widetilde{\mathbf{K}}^{\mathrm{T}}$, where the matrix $\widetilde{\mathbf{K}}^{\mathrm{T}}$ has terms proportional only to the feedback parameters γ and ω_0. This decomposition facilitates the use of modern control engineering techniques such as pole-placement and tests of controllability and observability (Ogata, 1990). We do not pursue this approach since, in general, these techniques require access to all dynamical variables or that they be reconstructed using mathematical models, an approach that is not in the spirit of most controlling chaos research.

Moving on to an example from optics, Gauthier (1998) demonstrated that feedback of the form prescribed by Eq. (22) may be ideally suited for stabilizing the USSs of lasers. For an idealized laser model, it was found theoretically that there exists a wide range of feedback parameters giving rise to stable behavior (known

as the *domain of control*) and the controller can automatically track slow variation or drift of the laser parameters. While it is well known that this idealized laser model does not describe quantitatively the behavior of typical lasers, these observations highlight the potential of the feedback schemes. Detailed studies of specific laser systems must be undertaken to ascertain whether the controlling chaos techniques will be useful in real-world applications.

For simplicity, consider a single mode, homogeneously broadened, resonant, two level laser whose dynamics is governed by the following set of dimensionless equations

$$\begin{aligned} \frac{dE}{dt} &= -\kappa(E - \upsilon + E_{\text{inj}}), \\ \frac{d\upsilon}{dt} &= -(\upsilon - Ew), \\ \frac{dw}{dt} &= -\gamma_{\parallel}(w + E\upsilon - w_p), \end{aligned} \tag{28}$$

where E is the laser field strength inside the cavity, υ (w) is the atomic polarization (population inversion), κ ($\gamma_{\parallel}$) is the cavity (atomic inversion) decay rate, w_p is the inversion due to the pumping process in the absence of a field, and E_{inj} accounts for the possibility of injecting a field into the cavity. In Eqs. (28), the field strength is normalized to its saturation value, the inversion to its value at the first laser threshold, the polarization to its value for a field at the saturation strength, and time to the inverse of the polarization decay rate. The dynamical state vector in state space is denoted by $\mathbf{z} = [E, \upsilon, w]^{\mathrm{T}}$.

For low pump rates ($w_p < 1$) the laser is below threshold and resides on the stable steady state $\mathbf{z}_*^0 = [0, 0, w_p]^{\mathrm{T}}$. At $w_p = 1$, the state $\mathbf{z}_*^0$ becomes unstable via a pitchfork bifurcation (the first laser threshold) and, for slightly higher pump rates, the system resides on either of two symmetric steady-states $\mathbf{z}_*^{\pm} = [\pm E_{ss}, \pm\upsilon_{ss}, 1]^{\mathrm{T}}$, where $E_{ss} = \upsilon_{ss} = \sqrt{w_p - 1}$. For a bad cavity ($\kappa > \gamma_{\parallel} + 1$) and high pump rates these steady states are destabilized via a Hopf bifurcation (the second laser threshold) and the system fluctuates in a stable periodic or chaotic manner. For example, Fig. 22 shows a projection of the chaotic attractor for $w_p = 17$, $\kappa = 4$, and $\gamma_{\parallel} = 0.5$. The locations of $\mathbf{z}_*^{\pm}$ are indicated by the solid dots. The practical goal of the controller is to stabilize either of these two states, corresponding to the case when the laser is generating a powerful, continuous-wave beam devoid of erratic intensity or frequency fluctuations. Fortuitously, feedback of the form given by Eq. (22) stabilizes always one of the lasing USS ($\mathbf{z}_*^{\pm}$) because it is incapable of stabilizing the non-lasing USS ($\mathbf{z}_*^0$), since this state is destabilized via a pitchfork bifurcation in the absence of control.

In the first feedback scheme investigated by Gauthier (1998), called 'incoherent control', the pump rate is adjusted about its nominal value $\overline{w}_p$ by a feedback

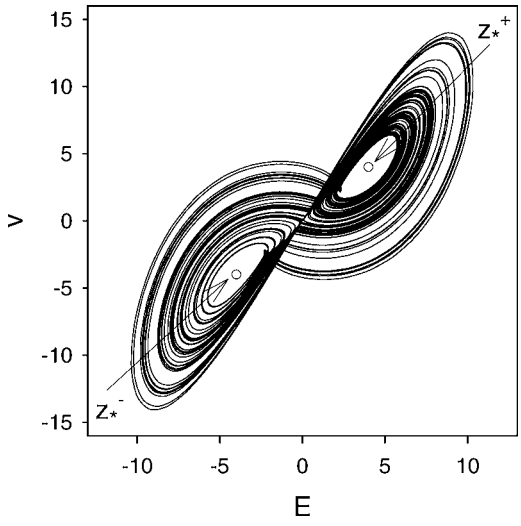

FIG. 22. Chaotic attractor of the single mode laser. From Gauthier (1998).

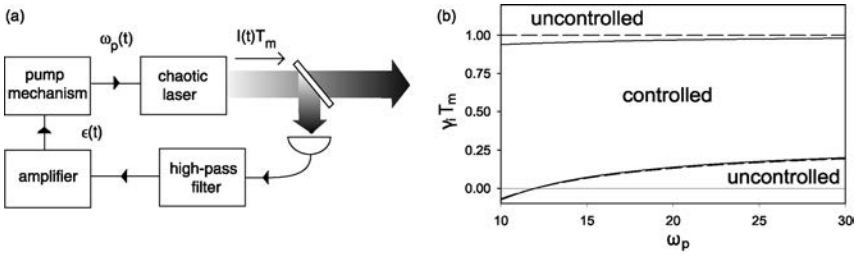

FIG. 23. (a) Possible realization of the 'incoherent' control scheme with its (b) associated domain of control. The USS is unstable in the absence of control at $w_p = 12$. From Gauthier (1998).

signal proportional to the high-pass-filtered intensity $I = T_m E^2$ of the beam generated by the laser and sensed by a square-law detector, where T_m is the intensity transmission coefficient of the laser output coupler, and I is normalized to the saturation intensity. A schematic of one possible realization of this feedback technique is shown in Fig. 23(a). The pump rate in the presence of feedback is given by $w_p = \overline{w}_p + \epsilon(t)$ where

$$\frac{d\epsilon}{dt} = -\omega_0 \epsilon + \gamma_i \frac{dI}{dt}. \tag{29}$$

The control law Eq. (29) is of the form of Eq. (22). For simplicity, Eq. (29) does not account for the control loop latency discussed in Section 3.2.3.

The stability of the USSs in the presence of feedback can be determined using the linear stability analysis outlined above. The laser dynamics (28) is linearized about the desired state and the range of feedback parameters ω_0 and γ_i rendering the state stable is determined using the Routh–Hurwitz criterion. Note that the local linear dynamics of the laser can be determined directly from experimental measurements. It is found that stabilization of the USSs is not overly sensitive to the parameter ω_0 so long as it is much smaller than the characteristic frequency of the chaotic fluctuations. For a narrow filter ($\omega_0 \ll \kappa, \gamma_\parallel, 1$), the approximate domain of control for either state $\mathbf{z}_*^+$ or $\mathbf{z}_*^-$ is given by

$$1 > \gamma_i > 1 - (1 + \gamma_\parallel + \kappa)(\kappa + \overline{w}_p)/2\kappa(\overline{w}_p - 1). \tag{30}$$

The precise domain (between the solid lines) is determined for $\kappa = 4$, $\gamma_\parallel = 0.5$, $\omega_0 = 0.1$, and $E_{\text{inj}} = 0$ and compared to the approximate domain (between the dashed lines) in Fig. 23(b). It is seen that control is possible for all w_p and the two results are in close agreement. Note that selecting between the states $\mathbf{z}_*^+$ and $\mathbf{z}_*^-$ is accomplished by the choice of initial conditions.

This analysis is applicable only for the case when the trajectory of the chaotic system is in a neighborhood of the USS, whereas the chaotic trajectory never visits this neighborhood as seen in Fig. 22. Direct numerical integration of Eqs. (28) and (29) indicates that the states are globally stable in the presence of feedback. However, the size of the transient control perturbations can often attain unphysical values. A method for circumventing this problem is suggested by Fig. 23(b).

A careful inspection of the figure reveals that the domain of control encompasses a horizontal band in the approximate range $0.9 > \gamma_i T_m > 0.3$, implying that the states can be controlled for all w_p without adjustment of γ_i. Thus, the control loop can automatically track slow changes or drift in the pump rate so long as the loop can adiabatically follow these changes (i.e., slow in comparison to the response time of the loop $\sim\omega_0^{-1}$). The procedure for stabilizing the USS using only small perturbations is to turn on control when the pump rate is low so that the USSs $\mathbf{z}_*^\pm$ are stable in the absence of control, set γ_i in the range between 0.3 and 0.9, then slowly adjust w_p to the desired value.

In the second feedback scheme, called 'coherent control', the control perturbation is an optical field E_{inj} injected into the laser whose nominal value is zero. It is generated all-optically by filtering a fraction of the optical field emitted by the laser with a short, high-finesse Fabry–Perot interferometer as shown schematically in Fig. 24(a). When the interferometer is adjusted so that one of its longitudinal modes coincides with the optical carrier frequency of the laser and its free-spectral-range is much larger than the spectral content of the chaotic fluctuations, the injected field is governed approximately by

$$\frac{dE_{\text{inj}}}{dt} = -\omega_0 E_{\text{inj}} + \gamma_c \sqrt{T_m} \frac{dE}{dt}, \tag{31}$$

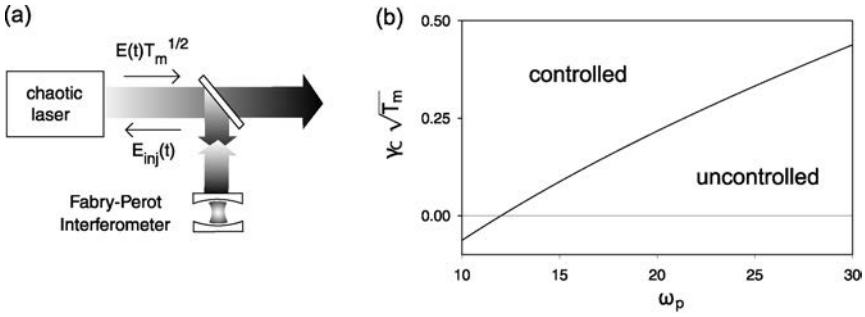

FIG. 24. (a) Possible realization of the 'coherent' control scheme with its (b) associated domain of control. From Gauthier (1998).

where an optical attenuator or amplifier in the beam path adjusts the feedback parameter γ_c and the cavity length and finesse adjusts the cut-off frequency ω_0. Note that E_{inj} vanishes when control is successful; this distinguishes the controlling chaos technique from other methods of frequency locking and narrowing of lasers using a field reflected from a Fabry–Perot interferometer.

The stability of the USSs in the presence of coherent feedback can be determined using the methods outlined in the previous discussion on incoherent control. The exact domain of control is shown in Fig. 24(b) for $\kappa = 4$, $\gamma_\parallel = 0.5$, $\omega_0 = 0.1$, and $\varepsilon = 0$. For a narrow filter, the domain for either state $\mathbf{z}_*^+$ or $\mathbf{z}_*^-$ is given approximately by

$$\gamma_c > \frac{1}{2\kappa}\big(\kappa(2\gamma_\parallel + 1)/(\gamma_\parallel + 1) + \gamma_\parallel + 1 - \big\{4\gamma_\parallel w_p\big[\kappa/(\gamma_\parallel + 1) - 1\big] + (\gamma_\parallel + 1)^2 - \kappa\big(6\gamma_\parallel^2 + 4\gamma_\parallel - \kappa - 2\big)\big/(\gamma_\parallel + 1)^2\big\}^{1/2}\big). \tag{32}$$

The approximate result is indistinguishable from the exact result shown in Fig. 24. As with incoherent control, it is seen that stabilization of the USS is effective for arbitrarily large pump rates. Also, the procedure for stabilization of a USS using only small perturbations is to turn on control when the pump rate is low so that the USSs $\mathbf{z}_*^\pm$ are stable in the absence of control, set γ_c to a large enough value (determined from Fig. 24(b)), then slowly adjust w_p to the desired value.

3.4. SUMMARY OF CONTROLLING CHAOS RESEARCH

In this section, we described methods for controlling complex periodic orbits (UPOs) and steady state behaviors (USSs) in optical systems. This research has taught us a lot about the underlying structure of chaotic systems and that there is, in fact, considerable order in chaos—the skeleton of UPOs and USSs. This order can be taken advantage of for potentially practical benefit. It serves as the structure on which chaotic dynamics can be controlled using small perturbations.

4. Synchronization

4.1. Introduction and Connection to Control

Huygens made the acute observation that two slightly out of step pendulum clocks synchronized when placed close to each other, but not when kept far apart (Sargent III et al., 1974). This discovery of the entrainment of coupled clocks has been seminal in the development of synchronized oscillators of all types. Synchronization of chaotic systems may be viewed as a generalization of the entrainment or synchronization of Huygens' coupled clocks. Now, the synchronized motion considered is not periodic, but chaotic.

Just as is the case for Huygens' clocks, two uncoupled chaotic systems will, after some transient time, evolve on their individual attractors in state space. The location of one has no relation to the other, which is particularly true for chaotic systems because of the extreme sensitivity to initial conditions. What happens if we couple them? Since coupling can be viewed as a form of control, it is not entirely surprising that coupling synchronizes the systems in some cases. That is, coupling can "lock" one system to the other, so that knowledge of the state of one system allows the prediction of the state of the other system. In a loose sense, we talk about chaos synchronization when some dynamic property that is uncorrelated when comparing two uncoupled chaotic oscillators becomes correlated when we couple the systems. Each of the systems remains chaotic even in the coupled case, but knowledge about one oscillator gives us predictive power about the second one.

Whereas it is the goal of chaos-control schemes to stabilize UPOs or USSs using small perturbations, synchronization can be viewed as an attempt to use small perturbations to control a dynamical system to a particular chaotic trajectory. For example, it is possible, in some cases, to achieve a replication of chaotic oscillations through the transmission of a single scalar signal from one high-dimensional dynamical system (the transmitter) to another high-dimensional dynamical system (the receiver). Furthermore, the coupling can be chosen such that the perturbations of the receiver-dynamics are zero when the receiver replicates the chaotic oscillations of the transmitter. In this sense, chaos synchronization may be viewed as a generalization of chaos control.

Chaos synchronization is also intimately linked with the observer problem in the control literature (Nijmeijer, 2001). This connection arises from asking: How does one construct a synchronizing system (or observer) for a given chaotic system? The purpose of this construction is to allow the dynamic state of the given chaotic system, which typically has 'inaccessible' degrees of freedom, to be determined using the synchronized system (the observer).

Several types of chaos synchronization can be distinguished depending on the dynamic property that is investigated. In the following, we use our own work to

illustrate the main types of synchronization, namely identical synchronization, generalized synchronization, and phase synchronization. (The interested reader may find further information in the book by Pikovsky et al. (2001) and the articles of Pecora et al. (1997b) and Boccaletti et al. (2002). Also, Uchida et al. (2005) provide a thorough review of chaos synchronization in optical systems.)

4.2. Identical Synchronization

Consider, as an example, a pair of identical and unidirectionally-coupled chaotic oscillators described by ordinary differential equations

$$\frac{d\mathbf{x}_T}{dt} = \mathbf{F}(\mathbf{x}_T), \tag{33}$$

$$\frac{d\mathbf{x}_R}{dt} = \mathbf{F}(\mathbf{x}_R) + c\mathbf{K}(\mathbf{x}_R - \mathbf{x}_T), \tag{34}$$

where $\mathbf{x}_T(t)$ denotes the n-dimensional state-space variable of the transmitter (or drive) system and $\mathbf{x}_R(t)$ the n-dimensional state-space variable of the receiver (or response) system, $\mathbf{F}$ is the nonlinear function governing the flow of a single oscillator, $\mathbf{K}$ is an $n \times n$ coupling matrix, and c is the scalar coupling strength.

Energy is dissipated in realistic devices. Therefore, the transmitter (and receiver) is modeled as a dissipative chaotic system. In this context, dissipative means that the volume of a ball of initial conditions in n-dimensional state-space will contract as the system evolves in time according to Eq. (33). As a consequence, the ball of initial conditions will be mapped, asymptotically, onto an attracting limit set, i.e. the chaotic attractor. In contrast, being chaotic, which is synonymous with extreme sensitivity to initial conditions, means that the distance between any two points in the ball of initial conditions will grow exponentially with time. This implies a stretching of the ball of initial conditions in at least one direction as the system evolves in time according to Eq. (33). Thus, the evolution of a dissipative chaotic system in its state-space is characterized both by contraction in some directions and by stretching in other directions.

The average rate of contraction and stretching is quantified by the *Lyapunov exponents* of the system (for a technical definition of Lyapunov exponents see Eckmann and Ruelle, 1985). For a chaotic system at least one Lyapunov exponent is positive, while the sum over all exponents is negative because of dissipation. Lyapunov exponents are useful quantities for characterizing chaotic systems because they are topological invariants, i.e. their values are independent of the chosen coordinate system. Furthermore, numerical methods to determine the exponents exist (Benettin et al., 1980; Eckmann and Ruelle, 1985).

In Eqs. (33) and (34), if transmitter and receiver are uncoupled ($c = 0$), then the chaotic attractor in the combined $2n$-dimensional state space is the product of the attractors of transmitter and receiver in their respective n-dimensional state

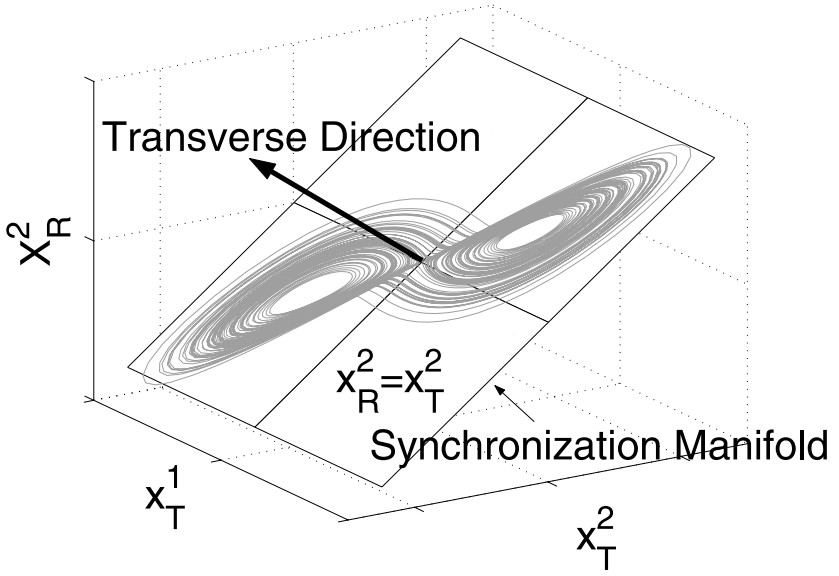

FIG. 25. Projection of the six-dimensional state space of two coupled Lorenz oscillators. The motion of the synchronized system takes place on a chaotic attractor, which is confined to a hyperplane (synchronization manifold) defined by $\mathbf{x}_R = \mathbf{x}_T$.

spaces. The $2n$-Lyapunov exponents of the combined system are those of, for example, the chaotic transmitter system with each value appearing twice. If transmitter and receiver are coupled ($c \neq 0$), then the attractor in the $2n$-dimensional state space will not be a simple product anymore and chaos synchronization becomes possible.

Identical synchronization (sometimes also referred to as complete synchronization) occurs when

$$\mathbf{x}_T(t) = \mathbf{x}_R(t) \tag{35}$$

is a stable solution of Eqs. (33) and (34). Geometrically, condition (35) implies that the attractor of the combined transmitter-response system in its $2n$-dimensional state space is confined to an n-dimensional hyperplane (or synchronization manifold), as depicted in Fig. 25 for the case of two coupled Lorenz systems. The stability of the synchronous solution (or, equivalently, the synchronization manifold) can sometimes be proven analytically, e.g., by using Lyapunov functions. In general, however, the local stability has to be determined numerically. One method is to compute the Lyapunov exponents; synchronization occurs if and only if all transverse Lyapunov exponents are negative (Pecora and Carroll, 1990). The transverse Lyapunov exponents (also known as condi-

tional Lyapunov exponents) are the average rate of exponential expansion or contraction in directions transverse to the synchronization manifold. In the case of unidirectionally-coupled identical transmitter and receiver systems, there are precisely n-transverse Lyapunov exponents. The remaining n-Lyapunov exponents characterize the chaotic dynamics within the synchronization manifold and have values identical to those of the chaotic transmitter.

The first experimental demonstration of identical synchronization in optical systems used Nd:YAG lasers (Roy and Thornburg, 1994). Since then, identical synchronization has been demonstrated in many optical and opto-electronic systems, including fiber ring lasers, which we discuss next.

In fiber lasers, the optical gain is provided by rare-earth elements (such as erbium, neodymium and ytterbium) embedded in silica fiber. Under optical pumping, those atoms provide light amplification at a characteristic wavelength; in the particular case of erbium that wavelength is of the order of 1.55 μm, which lies within the spectral region of minimal loss of silica fibers. For that reason, erbium-doped fiber amplifiers have been used widely since the mid 1990s in fiber-optics communication systems.

Laser emission is obtained in the system by providing feedback through closing the fiber on itself using a piece undoped silica fiber. A defining characteristic of such fiber ring lasers is that, due to the waveguiding properties of optical fiber, their cavities can be very long (on the order of tens of meters), orders of magnitude longer than most other lasers. For that reason, the frequency separation between consecutive longitudinal modes is very small (on the order of $\sim$1 MHz). Additionally, the amorphous character of the host medium leads to a very broad gain profile (on the order of hundreds of GHz). As a consequence, a large number of longitudinal cavity modes can experience gain and coexist inside the cavity, coupled through gain sharing. Hence, fiber lasers usually operate in a strongly multimode regime, and, consequently, their dynamics cannot be described in general by single-mode models.

For fiber lengths of tens of meters, the round-trip time taken by the light to travel once along the laser cavity is of the order of hundreds of nanoseconds. It is therefore natural to use a modeling approach based on delay-differential equations, which was done in a series of papers with increasingly detailed description of the laser physics (Williams and Roy, 1996; Williams et al., 1997; Abarbanel and Kennel, 1998; Abarbanel et al., 1999; Lewis et al., 2000). For example, in Abarbanel and Kennel (1998) and in Lewis et al. (2000), the behavior of two coupled erbium-doped fiber ring lasers operating in a high-dimensional chaotic regime was investigated, showing that the two lasers become identically synchronized if sufficient light from the first laser is injected into the second. The transmitter laser is modeled schematically as

$$\mathcal{E}_T(t+\tau_R) = \mathbf{M}\big(w_T(t), \mathcal{E}_T(t)\big), \tag{36}$$

$$\frac{dw_T(t)}{dt} = Q - 2\gamma\{w_T(t) + 1 + |\mathcal{E}_T(t)|^2(e^{Gw_T(t)} - 1)/G\}, \tag{37}$$

where $\mathcal{E}_T(t)$ is the complex envelope of the electric field, measured at a given reference point inside the cavity, and $w_T(t)$ is the averaged population inversion of the nonlinear medium. The propagation round-trip time around the cavity is τ_R, and $\mathbf{M}$ denotes the mapping of the electric field from time t to time $t + \tau_R$. The mapping $\mathbf{M}(w, \mathcal{E})$ takes into account birefringence, group velocity dispersion, gain dispersion, nonlinear polarization effects associated with the Kerr term, and the contribution of the pump light that is injected into the cavity (Lewis et al., 2000). In the equation for the population inversion (Eq. (37)), Q is the pumping strength, G the overall gain and γ is the decay time of the atomic transition. The receiver is an identical copy of the transmitter and is described by

$$\mathcal{E}_R(t + \tau_R) = \mathbf{M}\big(w_R(t), c\mathcal{E}_T(t) + (1 - c)\mathcal{E}_R(t)\big), \tag{38}$$

$$\frac{dw_R(t)}{dt} = Q - 2\gamma\{w_R(t) + 1 + |c\mathcal{E}_T(t) + (1 - c)\mathcal{E}_R(t)|^2(e^{Gw_R(t)} - 1)/G\}. \tag{39}$$

When $c = 0$, the lasers are uncoupled and run independently. If all of the physical parameters in the two laser subsystems are identical, the electric field in each laser visits the same chaotic attractor. However, $\mathcal{E}_T(t)$ and $\mathcal{E}_R(t)$, as well as $w_T(t)$ and $w_R(t)$, are uncorrelated due to the instabilities in the state-space of the system. As c increases away from zero, Lewis et al. (2000) find numerically that the lasers asymptotically achieve identical synchronization, $\mathcal{E}_T(t) = \mathcal{E}_R(t)$, and $w_T(t) = w_R(t)$, for a certain minimum coupling (as low as $c_{\text{crit}} \sim 1.3 \times 10^{-3}$) even though the population inversions are not physically coupled.

Identical synchronization is most easily demonstrated for the case $c = 1$, which is commonly referred to as open loop configuration. Inspection of Eqs. (36)–(39) shows that $\mathcal{E}_T(t) = \mathcal{E}_R(t)$ and $w_T(t) = w_R(t)$ is always a solution. Identical synchronization happens when this solution is asymptotically stable such that starting the transmitter and receiver from different initial conditions their dynamics will converge. To demonstrate asymptotic stability, consider Eqs. (37) and (39) with $c = 1$. It can be shown that any initial difference between the population inversion of the transmitter and the receiver evolves according to the equation

$$\frac{d[w_T(t) - w_R(t)]}{dt} = -2\gamma\{[w_T(t) - w_R(t)] + |\mathcal{E}_T(t)|^2 e^{Gw_R(t)} \times (e^{G[w_T(t) - w_R(t)]} - 1)/G\}. \tag{40}$$

Since $e^x - 1 \geqslant x$ for any real x,

$$\frac{d[w_T(t) - w_R(t)]}{dt} \leqslant -2\gamma[w_T(t) - w_R(t)](1 + |\mathcal{E}_T(t)|^2 e^{Gw_R(t)}), \tag{41}$$

so that $|w_T(t) - w_R(t)|$ tends to 0 faster than $e^{-2\gamma t}$. Using the exponential convergence of the receiver's population inversion to that of the transmitter, it is straightforward to see that the maps **M** for receiver and transmitter become identical, and therefore $\mathcal{E}_T(t) - \mathcal{E}_R(t)$ tends to 0 also. Thus, in the open loop configuration two erbium-doped fiber ring lasers synchronize identically.

Experimental demonstrations of the synchronization between chaotic fiber lasers exist. The first experimental observation of this phenomenon was made by VanWiggeren and Roy (1998a) using the experimental setup shown in Fig. 26(a). The transmitter is an erbium-doped fiber ring laser, whose dynamical regime can be manipulated by means of an intracavity polarization controller. The laser is set to operate in a chaotic regime, from which 10% of the intracavity radiation is extracted via a 90/10 output coupler and transmitted to the receiver. Half of this transmitted signal is injected into an erbium-doped fiber amplifier (EDFA) whose physical characteristics (fiber length, dopant concentration, and pump diode laser) are matched as closely as possible to those of the transmitter EDFA. It should be noted that the receiver output is not reinjected back into itself, i.e. the system operates in an open loop. A second 90/10 coupler in the transmitter cavity allows for the introduction of an external signal, whose role is discussed in Section 5, in the context of chaotic communications. Plot A in Fig. 26(b) shows a sample time trace of the transmitted field in the absence of an external signal. The state-space reconstruction of the dynamics displayed in plot A is shown in plot B and exhibits no low-dimensional structure. The signal detected by photodiode B (see experimental setup in Fig. 26(a)) after passing through the receiver s EDFA is shown in plot C. This signal has been shifted in time an amount $\tau = 51$ ns, equal to the time mismatch corresponding to the fiber length difference between the paths leading to photodiodes A and B. Visual inspection already indicates that the time series of the transmitter and receiver are very similar. The existence of synchronization is confirmed by plotting the output of the receiver (again shifted 51 ns) versus that of the transmitter; the resulting straight line with slope unity in this synchronization plot is a clear indicator of the occurrence of synchronization.

4.3. Generalized Synchronization

Identical synchronization is easy to recognize in experiment. However, it is a very restrictive definition of synchronization, which, for instance, doesn't allow the discussion of synchronization of non-identical systems. A first logical step toward relaxing the definition of synchronization is to require a (static) functional relationship of the two coupled chaotic systems instead of identity:

$$x_R(t) = F\big(x_T(t)\big). \tag{42}$$

This type of chaos synchronization was discussed for two mutually coupled systems in Afraimovich et al. (1986), and has been introduced for unidirectionally

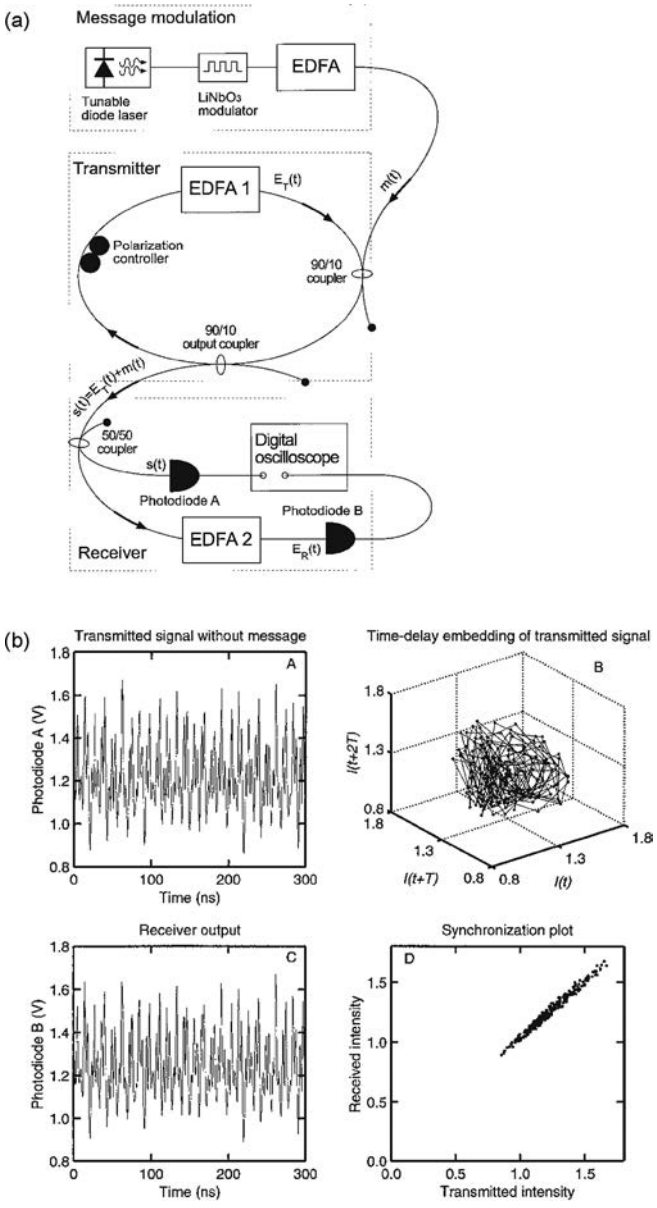

FIG. 26. (a) schematic experimental setup to observe synchronization of fiber-laser chaos. (b) experimental results showing the transmitter (A) and receiver (C) outputs, the state-space reconstruction plot of the transmitted signal (B) and the synchronization plot (D). From VanWiggeren and Roy (1998a).

coupled systems under the name of *generalized synchronization* by Rulkov et al. (1995). We restrict ourselves here to the discussion of unidirectionally coupled systems, where we have an autonomous transmitter (or drive system) and a receiver (or response system), which are characterized by their respective state-space variables $x_T(t)$ and $x_R(t)$.

Generalized synchronization has been shown to exist through predictability (Rulkov et al., 1995) or the existence of a functional relationship (Pecora et al., 1997a; Brown, 1998) between the transmitter and receiver. These approaches are often difficult to implement in experimental measurements due to the presence of noise and lack of precision in measurements. When replicas or duplicates of the receiver are available, the auxiliary-system method introduced by Abarbanel et al. (1996) can be used for detecting generalized synchronization. In this method, two or more receivers are coupled with the transmitter. If the receivers, starting from different initial conditions, display identical synchronization between them (after transients have disappeared), one can conclude that the receiver signal is synchronized with the transmitter in a generalized way (Kocarev and Parlitz, 1996a; Rulkov et al., 2001).

Most examples of generalized synchronization discussed in the literature consist of situations where the transmitter and receivers are different from each other, or those involving the same system operated at different parameter values (Lewis et al., 2000). One may expect that strongly coupled identical systems with similar parameter values display identical synchronization, if they synchronize at all. However, generalized synchronization of chaos can occur with identical transmitter and receivers with similar parameter values. This was shown by Uchida et al. (2003) (also McAllister et al., 2004), who used a two-longitudinal-mode Nd:YAG microchip laser as a laser source, as shown in Fig. 27(a). The total intensity of the laser output is detected by a photodiode and the voltage signal is fed back into an intracavity acousto-optic modulator (AOM) in the laser cavity through an electronic low pass filter with an amplifier. The loss of the laser cavity was modulated by the self-feedback signal through the AOM, which induced chaotic oscillations. Temporal waveforms of the laser output were measured by a digital oscilloscope and stored in a computer for later use as a drive signal. In order to test for synchronization, the same laser was used as a receiver, which ensured identical parameter settings between transmitter and receiver. The drive signal was sent to the AOM in the same laser cavity using an arbitrary waveform generator connected to the computer. The original feedback loop was disconnected (dashed line in Fig. 27(a)), i.e., the open loop configuration was used for the receiver (dotted line in Fig. 27(a)). The total intensity of the laser output was detected with a digital oscilloscope. Typical temporal waveforms of the transmitter and the receiver are shown in Fig. 27(b). There is no obvious correlation between the two outputs and the correlation plot between the transmitter and receiver waveforms (Fig. 27(c)) shows no evidence of identical synchronization. Next, the drive sig-

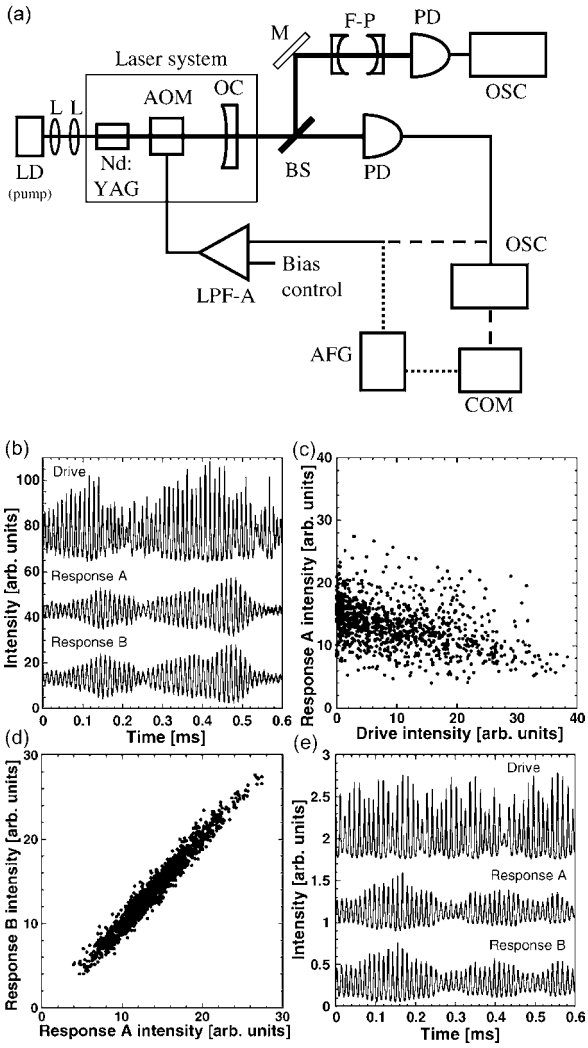

FIG. 27. (a) Experimental setup of a diode-pumped Nd:YAG microchip laser with optoelectronic feedback. The dashed line corresponds to the closed-loop transmitter, and the dotted line corresponds to the open-loop receiver. AFG, arbitrary function generator; AOM, acousto-optic modulator; BS, beam splitter; COM, computer; F-P, Fabry–Perot interferometer; L, lens; LD, laser diode for pumping; LPF-A, low pass filter and amplifier; M, mirror; Nd:YAG, Nd:YAG laser crystal; OC, output coupler; OSC, digital oscilloscope; PD, photodetector. (b) Temporal waveforms of experimentally measured total intensity of the transmitter and two receivers. (c) Correlation plots between the transmitter and receiver outputs. (d) Correlation plots between the two receiver outputs; (c) and (d) are obtained from (b). (e) Temporal waveforms of the total intensity as obtained from numerical calculations. From Uchida et al. (2003).

nal was fed back into the receiver laser repeatedly, in order to apply the auxiliary system method. Figure 27(b) shows two receiver outputs driven by the same drive signal at different times.

The correlation plot between the two receiver outputs shows linear correlation, as shown in Fig. 27(d). This implies that the receiver laser driven by the same drive signal always generates identical outputs, independent of initial conditions. Because the dynamics of the receiver laser are repeatable and reproducible, generalized synchronization can be achieved stably in this system. Numerical results obtained from Tang–Statz–deMars equations agree well with the experimental observations (Fig. 27(e)). Analysis of these equations reveals that modal dynamics is responsible for the occurrence of generalized synchronization in identical systems.

4.4. Phase Synchronization

Both identical synchronization and generalized synchronization are defined as deterministic relationships between all variables of the coupled systems. Phase synchronization is different. The definition of phase synchronization was inspired by the concept of frequency locking of periodic oscillators, where very minute coupling is sufficient to lock the phases of drive and response. That is, their oscillation period becomes identical, yet the amplitude of the oscillations of drive and response might be very different.

The concept of phase synchronization of chaotic systems such as lasers is based on the fact that, in some cases, the chaotic oscillations can be decomposed in terms of an amplitude and a phase. Under certain conditions, it can happen that the amplitudes of the chaotic oscillations of two coupled lasers are desynchronized, while a clear synchronization exists between the phases. This is called *phase synchronization* (Rosenblum et al., 1996). We note that "phase" in this context indicates a suitably defined phase of chaotic oscillations of laser intensity, not the optical phase of the electric field.

Let us illustrate the concept of phase synchronization with the example of a periodically driven chaotic Rössler oscillator, whose dynamics is described by

$$\begin{aligned} \dot{x} &= -(y+z), \\ \dot{y} &= -x + 0.15y + k\sin(\omega t), \\ \dot{z} &= 0.2 + z(x-10), \end{aligned} \tag{43}$$

where k denotes the coupling strength, and the drive frequency is close to the average frequency of the chaotic Rössler system, namely $\omega = 1.0335$. The projection of the Rössler attractor onto the x–y plane (see Fig. 28) reveals that we can introduce phase through an angle variable by simply going to cylindrical coordinates, yielding a phase $\phi = \arcsin(y/r)$, where $r = \sqrt{x^2 + y^2}$. A good

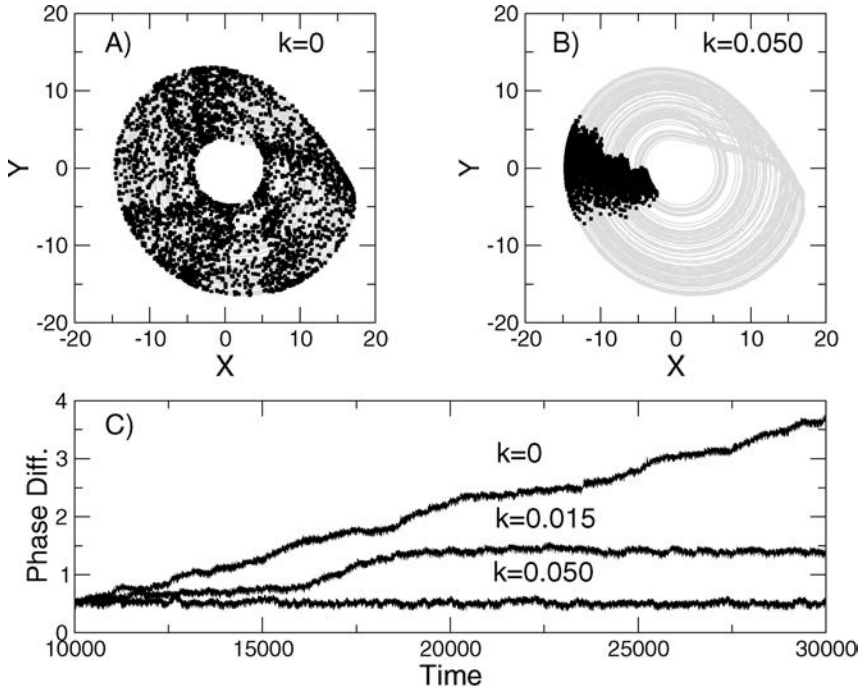

FIG. 28. Phase synchronization of a periodically driven Rössler oscillator. In (A) and (B) projections of the chaotic attractor onto the x–y plane are shown and the black squares are a stroboscopic plot in which the coordinates of the driven Rössler system are sampled after every full period of the drive. (A) In the uncoupled case, $k = 0$, the points spread relatively evenly over the whole attractor, which corresponds to a drift of the phase of the Rössler oscillator with respect to the drive. (B) Phase synchronization occurs for a coupling $k = 0.05$, as seen by the concentration of squares in one region of the attractor. In (C) the evolution of the phase difference $(\phi(t) - \omega t)/2\pi$ is plotted for different k.

measure for phase synchronization between the chaotic Rössler system and the periodic drive is the phase difference $\phi(t) - \omega t$. For weak or no coupling the phase difference varies either without bound in a random-walk like manner if the drive frequency equals the mean rate of phase increase of the chaotic oscillator or steadily increases (or decreases) if the drive frequency and mean oscillator frequency differ. This is shown in Fig. 28(C), where the evolution of the phase difference is depicted for the case of no coupling, weak coupling, and coupling above the synchronization threshold. For no coupling, the phase difference grows steadily. An increase in k to $k = 0.015$ leads to partial synchronization, where long periods of phase locking are interspersed by phase slips. The rate of slipping decreases continually as k increases, until the synchronization threshold is

reached. Above the synchronization threshold, there are no more phase slips and the phase difference is bounded by a fraction of 2π for all times.

Although phase synchronization has been observed in many experimental systems, the phenomena is still not completely understood. A central problem is that no general definition of "phase" exists that works for all chaotic systems. That is, only for very special chaotic oscillators are we able to introduce a phase variable in the straightforward manner discussed above and many alternative definitions of phase have been proposed and applied. One example is the use of the Gabor analytic signal (Gabor, 1946) defined through the Hilbert transform (Born and Wolf, 1999) of the intensity time series, as used in the experimental investigation of phase synchronization in a chaotic laser array by Deshazer et al. (2001).

The chaotic system of Deshazer et al. (2001) consists of three parallel, laterally coupled single-mode Nd:YAG laser arrays. Coupling through the electric fields of the individual beams exists only for adjacent pairs. Experimental intensity measurements are displayed in Figs. 29(a)–(c). The two outer lasers in the array (lasers 1 and 3) have nearly identical intensity fluctuations. However, no synchronization relationship is obvious between the center laser (laser 2) and the outer lasers (lasers 1 and 3), even though the center laser mediates the identical synchronization of the outer lasers.

To test for interdependence between the time series of the outer and center lasers, an analytic phase and a Gaussian filtered phase are introduced (see details in the article by Deshazer et al. (2001)). Phase synchronization between the outer and the center laser (lasers 1 and 2) is shown by plotting their relative phase versus time (Figs. 29(d)–(e)). Figure 29(d) shows the difference of the analytic signal phases for these lasers, which has a large range of variation ($\sim$130 rotations). Phase synchronization is not discernible. Next, in Fig. 29(e), the difference of the Gaussian filtered phase for these two lasers is plotted at different frequencies of the Gaussian filter. Synchronization of the side and central lasers in the frequency regime of 140 kHz is apparent immediately, since the flat portion of this plot extends across essentially the entire time of observation (solid line). Periods of phase synchronization and phase slipping are found in the less correlated frequency regime of 80 kHz (dotted line). No indication of synchronization is found when one of the component phases is replaced with a surrogate phase extracted from another experimental data set taken from this array under identical conditions (dashed line). These results illustrate that the detection of phase synchronization may require careful consideration of the nature of the time series measured. The time series considered in this experiment are of a distinctly nonstationary nature, and it is clearly advantageous to introduce a Gaussian filtered phase variable. One is then able to quantitatively assess phase synchronization for different frequency components of the dynamics.

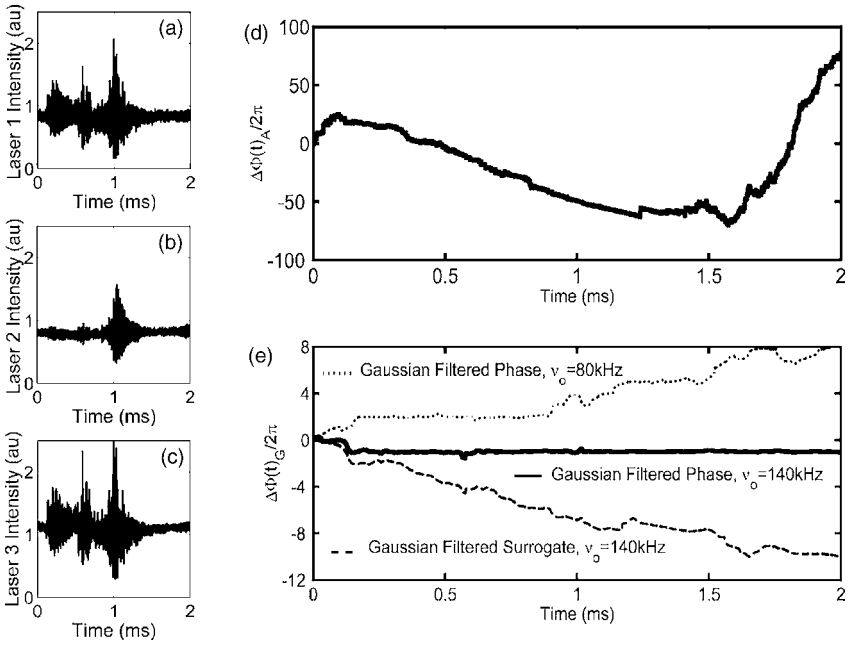

FIG. 29. (a)–(c) Experimental intensity time series showing chaotic bursts of three Nd:YAG lasers evanescently coupled in a linear array. (d), (e) Time series for the differences between the (d) analytic and (e) Gaussian filtered phases of the center and an outer laser. The solid line in (e) corresponds to a Gaussian filter centered at 140 kHz; for the dotted line it is centered at 80 kHz; and the dashed line is the phase difference with respect to a surrogate time series. From Deshazer et al. (2001).

4.5. SYNCHRONIZATION ERRORS

In realistic devices there is always noise and no two physical devices are exactly identical. One therefore has to consider the effects of noise and slight mismatches of transmitter and receiver on the quality of chaos synchronization. For simplicity, we focus on the case of identical synchronization, but similar considerations apply to generalized synchronization and phase synchronization.

As a concrete example consider the two coupled opto-electronic devices shown in Fig. 30(A) that were investigated theoretically by Abarbanel et al. (2001) and experimentally by Tang and Liu (2001b). The transmitter and receiver each consist of a single-mode semiconductor laser with time-delayed feedback formed by an optoelectronic loop from the laser optical output back to the bias current across the laser itself. This particular feedback is insensitive to the optical phase of the laser output, which simplifies experiments as compared to optical

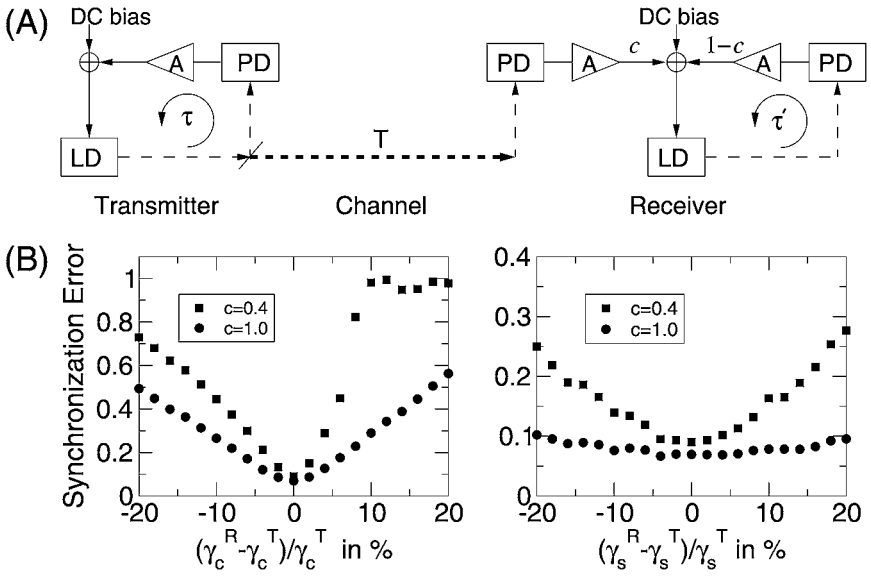

FIG. 30. Synchronization of two hyperchaotic opto-electronic devices with delayed feedback. (A) Setup. LD: laser diode; PD: photodetector; A: amplifier; τ: feedback delay time; T: transmission time. (B) Synchronization error from mismatches in the photon decay rate (γ_c) and the carrier decay rate (γ_s). From Abarbanel et al. (2001).

feedback schemes, such as those described in Section 2.2. The transmitter and receiver generate chaotic oscillations at gigahertz frequencies due to the interplay of laser nonlinearities and time-delayed feedback, which makes the state-space of the system formally infinite-dimensional. The two chaotic devices are coupled by injecting light from the chaotic transmitter system into the receiver with coupling strength c. The equations of motion describing the time-delay dynamics of the transmitter-receiver system read

$$\begin{cases} \dfrac{ds_T}{dt} = \gamma_c^T\big(\big[g(n_T, s_T) - 1\big]s_T\big) + 2\sqrt{s_T}F_T^{\mathrm{sp}}, \\ \dfrac{dn_T}{dt} = \gamma_s^T\big(\mathcal{J} - n_T - \mathcal{J}g(n_T, s_T)s_T\big) + \gamma_s^T\xi(\mathcal{J}+1)s_T(t-\tau), \end{cases} \tag{44}$$

$$\begin{cases} \dfrac{ds_R}{dt} = \gamma_c^R\big(\big[g(n_R, s_R) - 1\big]s_R\big) + 2\sqrt{s_R}F_R^{\mathrm{sp}}, \\ \dfrac{dn_R}{dt} = \gamma_s^R\big(\mathcal{J} - n_R - \mathcal{J}g(n_R, s_R)s_R\big) \\ \qquad\qquad + \gamma_s^R\xi(\mathcal{J}+1)\big(cs_T(t-\tau) + (1-c)s_R(t-\tau')\big), \end{cases} \tag{45}$$

where s is the intracavity photon density of the laser, n is the carrier density, $g(n, s)$ is the gain, $\mathcal{J}$ is the dc-bias current, γ_c is the photon decay rate, γ_s is the spontaneous carrier decay rate, τ is the feedback delay, and F^{sp} is the noise due to spontaneous emission. For the case without noise and equal parameters, i.e. $\gamma_c^T = \gamma_c^R$, $\gamma_s^T = \gamma_s^R$ and $\tau = \tau'$, the systems synchronize identically for coupling strengths $c \geqslant 0.1$, as shown by numerical simulations of Eqs. (44) and (45) as well as computations of the transverse Lyapunov exponents (Abarbanel et al., 2001).

In an experiment, the transmitter and receiver systems are inevitably different from each other. In this situation, identical synchronization is not a mathematical solution of the model equations. Nonetheless, the deviation from the identity solution can be small over some range of parameters.

An evaluation of the effect of parameter mismatches between the transmitter and the receiver on the quality of synchronization, quantified by the synchronization error

$$\mathcal{E} = \frac{\langle |s_T(t) - s_R(t)| \rangle}{\langle s_T(t) \rangle}, \tag{46}$$

is shown in Fig. 30(B) for the two coupling strengths $c = 0.4$ and $c = 1$. In these computations, a realistic level of spontaneous emission noise is present, so $\mathcal{E} > 0$ even for perfectly matched parameters. While the error is tolerable for a 5% or so mismatch at $c = 1$, for $c = 0.4$ the error is large for almost all mismatches. Thus, as one would expect, the open loop configuration ($c = 1$) is most robust with respect to parameter mismatch. This conclusion was confirmed experimentally by Tang and Liu (2001b), where approximate identical synchronization was found for a range of coupling strengths c with a minimum synchronization error for the open loop configuration.

The case of two coupled opto-electronic devices is an example of a system where the noise-free model with identical transmitter and receiver predicts identical synchronization (all transverse Lyapunov exponents are negative) and where the inclusion of noise and parameter mismatches does not destroy synchronized behavior in any essential way. In other words, in this example, the *asymptotic* stability of the synchronization manifold is a good predictor of synchronization in the physical system despite the presence of noise and parameter mismatch. However, this is not always true. Illing et al. (2002) show that slight parameter mismatches can lead to large synchronization errors in some systems even when no noise is present. In this case, synchronization errors arise due to the fact that even when the slightly mismatched systems exhibit generalized synchronization, the deviation of the manifold associated with generalized synchronization (defined by $x_R = F(x_T)$) from the hyperplane associated with identical synchronization can be large.

Aside from parameter mismatches, the presence of noise can prevent high quality synchronization. In some synchronization experiments where all transverse

Lyapunov exponents are negative, long intervals of synchronization are interrupted irregularly by large (comparable to the size of the chaotic attractor), brief desynchronization events. This behavior has been called *attractor bubbling* (Ashwin et al., 1994, 1996).

Ashwin et al. (1994, 1996) pointed out that the synchronization manifold may contain unstable sets that are embedded in or close to the chaotic attractor. These unstable sets, such as unstable periodic orbits, are characterized by positive transverse Lyapunov exponents, even though the transverse exponents characterizing the entire chaotic attractor are all negative. Near such sets, the manifold is locally repelling so that a small perturbation arising from experimental noise results in a brief excursion away from the synchronization manifold. These desynchronization events recur because the chaotic evolution of the system brings it into the neighborhood of the repelling set an infinite number of times.

This explanation implies that the transition from bubble-free synchronization to bubbling as the coupling strength is varied occurs when a set first becomes transversely unstable. Thus, a criterion for high-quality, bubble-free synchronization is that the largest transverse exponents characterizing each of the unstable sets embedded in the attractor must be negative. Since Lyapunov exponents are topological invariants, this criterion is independent of the choice of metric.

Unfortunately, it is impossible to apply this criterion since there are typically an infinite number of unstable sets embedded in a chaotic attractor whose stability must be determined. There is some indication that the criterion might be applied in an approximate sense because it has been suggested that a low-period UPO typically yields the largest exponent (Hunt and Ott, 1996). However, it is known that this conjecture does not hold for an attractor near a crisis (Zoldi and Greenside, 1998; Hunt and Ott, 1998; Yang et al., 2000).

To circumvent the problems associated with applying the criterion proposed by Ashwin et al. (1994), synchronization criteria that are much simpler to apply were suggested, e.g., by Gauthier and Bienfang (1996) and Brown and Rulkov (1997). Unfortunately, although simple to apply, these criteria are often too conservative: experimental systems synchronize even when the condition that guarantees synchronization is not satisfied. This was demonstrated by Blakely and Gauthier (2000) who compared regimes of high-quality synchronization observed in an experimental system of coupled hyperchaotic electronic oscillators to the predictions of the different criteria for high-quality synchronization.

In summary, both parameter mismatches and experimental noise can destroy high quality identical synchronization in certain chaotic systems. Furthermore, there is no simple and generally reliable way to determine how to couple two oscillators to achieve high-quality synchronization. Indeed, in many cases, the computationally most efficient approach is to include realistic levels of noise and parameter mismatches in the model and check synchronization quality by direct simulation.

4.6. Summary of Synchronizing Chaos Research

In this section, we described methods for synchronizing the behavior of two or more systems displaying chaotic behavior. This research drives home the fact that chaotic systems are acutely sensitive to tiny perturbations and that any behavior that is consistent with the system dynamics, including even chaotic behavior, can serve as a target state.

5. Communication

5.1. Introduction

Synchronization leads to communication—even when the signals used are chaotic. The main idea of chaos communication schemes is to mix the message with a chaotic carrier in the transmitter and to send the mixed signal to the receiver. At the receiver, the message can be recovered by comparing the transmitted mixed signal to the message-free chaotic carrier. The crux of synchronization based chaos communication is that it solves the problem of how to obtain the message-free chaotic carrier at the receiver. That is, although it is not possible to store the non-repeating chaotic carrier that is needed for message retrieval, the chaotic carrier can be regenerated at the receiver using chaos synchronization.

Communication based on chaotic synchronization was already proposed by Pecora and Carroll (1990) in their seminal paper on chaos synchronization and developed further by Frey (1993); Volkovskii and Rulkov (1993); Kocarev and Parlitz (1995); and Feldmann et al. (1996). The feasibility of chaos communication using synchronization was confirmed experimentally soon thereafter in electronic circuits (Kocarev et al., 1992; Cuomo and Oppenheim, 1993) and laser systems (VanWiggeren and Roy, 1998a, 1998b; Goedgebuer et al., 1998). Synchronization based communication is not the only known approach to chaos communication. For example, the unmodulated chaotic waveform can be transmitted along with the modulated signal (known as transmitted reference scheme) using either a separate channel or time division (Kolumban et al., 1998). Thus, reliable detection can be achieved at the expense of efficiency, since at least 3 dB of the signal-to-noise ratio is lost. Another method encodes the message into the symbolic dynamics of the chaotic transmitter (Hayes et al., 1993, 1994; Corron et al., 2002), with the result that the information can be read off simply by observing the transmitted signal. However, this method requires detailed and precise control of the transmitter dynamics, which is an extremely challenging task in high-speed optical systems. For this reason essentially all optical chaos communication schemes are based on chaos synchronization.

In the context of synchronization-based chaos communication, one key issue is how to mix the message with the chaotic carrier. One approach is *chaos masking*,

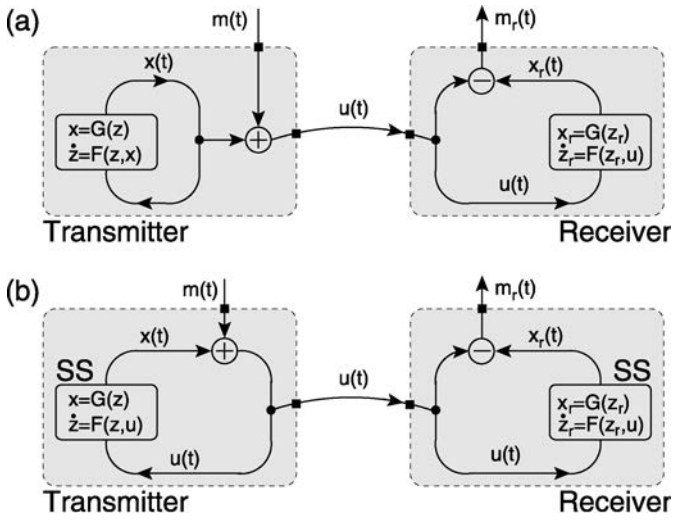

FIG. 31. Schematic of chaos communication based on synchronization where the message is encoded using (a) *chaos masking*, i.e. the message $m(t)$ is added to the transmitter signal without influencing the transmitter dynamics, and (b) *chaos modulation*, i.e. the message $m(t)$ is incorporated into the transmitter dynamics.

where the information signal $m(t)$ is added (or multiplied) to the chaotic signal $x(t)$ generated by a chaotic transmitter whose oscillations do not depend on the information $m(t)$, as shown in Fig. 31(a). The mixture $u(t) = x(t) + m(t)$ is transmitted to the receiver where it is used as a driving signal for the matched receiver. Various implementations of the matched receivers were proposed; see, for example, Carroll and Pecora (1993); Cuomo and Oppenheim (1993); Kocarev et al. (1992); Dedieu et al. (1993); Murali and Lakshmanan (1993); Yu et al. (1995), and references therein. The message is then recovered by subtracting (or dividing) the synchronized chaotic signal in the receiver (x_r) from the transmitted signal. The common shortcoming of such methods of communication is that the driving signal at the receiver ($u = x + m$), which is "distorted" by the message $m(t)$, does not match the corresponding "driving" signal in the transmitter (x) and perfect synchronization of transmitter and receiver dynamics is not possible. As a result, the recovered message $m_r(t)$ will always contain some traces of chaotic waveforms no matter how perfectly the parameters of the receiver match those of the transmitter.

In contrast, perfect synchronization and message recovery is possible, in principle, in chaos communication schemes that utilize *chaos modulation* to encode and decode information (Volkovskii and Rulkov, 1993; Halle et al., 1993; Frey, 1993; Kocarev and Parlitz, 1995; Feldmann et al., 1996; Parlitz et al., 1996). The key

idea of this approach is that the information signal $m(t)$ is injected into one of the feedback loops of the chaotic transmitter system, as depicted in Fig. 31(b). The feedback is selected in such a way that the remaining subsystem (SS) is conditionally stable. In this case, the distorted chaotic signal $u(t) = x(t) + m(t)$ returns back to the generator and drives the dynamics of the transmitter. The signal $u(t)$ is also transmitted to the receiver, where it drives the dynamics and generates oscillations of the receiver system that are identical to the chaotic oscillations in the transmitter. The message can be recovered using the open feedback loop of the receiver, as shown in Fig. 31(b). In this case (in the absence of noise) the information can be restored exactly after initial transients.

Since the first numerical proposal of communications with synchronized chaotic lasers was carried out in a solid-state Nd:YAG laser model by Colet and Roy (1994), many communication systems based on chaotic lasers have been investigated. We now turn to describe communication using fiber lasers as a representative example of optical chaos communication schemes (for more comprehensive reviews on optical chaos communication see Donati and Mirasso, 2002; Larger and Goedgebuer, 2004; Gavrielides et al., 2004; Ohtsubo, 2005, and Uchida et al., 2005).

5.2. Chaos Communication Using Fiber Lasers

In their theoretical analysis of chaos synchronization of fiber ring laser systems (see Section 4.2), Abarbanel and Kennel (1998) examined the possibility of using that property for communication purposes. They showed that the states of two fiber lasers can become synchronized even when a message $m(t)$ is added to the transmitter field $\mathbf{E}_T(t)$. Part of the resulting field $\mathbf{E}_T(t) + m(t)$ is used for transmission to the receiver and part for internal time-delayed feedback, which in turn determines the transmitter dynamics. Thus, they suggest a chaos modulation scheme (see Fig. 31) and demonstrate that subtraction of the synchronized receiver signal $\mathbf{E}_R(t)$ from the total transmitted signal allows the recovery of the message. As an example of the feasibility of their proposal, Abarbanel and Kennel (1998) used their communication scheme to model the transmission of a segment of speech, both analog and digital, at frequencies on the order of hundreds of MHz.

Several experimental demonstrations of chaotic communications in fiber lasers have been reported. VanWiggeren and Roy (1998a) demonstrated one of the first experiments for chaos communications using an erbium doped fiber ring laser (EDFRL), as shown in Fig. 26(a). The ability to produce chaos synchronization was discussed in Section 4.2. A small-amplitude, 10-MHz square-wave message is introduced into the transmitter's cavity via an output coupler (chaos modulation). Under these conditions synchronization between the receiver's output ($\mathbf{E}_R$)

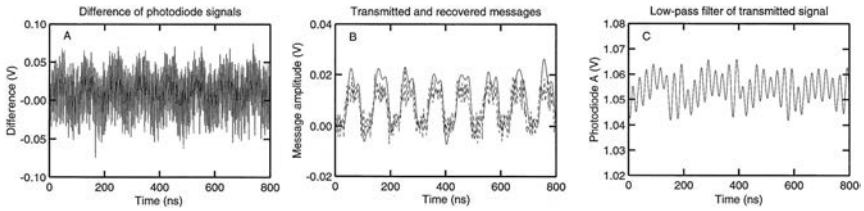

FIG. 32. Message recovery in the experimental setup of Fig. 26(a). (A): Difference between the signals of photodiodes A and B before filtering. (B): The same signal after low-pass filtering (solid line); the dashed line represents the original message (as detected by photodiode A when the transmitter erbium doped fiber amplifier (EDFA) is turned off). (C): Low-pass-filtered transmitter signal. From VanWiggeren and Roy (1998a).

and the transmitter's unperturbed electric field ($\mathbf{E}_T$, i.e. without the message) is preserved. To recover the message they subtract the signals from photodiodes A and B (Fig. 26). The result of such a subtraction is shown in Fig. 32. In the absence of low-pass filtering (Fig. 32(A)), not much trace of the original square-wave message is to be found, because photodiodes record only intensities, so that the resulting signal corresponds to

$$\left|\mathbf{E}_T(t) + m(t)\right|^2 - \left|\mathbf{E}_R(t)\right|^2 = 2\,\mathrm{Re}\left[\mathbf{E}_T(t)m(t)\right] + \left|m(t)\right|^2, \tag{47}$$

given that $\mathbf{E}_R(t) = \mathbf{E}_T(t)$. Low-pass filtering that signal difference reproduces the message intensity $|m(t)|^2$, since the typical frequency of the chaotic carrier fluctuations (hundreds of MHz) is much faster than the message frequency (10 MHz). Figure 32(B) shows the result of such low-pass filtering (solid line), and compares it with the original message (dashed line). The good quality of the message recovery is evident. When a similar filtering is applied to the raw transmitted signal (as detected by photodiode A), the result shows no trace of the original message (Fig. 32(C)).

As we have seen, the transmission bit-rate in the experimental implementation described above is limited by the requirement that the message frequency be sufficiently smaller than the characteristic frequency of the chaotic carrier so that message recovery can be performed by low-pass filtering of the subtracted signals. In order to overcome this limitation, VanWiggeren and Roy (1998b) modified their original experimental setup in such a way that the message was injected in the transmitter by acting upon an intracavity intensity modulator, as shown in the left panel of Fig. 33. This encoding results in a signal $m(t)(\mathbf{E}_{T1} + \mathbf{E}_{T2})$, ten percent of which is transmitted and ninety percent of which returns via a feedback loop to the transmitter fiber amplifier EDFA 1. This type of parametric encoding via chaos modulation requires decoding by division, instead of subtraction. Photodiode A at the receiver measures the intensity

$$\left|m(\mathbf{E}_{T1} + \mathbf{E}_{T2})\right|^2 = |m|^2|\mathbf{E}_{T1} + \mathbf{E}_{T2}|^2, \tag{48}$$

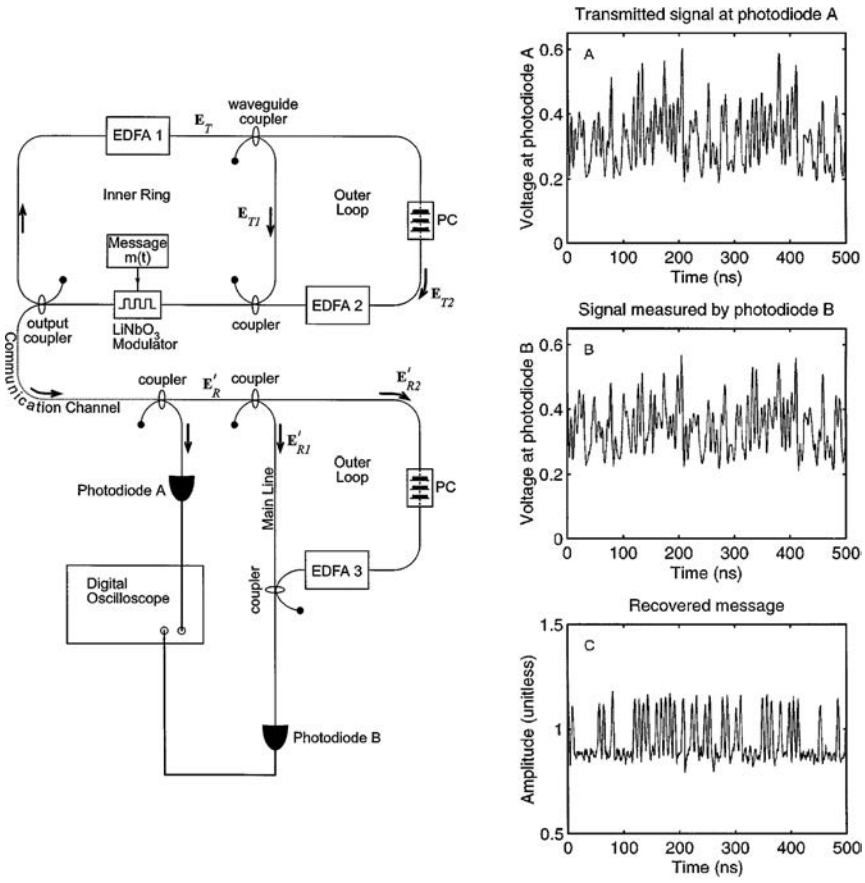

FIG. 33. A second experimental implementation of chaotic communications in coupled fiber lasers. Left: Experimental setup. Right: transmitted signal (top), signal after filtering by the receiver (middle), and result of dividing the two (bottom). From VanWiggeren and Roy (1998b).

whereas photodiode B measures $|\mathbf{E}'_{R1} + \mathbf{E}'_{R2}|^2$ and

$$\left|\mathbf{E}'_{R1} + \mathbf{E}'_{R2}\right|^2 = |\mathbf{E}_{T1} + \mathbf{E}_{T2}|^2 \tag{49}$$

under optimum conditions (VanWiggeren and Roy, 1998b). Dividing Eq. (48) by Eq. (49) gives the message $|m|^2$. Therefore, no low-pass filtering of the decoded signal is required, and the frequency limitation discussed above disappears. Successful transmission of a 126 Mbits/sec pseudorandom digital message is observed, as shown in the right plot of Fig. 33.

In this new experimental setup, the structures of the transmitter and receiver were modified by the addition of a second fiber loop, which introduced the re-

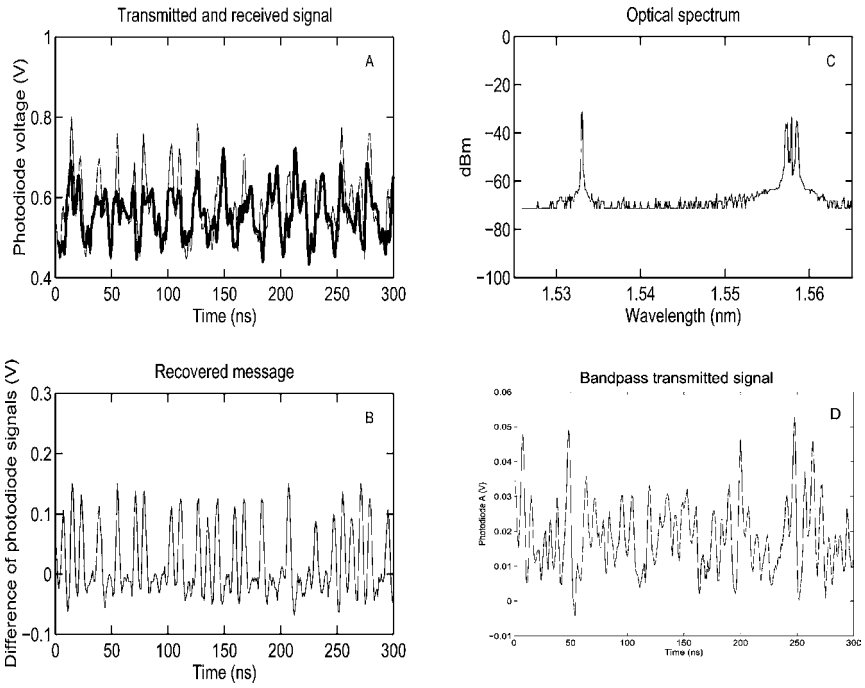

FIG. 34. (A) shows both the transmitted signal measured by photodiode A (thin line) and the signal measured by photodiode B (thick-line). (B) shows the results of subtracting the thick-line from the thin-line. (C) gives an optical spectrum showing the lasing wavelengths of the EDFRL. The message injection is occurring at a wavelength of 1.533 μm. (D) The transmitted signal after passing through a 1 nm bandpass filter at 1.533 μm. The chaotic light at this wavelength still masks the message. From VanWiggeren and Roy (1999).

quirement of multiple parameter matching for extraction of the message. In this case, accurate recovery of the message requires multiple matched parameters in the receiver. The geometrical configuration of the receiver must be the same as in the transmitter. The lengths of the fiber in the outer loop and the time-delay between photodiode A and B must be matched fairly precisely. Finally, the relative power levels in the receiver must be properly matched to the power levels in the transmitter. This method suggests that more complicated geometries and systems requiring additional parameters for message recovery may also be possible to construct using an EDFRL as a basic element.

VanWiggeren and Roy (1999) also performed experiments with message injection at wavelengths which were not resonant with the lasing wavelength of the ring laser. Figure 34(A) shows signals measured by photodiodes A and B when the wavelength of the injected message is 1533.01 nm. In this case the fiber amplifiers

were pumped at about 85 mW, many times threshold. This resulted in an optical power in the ring of 9.1 dBm without any message injection. The injected message power was −3.1 dBm. The subtraction of the traces in Fig. 34(A) is seen in Fig. 34(B). Once again, the same pattern of bits is obtained. The optical spectrum (Fig. 34(C)) shows two distinct peaks. The first of these peaks (1533 nm) corresponds to the message injection, whereas the second peak (1558 nm) corresponds to the natural lasing wavelength of the ring laser. The very broad line-width is characteristic of the EDFRL. The message light at 1533 nm stimulates the laser to emit at the same wavelength and the fraction of the light that remains in the ring continues to circulate stimulating additional emission. Consequently, the light detected at 1533 nm consists of a combination of the message itself plus chaotic light produced by the laser.

If a bandpass filter was used to isolate the message wavelength (1533.01 nm), it was observed that the message was well obscured by the chaotic laser light. Figure 34(D) shows one of these measurements. The sequence of bits is not visible even after isolating just the message wavelength. This experiment indicates that wavelength division multiplexing may be possible, while still using a chaotic waveform as carrier. In summary, the message wavelength can be varied around the natural lasing wavelength of the EDFRL and chaotic communication can still occur.

Bit-rates of 125 Mbits/s and 250 Mbits/s (for a non-return to zero waveform) were demonstrated by VanWiggeren and Roy (1999). Taking full advantage of the large bandwidth available in the optical system would permit even faster rates, but these experiments were limited by the bandwidth of their photodiodes (125 MHz 3-dB roll-off) and oscilloscope (1 GS/s).

5.3. Adverse Effects of Realistic Communication Channels

All practical communication channels introduce signal distortions that alter the chaotic waveform shape, resulting in received chaotic oscillations that do not precisely represent the transmitted oscillations. Channel noise, filtering, attenuation variability and other distortions in the channel corrupt the chaotic carrier and information signal. The presence of these channel distortions significantly hamper the onset of identical synchronization of the chaotic systems and imperfect synchronization results in information loss.

As an example, Abarbanel et al. (2001) considered information loss due to signal distortions in an open air channel for a communication system based on the synchronized opto-electronic devices described in Section 4.5 (see Fig. 35(A)). Figure 35(B) summarizes the information loss of the proposed communication scheme due to channel noise by showing the bit error rate (BER) versus the signal to noise ratio (SNR), where the latter is defined as the energy per bit divided by the

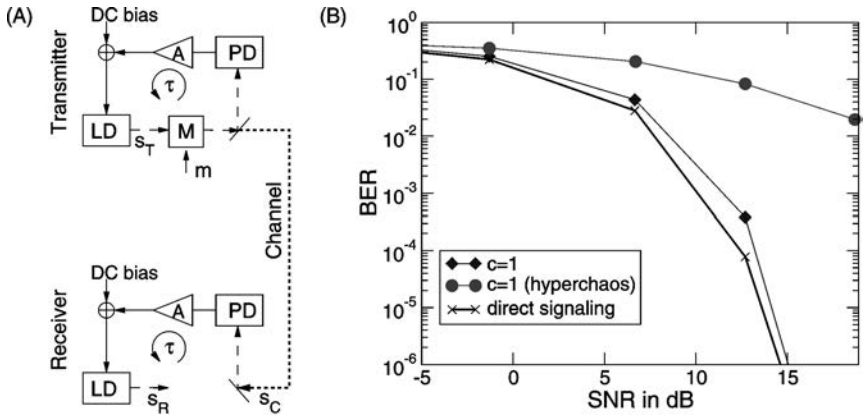

FIG. 35. (A) Chaos communication setup based on coupled optoelectronic devices in an open loop configuration ($c = 1$). LD: laser diode, PD: photo-diode, M: electro-optic modulator which multiplicatively modulates information onto the light intensity. (B) Numerical estimated bit error rate (BER) versus effective signal to noise ratio (SNR). Adapted from Abarbanel et al. (2001).

spectral density of the noise. Results are shown of calculations for the open loop configuration ($c = 1$), and, as a reference, the case of "direct signaling", where it is assumed that the receiver has a perfect copy of the transmitter's chaotic carrier signal. In general, the BER curves for synchronization-based chaos communication lie to the right of the curve for direct signaling for any non-zero coupling because some channel noise enters the feedback loop of the receiver. This noise causes desynchronization and thus information loss in addition to the information loss that results from channel-noise-induced bit flips.

It is seen that one of the chaos-communication BER curves (diamond-symbol) is close to the direct-signaling curve, indicating good synchronization of transmitter and receiver despite the noisy channel. This case corresponds to a situation where the device dynamics is in a regime of low-dimensional chaos, i.e. the Lyapunov dimension D_L of the chaotic attractor is in the range of three to four. In contrast, the chaos-communication BER curve shown with circle symbols in Fig. 35(B) is far to the right of the direct-signaling curve, implying substantial information losses due to noise-induced desynchronization events. This curve corresponds to the case of high-dimensional chaos ($D_L > 5$). Nevertheless, even for the case of high-dimensional chaos, the noise entering the feedback loop does not cause global desynchronization and thus it is still possible to communicate. This result demonstrates the structural stability of the synchronized state.

In the example above, information is encoded in the signal amplitude and no error correction codes are applied. In this context, reliable communication (low BER) can be achieved only for low noise levels in the communication channel

(SNR $>$ 1) even for the direct signaling case, which requires no chaos synchronization. The potentially significant additional information losses for chaos communication schemes that result because of imperfect synchronization can be largely avoided through a careful choice of the chaotic carrier signal. Furthermore, the levels of channel-noise that are required for reliable communication can be straightforwardly achieved in communication applications that use optical fiber links (Argyris et al., 2005) and, of course, in bench-top free-space experiments. The latter was conclusively demonstrated by Tang and Liu (2001a) who achieved 2.5 Gbit/s chaos communication.

5.4. Minimizing the Effect of Channel Distortions on Synchronization

The enhanced sensitivity to chaotic signal waveform shape distortions and the resulting problems with chaos synchronization are major challenges for practical implementation of chaos-based communications systems. In some cases, this challenge is overcome by correcting at the receiver the signal waveform distortions that arise in the communication channel. This was done, for example, in the successful demonstration of chaos communication by Argyris et al. (2005) mentioned in Section 2.3.

Another way to minimize the effect of channel distortions was suggested by Rulkov and Volkovskii (1993) who substituted continuous chaotic waveforms with chaotically-timed pulse sequences. Each pulse in the sequence has identical shape, but the time delay between them varies chaotically. Since the information about the state of the chaotic system is contained *entirely* in the timing between pulses, the distortions that affect the pulse shape do not significantly influence the ability of the chaotic pulse generators to synchronize. Therefore, synchronizing chaotic impulse generators can be utilized in communications schemes for realistic channels and, at the same time, allow the use of filters for noise reduction. The information can be encoded in the pulse train by alteration of time position of pulses with respect to chaotic carrier. This is the essence of the Chaotic Pulse Position Modulation (CPPM) system described by Sushchik et al. (2000). The ability of the self-synchronizing CPPM method to communicate in the presence of significant non-stationary signal distortions in the channel has been studied experimentally using a free-space laser communication link by Rulkov et al. (2002).

A schematic representation of the chaotic free-space laser communication system is shown in Fig. 36(a). Here, the communication carrier signal consists of a sequence of optical pulses that travel through air. The CPPM communication method encodes information in the interpulse intervals and can therefore tolerate strong signal distortions and amplitude variations like the ones caused by atmospheric turbulence as long as fluctuations of the propagation time in the turbulent channel remain small.

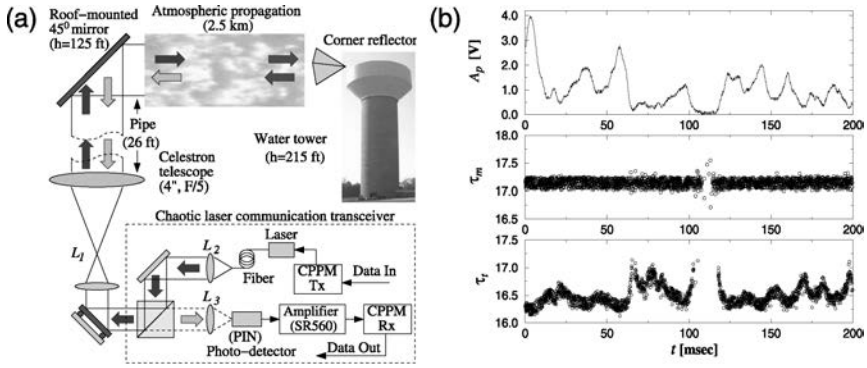

FIG. 36. Robust chaos communication over a free-space laser link. (a) Experimental setup. (b) Fluctuations of the CPPM pulses after traveling through atmospheric turbulence. Pulse amplitude A_p measured in volts at the output of the amplifier (top). Propagation times τ_m (middle) and τ_t (bottom). From Rulkov et al. (2002).

Figure 36(b) illustrates the severe pulse amplitude fluctuations of the signal entering the CPPM demodulator. It also shows that the pulse propagation time τ_m, which is measured between the leading front of the TTL pulse applied to the laser and the maximal point of the received pulse, varies only within a 0.2 μs time interval. However, in order to trigger the CPPM demodulator circuit, the received pulse amplitude has to exceed a certain threshold level. Therefore, the actual delay time τ_t, as seen by the transceiver, depends on the amplitude of the received pulses and fluctuates (see Fig. 36, bottom). Nevertheless, the variations of the pulse propagation time are small enough for the CPPM controller to self-synchronize and to maintain the stability of the communication link.

The gaps visible in Fig. 36(b) are caused by pulse amplitude fading when the pulse amplitude falls to the photo-receiver noise level, which is below the threshold level. The gaps are audible as occasional clicks when using the free-space laser communication system for real-time voice communication. They are the main contribution to the total BER of 1.92×10^{-2} measured in this experiment. Indeed, errors that are not related to the complete failure of the channel because of fading instances contributed to the BER only $\sim 5.5 \times 10^{-5}$. Thus, chaos communication using pulses and encoding information in the timing of the pulses appears to be a particularly robust communication scheme.

5.5. SUMMARY OF CHAOS COMMUNICATION RESEARCH

Chaos communication research has shown that gigabit-per-second transmission rates and very low bit-error rates, comparable to those of traditional communication systems, can be achieved. Thus, within little more than a decade, optical

chaos communication developed from an idea to a communication technology that can now be compared in a meaningful way to traditional communication approaches.

There are clearly practical applications of such non-traditional communication systems that one can envision such as cost-effective private optical communication. However, in our opinion, the main merit of the research on chaos communication is that it challenges us to think more deeply about fundamental issues of information transmission. Whereas most traditional communication techniques utilize regular and repeating sinusoidal signals, chaos communication shows that parties can communicate equally well using irregular signals that never repeat exactly. This research generalizes standard communication approaches and provides insights about information transmission in biological systems, where non-sinusoidal, pulse-like waveforms are used to convey information.

6. Spatio-Temporal Chaos and Patterns

Spatio-temporal chaos and pattern formation can often take place in a nonlinear optical device when the Fresnel number is large; that is, when the device can support a large number of transverse modes. The behavior can often be visualized by measuring the intensity profile of the light generated by the device in a plane that is perpendicular to the propagation direction. For some time, it was thought that transverse behavior was just too complex (too high-dimensional) to be responsive to the control and synchronization methods described in the previous sections. But we see below that this is not the case.

6.1. Spatio-Temporal Chaos Communication

All communication systems discussed in Section 5 involve serial transmission of data through a single communication channel, using temporal chaotic signals as information carriers. A generalization of this approach to systems with spatial degrees of freedom would enable the use of spatio-temporal chaos for the parallel transfer of information, which would yield a substantial increase in channel capacity. Implementing a parallel chaotic communication scheme in electronic systems would be a complex task (due mainly to the need of a comprehensive extended coupling between transmitter and receiver). Optical systems, on the other hand, provide a natural arena for the parallel transfer of information, as we review in what follows.

Multichannel chaotic communications have been recently proposed in models of multimode semiconductor lasers with optical feedback by White and Moloney (1999) (see also Buldú et al., 2004). In that case, only variations of

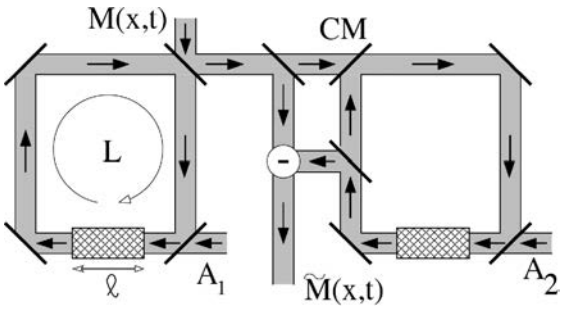

FIG. 37. Scheme for communicating spatio-temporal information using optical chaos. CM is a coupling mirror. Adapted from García-Ojalvo and Roy (2001b).

the electric field along its propagation direction are considered. Information is encoded in the different longitudinal cavity modes, giving rise to a technique for multiplexing. Spatio-temporal communication, on the other hand, utilizes the inherent large scale parallelism of information transfer that is possible with broad-area optical wavefronts. As in the previous systems considered, spatio-temporal chaotic communications require the existence of synchronization between transmitter and receiver. Synchronization of spatio-temporal chaos has been investigated extensively in arrays of nonlinear oscillators (Kocarev and Parlitz, 1996b) and in model partial differential equations (Amengual et al., 1997; Kocarev et al., 1997).

García-Ojalvo and Roy (2001b) proposed a communication system based on the synchronization of the spatio-temporal chaos generated by a broad-area nonlinear optical cavity. The setup is shown schematically in Fig. 37. Two optical ring cavities are unidirectionally coupled by a light beam extracted from the left ring (the transmitter) and partially injected into the right one (the receiver). Each cavity contains a broad-area nonlinear absorbing medium, and is subject to a continuously injected plane wave A_i. Light diffraction is taken into account during propagation through the medium, in such a way that a nonuniform distribution of light in the plane transverse to the propagation direction appears. In fact, an infinite number of transverse modes can oscillate within the cavity.

In the absence of a message, the transmitter is a standard nonlinear ring cavity, well known to exhibit temporal optical chaos (Ikeda, 1979). When transverse effects due to light diffraction are taken into account, a rich variety of spatio-temporal instabilities appear, including solitary waves (McLaughlin et al., 1983) and spatio-temporal chaos (Sauer and Kaiser, 1996; Le Berre et al., 1997). This latter behavior is the one in which we are interested here, since such chaotic waveforms can be used as information carriers. The propagation of light through the nonlinear medium can be described by the following equation for the slowly-varying complex envelope $\mathcal{E}_n(\mathbf{x}, z)$ of the electric field (assumed to be linearly

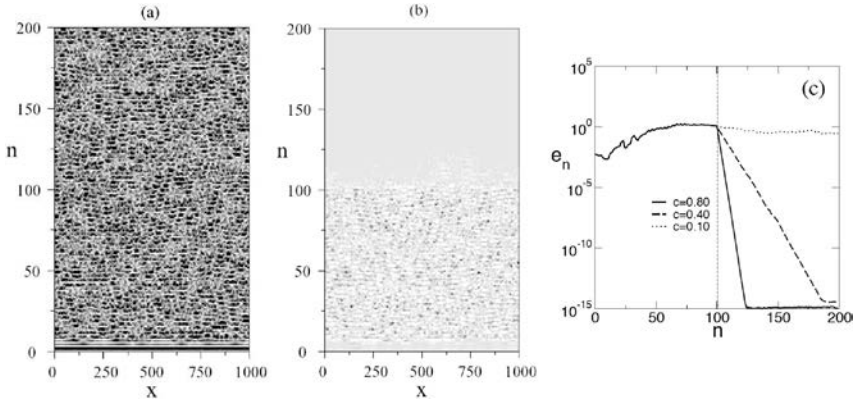

FIG. 38. (a) Space–time representation of a spatio-temporal chaotic state. (b) Intensity difference between the transmitter and the receiver; coupling is switched on at $n = 100$. (c) Temporal evolution of the synchronization error (see text) for the case shown in plot (b). Parameters common to the two cavities are $\alpha = 100.0$, $\Delta \leqslant -10.0$, $R = 0.9$, $T = 0.1$, $k = 100.0$, $\ell = 0.01$, $L = 0.015$, $A = 7.0$. In (b), $c = 0.4$. From García-Ojalvo and Roy (2001a).

polarized) in the nth passage through the resonator (García-Ojalvo and Roy, 2001b):

$$\frac{\partial \mathcal{E}_n(\mathbf{x}, z)}{\partial z} = \frac{i}{2k}\nabla^2 \mathcal{E}_n(\mathbf{x}, z) - \frac{\alpha(1 + i\Delta)}{1 + 4|\mathcal{E}_n|^2}\mathcal{E}_n(\mathbf{x}, z). \tag{50}$$

The first term on the right-hand side of Eq. (50) describes diffraction, and the second saturable absorption. The propagation direction is denoted by z, whereas $\mathbf{x}$ is a vector in the plane orthogonal to the propagation direction. Equation (50) obeys the boundary condition

$$\mathcal{E}_n(\mathbf{x}, 0) = \sqrt{T}A + R\exp(ikL)\mathcal{E}_{n-1}(\mathbf{x}, \ell), \tag{51}$$

which corresponds to an infinite-dimensional map. The value $z = 0$ in Eq. (51) denotes the input of the nonlinear medium, which has length ℓ. The total length of the cavity is L. Other parameters of the model are the absorption coefficient α of the medium, the detuning Δ between the atomic transition and cavity resonance frequencies, the transmittivity T of the input mirror, and the total return coefficient R of the cavity (fraction of light intensity remaining in the cavity after one round trip). The injected signal, with amplitude A and wavenumber k, is taken to be in resonance with a longitudinal cavity mode.

Previous studies by Sauer and Kaiser (1996) have shown that, for $\Delta < 0$, model Eqs. (50) and (51) exhibits irregular dynamics in both space and time for A large enough. An example of this regime is shown in Fig. 38(a). This spatio-temporally chaotic behavior can become synchronized to that of a second cavity,

also operating in a chaotic regime, coupled to the first one as shown in Fig. 37. The coupling mechanism can be modeled by:

$$\begin{aligned}\mathcal{E}_n^{(1)}(\mathbf{x},0) &= \mathcal{F}^{(1)}\big[\mathcal{E}_{n-1}^{(1)}(\mathbf{x},\ell)\big],\\ \mathcal{E}_n^{(2)}(\mathbf{x},0) &= \mathcal{F}^{(2)}\big[(1-c)\mathcal{E}_{n-1}^{(2)}(\mathbf{x},\ell)+c\mathcal{E}_{n-1}^{(1)}(\mathbf{x},\ell)\big]\end{aligned} \tag{52}$$

where the application $\mathcal{F}^{(i)}$ represents the action of the map (51) in every round trip. The coupling coefficient c is given by the transmittivity of the coupling mirror CM (Fig. 37). The super-indices 1 and 2 represent the transmitter and receiver, respectively. Junge and Parlitz (2000) have shown that local sensor coupling is enough to achieve synchronization of spatio-temporal chaos in model continuous equations. In the optical model shown in Eqs. (50)–(51), however, the whole spatial domain can be coupled to the receiver in a natural way. Figure 38(b) shows a space-time representation of the intensity difference between the transmitter and the receiver before and after coupling between the two systems is activated (at the 100th round-trip). The initially uncoupled systems evolve in time starting from arbitrary initial conditions, and after 100 round trips, when their unsynchronized chaotic dynamics is fully developed, coupling is switched on, which results in a rapid synchronization. The synchronization efficiency can be quantified by means of the spatially-averaged synchronization error defined by Kocarev et al. (1997):

$$e_n = \sqrt{\frac{1}{S}\int_S \big|\mathcal{E}_n^{(1)}(\mathbf{x},\ell)-\mathcal{E}_n^{(2)}(\mathbf{x},\ell)\big|^2\,d\mathbf{x}}, \tag{53}$$

where S is the size of the system. The temporal evolution of this quantity is shown in Fig. 38(c) for three values of the coupling coefficient c. Model Eqs. (50) and (51) have been numerically integrated in a 1-d lattice of 1000 cells of size $dx = 0.1$ spatial units, using a pseudospectral code for the propagation in Eq. (50). The results indicate that, for large enough coupling coefficient c, the synchronization error decreases exponentially as soon as coupling is switched on, with a characteristic time that increases with c. In order to encode and decode information in space and time, one can modify the scheme of Eqs. (52) according to Fig. 37, which leads to:

$$\begin{aligned}\mathcal{E}_n^{(1)}(\mathbf{x},0) &= \mathcal{F}^{(1)}\big[\mathcal{E}_{n-1}^{(1)}(\mathbf{x},\ell)+M_{n-1}(\mathbf{x})\big],\\ \mathcal{E}_n^{(2)}(\mathbf{x},0) &= \mathcal{F}^{(2)}\big[(1-c)\mathcal{E}_{n-1}^{(2)}(\mathbf{x},\ell)+c\big(\mathcal{E}_{n-1}^{(1)}(\mathbf{x},\ell)+M_{n-1}(\mathbf{x})\big)\big].\end{aligned} \tag{54}$$

Upon synchronization between transmitter and receiver, the message can be decoded by simply subtracting the transmitted signal and the one coming from the receiver: $\widetilde{M}_n(\mathbf{x}) = \mathcal{E}_n^{(1)}(\mathbf{x},\ell) + M_n(\mathbf{x}) - \mathcal{E}_n^{(2)}(\mathbf{x},\ell)$. For identical parameters of the transmitter and the receiver (the situation considered so far), it can be seen analytically in a straightforward way that, as the coupling coefficient c tends to 1,

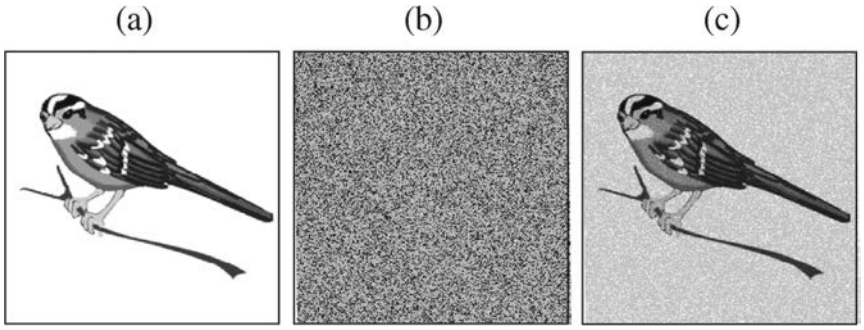

FIG. 39. Transmission of a 2-d spatio-temporal static image. (a) Input image; (b) real part of the transmitted signal at a certain time; (c) recovered data. Parameters are those of Fig. 38, plus $c = 0.7$. From García-Ojalvo and Roy (2001b).

the difference $|\mathcal{E}_n^{(1)} - \mathcal{E}_n^{(2)}| \to 0\ \forall \mathbf{x}$, which corresponds to perfect synchronization, and hence to perfect message recovery. It should be noted that the message is not merely added to the chaotic carrier, but rather the former is driving the nonlinear transmitter itself (i.e., chaos modulation). Therefore, the amplitude of the message need not be much smaller than that of the chaotic signal to provide good masking of the information.

Figure 39 shows an example of data encoded and decoded using the scheme described above, where a static 2-d image has been transmitted in space and time with a coupling coefficient $c = 0.7$. The left plot depicts the input image, the middle plot the real part of the transmitted signal (a snapshot of it, in this case), and the right plot the recovered data. The message amplitude maximum is 0.01 (this value should be compared to the maximum intensity of the chaotic carrier, which oscillates between 1 and 10, approximately, for the parameters chosen). Simulations in this case were performed on a square array with 256×256 pixels of width $dx = 1.0$. The image is clearly recognizable even though the coupling coefficient is now as low as 0.7.

Figure 39 shows qualitatively that, even though coupling between transmitter and receiver is not complete, information varying in time and space can be successfully transmitted and recovered with the setup described in Fig. 37. In order to have a quantitative measure of this effect, one can estimate the mutual information between the input and output message signals, and its dependence on several system parameters. To that end, one defines the entropy H of the message and the mutual information I between the original and recovered messages as

$$H_{\text{input}} = -\sum_x p(x) \ln p(x), \qquad I = -\sum_{x,y} p(x, y) \ln \frac{p(x)p(y)}{p(x, y)}, \tag{55}$$

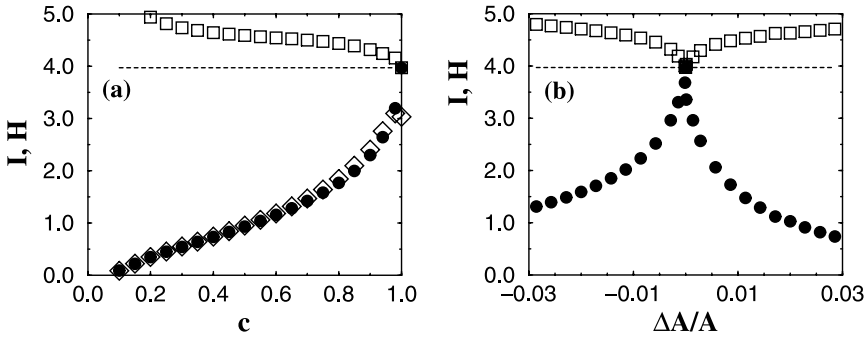

FIG. 40. Information-theory characterization of 1-d message transmission. Full circles: mutual information I; empty squares: entropy H of the recovered data; horizontal dashed line: entropy of the original image. Empty diamonds are the values of I in the presence of noise (see text). Parameters are those of Fig. 38. From García-Ojalvo and Roy (2001b).

where x and y are the values of M and $\widetilde{M}$ discretized in space and time, $p(x)$ and $p(y)$ are their corresponding probability distributions, and $p(x, y)$ is the joint probability. The entropy H_{output} of the recovered message is defined analogously to H_{input}. Note that, according to its definition, the mutual information is $I = 0$ for completely independent data sets, and $I = H_{\text{input}}$ when the two messages are identical.

Figure 40(a) shows the value of the mutual information I, versus the coupling coefficient c, for the transmission of a 1-d message (García-Ojalvo and Roy, 2001b). As c increases, I grows from 0 to 4.0 (perfect recovery), corresponding to the entropy of the input image, given by the horizontal dashed line in the figure. This result shows that, even though good synchronization appears for $c \gtrsim 0.4$, satisfactory message recovery requires coupling coefficients closer to unity. This can also be seen by examining the behavior of the entropy H of the recovered image, plotted as empty squares in Fig. 40(a): for values of c substantially smaller than 1, the entropy of the recovered data is appreciably larger than that of the input message, indicating a higher degree of randomness in the former. Finally, the behavior of the mutual information in the presence of noise is shown as empty diamonds in Fig. 40(a). Uncorrelated, uniformly distributed noise is added continuously to the communication channel, with an amplitude 1% that of the message (García-Ojalvo and Roy, 2001b).

The discussion above has considered so far identical parameters between emitter and receiver. In a realistic implementation, however, parameter mismatches will exist between both devices. A systematic study of the synchronization error between mismatched cavities shows that the most sensitive parameter in this respect is the amplitude A of the injected signal (García-Ojalvo and Roy, 2001b). The data plotted in Fig. 40(b) indicate that a slight mismatch in the value of A

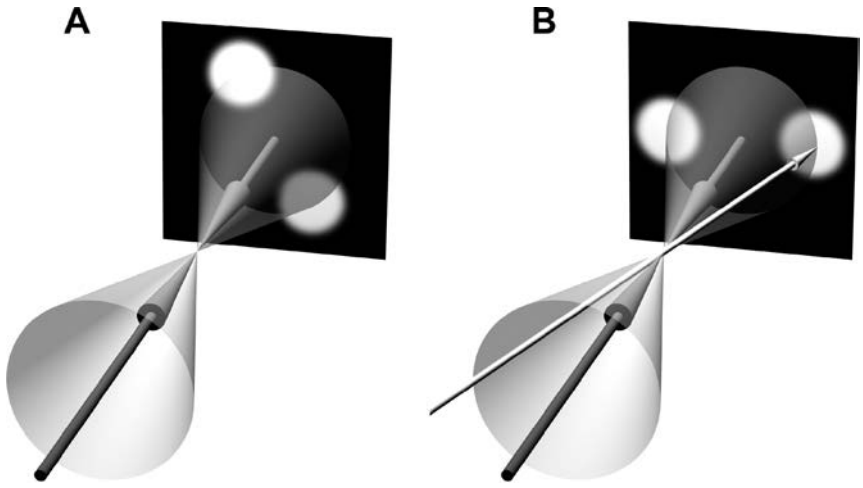

FIG. 41. The two states of the switch. (A) The off state. Weak symmetry breaking results in a two-spot output pattern. (B) The on state. A weak switching beam (light gray), directed along the cone, causes the output pattern to rotate. The state of polarization of the switching beam (light gray) is linear and orthogonal to that of the pump beams (dark gray). From Dawes et al. (2005).

degrades message recovery, by leading to values of I much smaller that the entropy of the input message, and to a recovered message with substantially larger entropy than the original.

6.2. ALL-OPTICAL SWITCHING

As discussed in the previous section, complex spatial patterns are very sensitive to tiny perturbations and can be readily synchronized. Recently, Dawes et al. (2005) reported the realization of an all-optical switch that relies on this extreme sensitivity, allowing it to operate at extremely low light levels. It consists of laser beams counterpropagating through a warm rubidium vapor that induce an off-axis optical pattern. A switching laser beam perturbs the pattern, causing it to rotate even when the power in the switching beam is much lower than the power in the pattern, as shown schematically in Fig. 41. The observed switching energy density is very low, suggesting the exciting possibility that the switch might operate at the single-photon level with system optimization.

Potential applications for a single-photon device are as a router in quantum information networks, as a highly efficient single-photon detector, or as a 'photon-number detector'. Unfortunately, the nonlinear optical interaction strength of most materials is so small that achieving single-photon switching is exceedingly difficult. This problem may be solved through modern quantum-interference methods,

where the nonlinear interaction strength can be increased by many orders-of-magnitude (Lukin, 2003; Braje et al., 2003). Another desirable property of all-optical switches is that the output beams are controlled by a weaker switching beam so they can be used as cascaded classical or quantum computational elements (Keys, 1970). Current switches, however, tend to control a weak beam with a strong one.

The experimental setup of Dawes et al. (2005) consisted of a weak switching beam that controls the direction of laser beams emerging from a warm laser-pumped rubidium vapor. Two pump laser beams counterpropagated through the vapor and induced an instability that generated new beams of light (i.e., a transverse optical pattern) when the power of the pump beams was above a critical level. The instability arises from mirror-less parametric self-oscillation (Lugiato, 1994; Silberberg and Bar-Joseph, 1984; Khitrova et al., 1988; Maître et al., 1995; Firth et al., 1990; Gauthier et al., 1990; Zibrov et al., 1999) due to the strong nonlinear coupling between the laser beams and atoms. Mirror-less self-oscillation occurs when the parametric gain due to nonlinear wave-mixing processes becomes infinite. Under this condition, infinitesimal fluctuations in the electromagnetic field strength trigger the generation of new beams of light. The threshold for this instability is lowest (and the parametric gain enhanced) when the frequency of the pump beams is set near the ^{87}Rb $5S_{1/2} \leftrightarrow 5P_{3/2}$ resonance (transition wavelength $\lambda = 780$ nm). The setup is extremely simple in comparison to most other low-light-level all-optical switching methods (Braje et al., 2003) and the spectral characteristics of the switching and output light match well with recently demonstrated single-photon sources and storage media (van der Wal et al., 2003; McKeever et al., 2004).

For a perfectly symmetric experimental setup, the instability-generated light (referred to henceforth as the 'output' light) would be emitted both forward and backward along cones centered on the pump beams. The angle between the pump-beam axis and the cone was of the order of $\sim$5 mrad and is determined by competition between two different nonlinear optical processes: backward four-wave mixing in the phase-conjugation geometry and forward four-wave mixing (Maître et al., 1995; Firth et al., 1990). The generated light has a state-of-polarization that is linear and orthogonal to that of the linearly co-polarized pump beams (Gauthier et al., 1990); hence, it was easy to separate the output and pump light using polarizing elements. Once separated, the output light propagating in one direction (say, the forward direction) can appear as a ring on a measurement screen that is perpendicular to the propagation direction and in the far field. This ring is known as a transverse optical pattern (Lugiato, 1994). Weak symmetry breaking caused by slight imperfections in the experimental setup reduced the symmetry of the optical pattern and selects its orientation (Maître et al., 1995). For high pump powers, Dawes et al. (2005) observed that the pattern consists of 6 spots with 6-fold symmetry. For lower powers near the instability threshold, only two

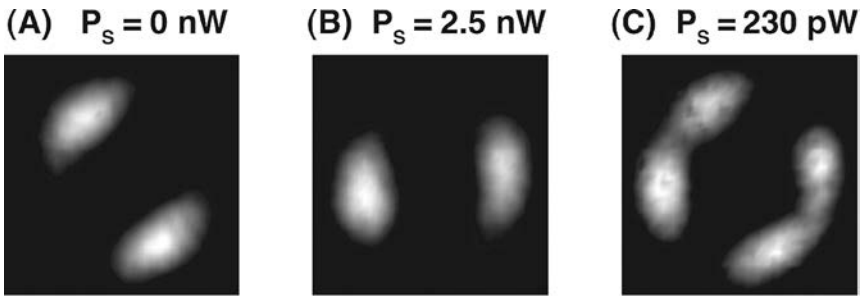

FIG. 42. Low-light-level all-optical switching. (A) The off state with $P_s = 0$. The output light forms a two-spot transverse optical pattern. (B) The on state with $P_s = 2.5$ nW. The two-spot output pattern is rotated by $-60°$. (C) The on state with $P_s = 230$ pW. Approximately half the output power is rotated by $-60°$. From Dawes et al. (2005).

spots appeared in the far field in both directions (forward and backward). The azimuthal angle of the spots (and the corresponding beams) was dictated by the system asymmetry, which could be adjusted by slight misalignment of the pump beams or application of a weak magnetic field. The orientation of the spots was stable for several minutes in the absence of a switching beam; this is in contrast to the single-feedback-mirror experiments analyzed by Le Berre et al. (1990).

In the all-optical switch, the direction of the bright output beams (total power P_{out}) was controlled by applying a weak switching laser beam whose state of polarization was linear and orthogonal to that of the pump-beams (Fig. 41). The azimuthal angle of the output beams was extremely sensitive to tiny perturbations because the symmetry breaking of their setup was so small. Directing the switching beam along the conical surface at a different azimuthal angle (see Fig. 41(B)) causes the output beams to rotate to a new angle, while P_{out} remained essentially unchanged. Typically, the orientation of the output beams rotated to the direction of the switching beam and they found that the pattern was most easily perturbed when the switching beam is injected at azimuthal angles of $\pm 60°$, thereby preserving the 6-fold symmetry of the pattern observed for higher pump powers.

Dawes et al. (2005) investigate the behavior of the switch for two values of the peak power P_s of the switching beam, where the spots rotate by $-60°$ in the presence of a switching beam. In the absence of a switching beam ($P_s = 0$), they observed the pattern shown in Fig. 42(A), where $P_{\text{out}} = 1.5$ μW and the total power emitted from the vapor cell in the forward direction in both states of polarization was 19 μW. For the higher power switching beam ($P_s = 2.5$ nW), they observed complete rotation of the output beams (Fig. 42(B)), whereas they found that only approximately half the power in the beams rotated to the new azimuthal angle (Fig. 42(C)) at the lower switching power ($P_s = 230$ pW). However, they observed high-contrast switching in both cases.

Under the conditions shown in Fig. 42(B), the total power in the output beams is much larger than the switching power: at least a factor of 600 larger. Furthermore, based on the response time τ of the switch (found to be $\sim$4 μs), the number of photons needed to change its state is given by $N_p = \tau P_s / E_p = 40{,}000$, where $E_p = 2.55 \times 10^{-19}$ J is the photon energy, and the switching energy is equal to $N_p E_p = 10$ femtoJ.

Another metric to characterize low-light-level switches is the energy density $\mathcal{E}$, given in units of photons per $(\lambda^2/2\pi)$. This metric gives the number of photons needed to actuate a switch whose transverse dimension has been reduced as small as possible—the diffraction limit of the interacting beams (Keys, 1970). For the spot size of the switching beam used in our experiment ($1/e$ intensity radius of 166 μm), Dawes et al. (2005) found that $\mathcal{E} \sim 4.4 \times 10^{-2}$ photons/$(\lambda^2/2\pi)$, corresponding to 11 zeptoJ/$(\lambda^2/2\pi)$.

They observed similar behavior for the lower switching power, as shown in Fig. 42(C). In this case, a weak switching beam controlled output beams that were 6,500 times stronger. The switching time was observed to be somewhat faster ($\tau \sim 3$ μs), possibly due to the fact that only part of the output light rotates to the new angle. Using this response time, they found $N_p = 2{,}700$ photons, $N_p E_p = 690$ attoJ, and $\mathcal{E} \sim 3 \times 10^{-3}$ photons/$(\lambda^2/2\pi)$ [770 yoctoJ/$(\lambda^2/2\pi)$].

These results demonstrate that a switch based on transverse optical patterns is a promising candidate for low-level, possibly single-photon computation and communication systems. It exhibits much higher sensitivity than other devices and can be realized using a simple experimental setup. It is cascadable in that a very weak beam switches a stronger one so that the output of one switch could be used to drive the input of another—a required characteristic of switches in general purpose computers. Additionally, this switch could be used as a router if information is impressed on the output light (e.g., by modulating the pump beams).

7. Outlook

Research on controlling optical chaos, spatio-temporal dynamics, and patterns is a vibrant field and we anticipate that the fundamental research results described in this chapter will begin to appear in practical devices and systems. We anticipate that the focus of much of the future fundamental work will be directed toward spatio-temporal systems where our understanding of the underlying orderly structure is not as complete as in lower-dimension dynamical systems.

8. Acknowledgement

L.I. and D.J.G. gratefully acknowledge the long-term financial support of the US Army Research Office, most recently supported by grant # W911NF-05-1-0228

and fruitful collaborations with many members of the Duke Center for Nonlinear and Complex Systems. R.R. acknowledges the financial support of the NSF and ONR, and is most grateful to his students and collaborators for making research such an enjoyable experience over the years.

9. References

Abarbanel, H.D.I., Kennel, M.B. (1998). Synchronizing high-dimensional chaotic optical ring dynamics. *Phys. Rev. Lett.* **80**, 3153–3156.

Abarbanel, H.D.I., Kennel, M.B., Buhl, M., Lewis, C.T. (1999). Chaotic dynamics in erbium-doped fiber ring lasers. *Phys. Rev. A* **60**, 2360–2374.

Abarbanel, H.D.I., Kennel, M.B., Illing, L., Tang, S., Chen, H.F., Liu, J.M. (2001). Synchronization and communication using semiconductor lasers with optoelectronic feedback. *IEEE J. Quantum Electron.* **37**, 1301–1311.

Abarbanel, H.D.I., Rulkov, N.F., Sushchik, M.M. (1996). Generalized synchronization of chaos: The auxiliary system approach. *Phys. Rev. E* **53**, 4528–4535.

Afraimovich, V.S., Verichev, N.N., Rabinovich, M.I. (1986). Stochastic synchronization of oscillation in dissipative systems. *Radiophys. and Quantum Electronics* **29**, 795–803.

Ahlborn, A., Parlitz, U. (2004). Stabilizing unstable steady states using multiple delay feedback control. *Phys. Rev. Lett.* **93** , 264101/1–4.

Amengual, A., Hernández-García, E., Montagne, R., Miguel, M.S. (1997). Synchronization of spatio-temporal chaos: The regime of coupled spatio-temporal intermittency. *Phys. Rev. Lett.* **78**, 4379–4382.

Anthon, D., Sipes, D., Pier, T., Ressl, M. (1992). Intracavity doubling of CW diode-pumped Nd:YAG lasers with KTP. *IEEE J. Quantum Electron.* **28**, 1148–1157.

Argyris, A., Syvridis, D., Larger, L., Annovazzi-Lodi, V., Colet, P., Fischer, I., García-Ojalvo, J., Mirasso, C.R., Pesquera, L., Shore, K.A. (2005). Chaos-based communications at high bit rates using commercial fibre-optic links. *Nature* **437**, 343–346.

Ashwin, P., Buescu, J., Stewart, I. (1994). Bubbling of attractors and synchronization of chaotic oscillators. *Phys. Lett. A* **193**, 126–139.

Ashwin, P., Buescu, J., Stewart, I. (1996). From attractor to chaotic saddle: A tale of transverse instability. *Nonlinearity* **9**, 703–737.

Baer, T. (1986). Large amplitude fluctuations due to longitudinal mode coupling in diode-pumped intracavity-doubled Nd:YAG lasers. *J. Opt. Soc. Amer. A* **83**, 1175–1180.

Barland, S., Tredicce, J., Brambilla, M., Lugiato, L., Balle, S., Giudicl, M., Maggipinto, T., Spinelli, L., Tissoni, G., Knodl, T., Miller, M., Jager, R. (2002). Cavity solitons as pixels in semiconductor microcavities. *Nature* **419**, 699–702.

Benettin, G., Galgani, L., Giorgilli, A., Strelcyn, J.-M. (1980). Lyapunov characteristic exponents for smooth dynamical systems and for Hamiltonian systems: A method for computing all of them. Part 2: Numerical application. *Meccanica* **15**, 21–30.

Bielawski, S., Bouazaoui, M., Derozier, D., Glorieux, P. (1993). Stabilization and characterization of unstable steady states in a laser. *Phys. Rev. A* **47**, 3276–3279.

Blakely, J.N., Gauthier, D.J. (2000). Attractor bubbling in coupled hyperchaotic oscillators. *Internat. J. Bifur. Chaos Appl. Sci. Engrg.* **10**, 835–847.

Blakely, J.N., Illing, L., Gauthier, D.J. (2004a). Controlling fast chaos in delay dynamical systems. *Phys. Rev. Lett.* **92**, 193901/1–4.

Blakely, J.N., Illing, L., Gauthier, D.J. (2004b). High-speed chaos in an optical feedback system with flexible timescales. *IEEE J. Quantum Electron.* **40**, 299–305.

Bleich, M.E., Socolar, J.E.S. (1996). Stability of periodic orbits controlled by time-delay feedback. *Phys. Lett. A* **210**, 87–94.
Boccaletti, S., Kurths, J., Osipov, G., Valladares, D.L., Zhou, C.S. (2002). The synchronization of chaotic systems. *Phys. Rep.* **366**, 1–101.
Born, M., Wolf, E. (1999). "Principles of Optics", seventh ed. Cambridge University Press, New York.
Bracikowski, C., Roy, R. (1991). Chaos in a multimode solid-state laser system. *Chaos* **1**, 49–64.
Braje, D.A., Balić, B., Yin, G.Y., Harris, S.E. (2003). Low-light-level nonlinear optics with slow light. *Phys. Rev. Lett.* **68**, 041801/1–4.
Brown, R. (1998). Approximating the mapping between systems exhibiting generalized synchronization. *Phys. Rev. Lett.* **81**, 4835–4838.
Brown, R., Rulkov, N. (1997). Synchronization of chaotic systems: Transverse stability of trajectories in invariant manifolds. *Chaos* **7**, 395–413.
Buldú, J., García-Ojalvo, J., Torrent, M. (2004). Multimode synchronization and communication using unidirectionally coupled semiconductor lasers. *IEEE J. Quantum Electron.* **40**, 640–650.
Carroll, T., Triandaf, I., Schwartz, I., Pecora, L. (1992). Tracking unstable orbits in an experiment. *Phys. Rev. A* **46**, 6189–6192.
Carroll, T.L., Pecora, L.M. (1993). Cascading synchronized chaotic systems. *Phys. D* **67**, 126–140.
Chang, A., Bienfang, J., Hall, G., Gardner, J., Gauthier, D. (1998). Stabilizing unstable steady states using extended time-delay autosynchronization. *Chaos* **8**, 782–790.
Colet, P., Roy, R. (1994). Digital communication with synchronized chaotic lasers. *Opt. Lett.* **19**, 2056–2058.
Collins, R.J., Nelson, D.F., Schawlow, A.L., Bond, W., Garrett, C.G.B., Kaiser, W. (1960). Coherence, narrowing, directionality, and relaxation oscillations in the light emission from ruby. *Phys. Rev. Lett.* **5**, 303–305.
Corron, N., Hopper, B., Pethel, S. (2003). Limiter control of a chaotic RF transistor oscillator. *Internat. J. Bifur. Chaos Appl. Sci. Engrg.* **13**, 957–961.
Corron, N.J., Pethel, S.D., Myneni, K. (2002). Synchronizing the information content of a chaotic map and flow via symbolic dynamics. *Phys. Rev. E* **66**, 036204/1–5.
Cuomo, K.M., Oppenheim, A.V. (1993). Circuit implementation of synchronized chaos with applications to communications. *Phys. Rev. Lett.* **71**, 65–68.
Dawes, A.M.C., Illing, L., Clark, S.M., Gauthier, D.J. (2005). All-optical switching in rubidium vapor. *Science* **308**, 672–674.
Dedieu, H., Kennedy, M.P., Hasler, M. (1993). Chaos shift keying: Modulation and demodulation of a chaotic carrier using self-synchronizing Chua's circuits. *IEEE Trans. Circuits Syst.* **40**, 634–642.
Deshazer, D., Breban, R., Ott, E., Roy, R. (2001). Detecting phase synchronization in a chaotic laser array. *Phys. Rev. Lett.* **87**, 044101/1–4.
Donati, S., Mirasso, C.R. (2002). Introduction to the feature section on optical chaos and applications to cryptography. *IEEE J. Quantum Electron.* **38**, 1138–1140.
Eckmann, J.-P., Ruelle, D. (1985). Ergodic theory of chaos and strange attractors. *Rev. Mod. Phys.* **57**, 617–656.
Feldmann, U., Hasler, M., Schwarz, W. (1996). Communication by chaotic signals: The inverse system approach. *Internat. J. Ciruit Theory Appl.* **24**, 551–579.
Firth, W.J., Fitzgerald, A., Paré, C. (1990). Transverse instabilities due to counterpropagation in Kerr media. *J. Opt. Soc. Amer. B* **7**, 1087–1097.
Frey, D.R. (1993). Chaotic digital encoding: An approach to secure communication. *IEEE Trans. Circuits Syst.* **40**, 660–666.
Fujisaka, H., Yamada, T. (1983). Stability theory of synchronized motion in coupled-oscillator systems. *Prog. Theor. Phys.* **69**, 32–47.
Gabor, D. (1946). Theory of communication. *J. IEE (London)* **93**, 429–457.
García-Ojalvo, J., Roy, R. (2001a). Parallel communication with optical spatio-temporal chaos. *IEEE Trans. Circuits Syst. Part I* **48**, 1491–1497.

García-Ojalvo, J., Roy, R. (2001b). Spatiotemporal communication with synchronized optical chaos. *Phys. Rev. Lett.* **86**, 5204–5207.

Gastaud, N., Poinsot, S., Larger, L., Merolla, J.-M., Hanna, M., Goedgebuer, J.-P., Malassenet, F. (2004). Electro-optical chaos for multi-10 Gbit/s optical transmissions. *Electron. Lett.* **40**, 898–899.

Gauthier, D. (1998). Controlling lasers by use of extended time-delay autosynchronization. *Opt. Lett.* **23**, 703–705.

Gauthier, D., Sukow, D., Concannon, H., Socolar, J. (1994). Stabilizing unstable periodic orbits in a fast diode resonator using continuous time-delay autosynchronization. *Phys. Rev. E* **50**, 2343–2346.

Gauthier, D.J. (2003). Resource letter: CC-1: Controlling chaos. *Amer. J. Phys.* **71**, 750–759.

Gauthier, D.J., Bienfang, J.C. (1996). Intermittent loss of synchronization in coupled chaotic oscillators: Toward a new criterion for high-quality synchronization. *Phys. Rev. Lett.* **77**, 1751–1754.

Gauthier, D.J., Malcuit, M.S., Gaeta, A.L., Boyd, R.W. (1990). Polarization bistability of counterpropagating laser beams. *Phys. Rev. Lett.* **64**, 1721–1724.

Gavrielides, A.T., Lenstra, D., Simpson, T.B., Othsubo, J. (2004). Introduction to the special issue on nonlinear optics. *IEEE J. Selected Topics Quantum Electron.* **10**, 859–861.

Gills, Z., Iwata, C., Roy, R., Schwartz, I.B., Triandaf, I. (1992). Tracking unstable steady states: Extending the stability regime of a multimode laser system. *Phys. Rev. Lett.* **69**, 3169–3172.

Goedgebuer, J.P., Larger, L., Porte, H. (1998). Optical cryptosystem based on synchronization of hyperchaos generated by a delayed feedback tunable laser diode. *Phys. Rev. Lett.* **80**, 2249–2252.

Goedgebuer, J.-P., Levy, P., Larger, L., Chen, C.-C., Rhodes, W.T. (2002). Optical communication with synchronized hyperchaos generated electrooptically. *IEEE J. Quantum Electron.* **38**, 1178–1183.

Haken, H. (1975). Analogy between higher instabilities in fluids and lasers. *Phys. Lett. A* **53A**, 77–78.

Halle, K.S., Wu, C.W., Itoh, M., Chua, L.O. (1993). Spread spectrum communication through modulation of chaos. *Internat. J. Bifur. Chaos Appl. Sci. Engrg.* **3**, 469–477.

Hayes, S., Grebogi, C., Ott, E. (1993). Communication with chaos. *Phys. Rev. Lett.* **70**, 3031–3034.

Hayes, S., Grebogi, C., Ott, E., Mark, A. (1994). Experimental control of chaos for communication. *Phys. Rev. Lett.* **73**, 1781–1784.

Hong, Y., Lee, M.W., Spencer, P.S., Shore, K.A. (2004). Synchronization of chaos in unidirectionally coupled vertical-cavity surface-emitting semiconductor lasers. *Opt. Lett.* **29**, 1215–1217.

Hunt, B., Ott, E. (1996). Optimal periodic orbits of chaotic systems. *Phys. Rev. Lett.* **76**, 2254–2257.

Hunt, B., Ott, E. (1998). A reply to the comment by Scott M. Zoldi and Henry S. Greenside. *Phys. Rev. Lett.* **80**, 1791.

Hunt, E.R. (1991). Stabilizing high-period orbits in a chaotic system: The diode resonator. *Phys. Rev. Lett.* **67**, 1953–1955.

Hunt, E.R., Johnson, G. (1993). Keeping chaos at bay. *IEEE Spectrum* **30**, 32–36.

Ikeda, K. (1979). Multiple-valued stationary state and its instability of the transmitted light by a ring cavity system. *Opt. Commun.* **30**, 257–261.

Ikeda, K., Kondo, K., Akimoto, O. (1982). Successive higher-harmonic bifurcations in systems with delayed feedback. *Phys. Rev. Lett.* **49**, 1467–1470.

Ilday, F., Buckley, J., Lim, H., Wise, F., Clark, W. (2003). Generation of 50-fs, 5-nJ pulses at 1.03 μm from a wave-breaking-free fiber laser. *Opt. Lett.* **28**, 1365–1367.

Illing, L., Bröcker, J., Kocarev, L., Parlitz, U., Abarbanel, H.D.I. (2002). When are synchronization errors small? *Phys. Rev. E* **66**, 036299/1–8.

James, G., Harrell II, E.M., Bracikowski, C., Wiesenfeld, K., Roy, R. (1990). Elimination of chaos in an intracavity-doubled Nd:YAG laser. *Opt. Lett.* **15**, 1141–1143.

Johnson, G., Hunt, E.R. (1993). Maintaining stability in Chua's circuit driven into regions of oscillation and chaos. *J. Circuits Syst. Comput.* **3**, 119–123.

Junge, L., Parlitz, U. (2000). Synchronization and control of coupled Ginzburg–Landau equations using local coupling. *Phys. Rev. E* **61**, 3736–3742.

Just, W., Bernard, T., Ostheimer, M., Reibold, E., Benner, H. (1997). Mechanism of time-delayed feedback control. *Phys. Rev. Lett.* **78**, 203–206.

Keys, R. (1970). Power dissipation in information processing. *Science* **168**, 796–801.

Khitrova, G., Valley, J.F., Gibbs, H.M. (1988). Gain-feedback approach to optical instabilities in sodium vapor. *Phys. Rev. Lett.* **60**, 1126–1129.

Kocarev, L., Halle, K.S., Eckert, K., Chua, L.O., Parlitz, U. (1992). Experimental demonstration of secure communications via chaotic synchronization. *Internat. J. Bifur. Chaos Appl. Sci. Engrg.* **2**, 709–713.

Kocarev, L., Parlitz, U. (1995). General approach for chaotic synchronization with applications to communication. *Phys. Rev. Lett.* **74**, 5028–5031.

Kocarev, L., Parlitz, U. (1996a). Generalized synchronization, predictability, and equivalence of unidirectionally coupled dynamical systems. *Phys. Rev. Lett.* **76**, 1816–1819.

Kocarev, L., Parlitz, U. (1996b). Synchronizing spatio-temporal chaos in coupled nonlinear oscillators. *Phys. Rev. Lett.* **77**, 2206–2209.

Kocarev, L., Tasev, Z., Parlitz, U. (1997). Synchronizing spatio-temporal chaos of partial differential equations. *Phys. Rev. Lett.* **79**, 5–54.

Kolumban, G., Kis, G., Jákó, Z., Kennedy, M.P. (1998). FM-DCSK: A robust modulation scheme for chaotic communications. *IEICE Trans. Fund. Electron. Commun. Comput. Sci.* **E81-A** (9), 1798–1802.

Larger, L., Goedgebuer, J.-P. (2004). Encryption using chaotic dynamics for optical telecommunications. *C.R. Phys.* **5**, 609–611.

Le Berre, M., Patrascu, A., Ressayre, E., Tallet, A. (1997). Localized structures in chaotic patterns: From disorder to ordering. *Phys. Rev. A* **56**, 3150–3160.

Le Berre, M., Ressayre, E., Tallet, A., Zondy, J.-J. (1990). Linear analysis of single-feedback-mirror spatio-temporal instabilities. *J. Opt. Soc. Amer. B* **7**, 1346–1360.

Lewis, C.T., Abarbanel, H.D.I., Kennel, M.B., Buhl, M., Illing, L. (2000). Synchronization of chaotic oscillations in doped fiber ring lasers. *Phys. Rev. E* **63**, 016215/1–15.

Lorenz, E.N. (1963). Deterministic nonperiodic flow. *J. Atmos. Sci.* **20**, 130–141.

Lorenz, E.N. (1993). "The Essence of Chaos". University of Washington Press, Seattle, WA.

Lugiato, L.A. (1994). Transverse nonlinear optics: Introduction and review. *Chaos, Solitons & Fractals* **4**, 1251–1258.

Lukin, M.D. (2003). Colloquium: Trapping and manipulating photon states in atomic ensembles. *Rev. Mod. Phys.* **75**, 457–472.

Maître, A., Petrossian, A., Blouin, A., Pinard, M., Grynberg, G. (1995). Spatio-temporal instability for counterpropagating beams in rubidium vapor. *Opt. Commun.* **116**, 153–158.

McAllister, R., Uchida, A., Meucci, R., Roy, R. (2004). Generalized synchronization of chaos: Experiments on a two-mode microchip laser with optoelectronic feedback. *Phys. D* **195**, 244–262.

McKeever, J., Boca, A., Boozer, A.D., Miller, R., Buck, J.R., Kuzmich, A., Kimble, H.J. (2004). Deterministic generation of single photons from one atom trapped in a cavity. *Science* **303**, 1992–1994.

McLaughlin, D.W., Moloney, J.V., Newell, A.C. (1983). Solitary waves as fixed points of infinite-dimensional maps in an optical bistable ring cavity. *Phys. Rev. Lett.* **51**, 75–78.

Mulet, J., Mirasso, C., Heil, T., Fischer, I. (2004). Synchronization scenario of two distant mutually coupled semiconductor lasers. *J. Opt. B, Quantum Semiclassical Opt.* **6**, 97–105.

Murali, K., Lakshmanan, M. (1993). Transmission of signals by synchronization in a chaotic Van der Pol–Duffing oscillator. *Phys. Rev. E* **48**, 1624–1626.

Nakajima, H. (1997). On analytical properties of delayed feedback control of chaos. *Phys. Lett. A* **232**, 207–210.

Nelson, D.F., Boyle, W.S. (1962). A continuously operating ruby optical maser. *Appl. Opt.* **1**, 181–183.
Nijmeijer, H. (2001). A dynamical control view on synchronization. *Phys. D* **154**, 219–228.
Ogata, K. (1990). "Modern Control Engineering", second ed. Prentice-Hall, Englewood Cliffs, NJ.
Ohtsubo, J. (2005). "Semiconductor Lasers: Stability, Instability and Chaos". In: *Springer Series in Optical Sciences*, vol. 111. Springer, Heidelberg.
Oka, M., Kubota, S. (1988). Stable intracavity doubling of orthogonal linearly polarized modes in diode-pumped Nd:YAG lasers. *Opt. Lett.* **13**, 805–807.
Ott, E., Grebogi, C., Yorke, J.A. (1990). Controlling chaos. *Phys. Rev. Lett.* **64**, 1196–1199.
Parlitz, U., Kocarev, L., Stojanovski, T., Preckel, H. (1996). Encoding messages using chaotic synchronization. *Phys. Rev. E* **53**, 4351–4361.
Parmananda, P., Rhode, M., Johnson, G., Rollins, R., Dewald, H., Markworth, A. (1994). Stabilization of unstable steady-states in an electrochemical system using derivative control. *Phys. Rev. E* **49**, 5007–5013.
Pastur, L., Gostiaux, L., Bortolozzo, U., Boccaletti, S., Ramazza, P. (2004). Experimental targeting and control of spatio-temporal chaos in nonlinear optics. *Phys. Rev. Lett.* **93**, 063902/1–4.
Pecora, L.M., Carroll, T.L. (1990). Synchronization in chaotic systems. *Phys. Rev. Lett.* **64**, 821–824.
Pecora, L.M., Carroll, T.L., Heagy, J.F. (1997a). Statistics for continuity and differentiability: An application to attractor reconstruction from time series. *Fields Inst. Commun.* **11**, 49–62.
Pecora, L.M., Carroll, T.L., Johnson, G.A., Mar, D.J., Heagy, J.F. (1997b). Fundamentals of synchronization in chaotic systems, concepts, and applications. *Chaos* **7**, 520–543.
Pikovsky, A., Rosenblum, M., Kurths, J. (2001). "Synchronization". Cambridge University Press, Cambridge.
Pyragas, K. (1992). Continuous control of chaos by self-controlling feedback. *Phys. Lett. A* **170**, 421–428.
Pyragas, K. (1995). Control of chaos via extended delay feedback. *Phys. Lett. A* **206**, 323–330.
Pyragas, K., Tamasevicius, A. (1993). Experimental control of chaos by delayed self-controlling feedback. *Phys. Lett. A* **180**, 99–102.
Qu, Z., Hu, G., Ma, B. (1993). Controlling chaos via continuous feedback. *Phys. Lett. A* **178**, 265–270.
Romeiras, F.J., Grebogi, C., Ott, E., Dayawansa, W.P. (1992). Controlling chaotic dynamical systems. *Phys. D* **58**, 165–192.
Rosenblum, M.G., Pikovsky, A.S., Kurths, J. (1996). Phase synchronization of chaotic oscillators. *Phys. Rev. Lett.* **76**, 1804–1807.
Roy, R., Gills, Z., Thornburg Jr., K.S. (1994). Controlling chaotic lasers. *Opt. Photonics News* **5**, 8–15.
Roy, R., Murphy Jr., T.W., Maier, T.D., Gills, Z., Hunt, E.R. (1992). Dynamical control of a chaotic laser: Experimental stabilization of a globally coupled system. *Phys. Rev. Lett.* **68**, 1259–1262.
Roy, R., Thornburg Jr., K.S. (1994). Experimental synchronization of chaotic lasers. *Phys. Rev. Lett.* **72**, 2009–2012.
Rulkov, N., Afraimovich, V., Lewis, C.T., Chazottes, J.R., Cordonet, A. (2001). Multivalued mappings in generalized chaos synchronization. *Phys. Rev. E* **64**, 016217/1–11.
Rulkov, N.F., Sushchik, M.M., Tsimring, L.S., Abarbanel, H.D.I. (1995). Generalized synchronization of chaos in directionally coupled chaotic systems. *Phys. Rev. E* **51**, 980–994.
Rulkov, N.F., Volkovskii, A.R. (1993). Synchronization of pulse-coupled chaotic oscillators. In: "Proceedings of the 2nd Experimental Chaos Conference", pp. 106–115.
Rulkov, N.F., Vorontsov, M.A., Illing, L. (2002). Chaotic free-space laser communication over a turbulent channel. *Phys. Rev. Lett.* **89**, 277905/1–4.
Sargent III, M., Scully, M.O., Lamb Jr., W.E. (1974). "Laser Physics". Addison-Wesley, Reading, MA, p. 52.
Sauer, M., Kaiser, F. (1996). Synchronized spatio-temporal chaos and spatio-temporal on-off intermittency in a nonlinear ring cavity. *Phys. Rev. E* **54**, 2468–2473.
Schwarz, I.B., Triandaf, I. (1992). Tracking unstable orbits in experiments. *Phys. Rev. A* **46**, 7439–7444.

Shinbrot, T., Grebogi, C., Ott, E., Yorke, J.A. (1993). Using small perturbations to control chaos. *Nature* **363**, 411–417.

Silberberg, Y., Bar-Joseph, I. (1984). Optical instabilities in a nonlinear Kerr medium. *J. Opt. Soc. Amer. B* **1**, 662–670.

Socolar, J., Sukow, D., Gauthier, D. (1994). Stabilizing unstable periodic orbits in fast dynamical systems. *Phys. Rev. E* **50**, 3245–3248.

Sugawara, T., Tachikawa, M., Tsukamoto, T., Shimizu, T. (1994). Observation of synchronization in laser chaos. *Phys. Rev. Lett.* **72**, 3502–3505.

Sukow, D.W., Bleich, M.E., Gauthier, D.J., Socolar, J.E.S. (1997). Controlling chaos in fast dynamical systems: Experimental results and theoretical analysis. *Chaos* **7**, 560–576.

Sushchik Jr., M., Rulkov, N.F., Larson, L., Tsimring, L., Abarbanel, H.D.I., Yao, K., Volkovskii, A. (2000). Chaotic pulse position modulation: A robust method of communicating with chaos. *IEEE Commun. Lett.* **4**, 128–130.

Tang, S., Liu, J.M. (2001a). Message encoding-decoding at 2.5 Gbits/s through synchronization of chaotic pulsing semiconductor lasers. *Opt. Lett.* **26**, 1843–1845.

Tang, S., Liu, J.M. (2001b). Synchronization of high-frequency chaotic optical pulses. *Opt. Lett.* **26**, 596–598.

Uchida, A., McAllister, R., Meucci, R., Roy, R. (2003). Generalized synchronization of chaos in identical systems with hidden degrees of freedom. *Phys. Rev. Lett.* **91**, 174101/1–4.

Uchida, A., Rogister, F., García-Ojalvo, J., Roy, R. (2005). Synchronization and communication with chaotic laser systems. In: *Progress in Optics*, vol. 48. North-Holland, Amsterdam, pp. 203–342.

Ushio, T. (1996). Limitations of delayed feedback control in nonlinear discrete-time systems. *IEEE Trans. Circuits Syst.* **43**, 815–816.

van der Wal, C.H., Eisaman, M.D., Andre, A., Walsworth, R.L., Phillips, D.F., Zibrov, A.S., Lukin, M.D. (2003). Atomic memory for correlated photon states. *Science* **301**, 196–200.

VanWiggeren, G., Roy, R. (1998a). Communication with chaotic lasers. *Science* **279**, 1198–1200.

VanWiggeren, G., Roy, R. (1998b). Optical communication with chaotic waveforms. *Phys. Rev. Lett.* **81**, 3547–3550.

VanWiggeren, G.D., Roy, R. (1999). Chaotic communication using time-delayed optical systems. *Internat. J. Bifur. Chaos Appl. Sci. Engrg.* **9**, 2129–2156.

Volkovskii, A.R., Rulkov, N.F. (1993). Synchronous chaotic response of a nonlinear oscillator system as a principle for the detection of the information component of chaos. *Tech. Phys. Lett.* **19**, 97–99.

White, J., Moloney, J. (1999). Multichannel communication using an infinite dimensional spatio-temporal chaotic system. *Phys. Rev. A* **59**, 2422–2426.

Williams, Q.L., García-Ojalvo, J., Roy, R. (1997). Fast intracavity polarization dynamics of an erbium-doped fiber ring laser: Inclusion of stochastic effects. *Phys. Rev. A* **55**, 2376–2386.

Williams, Q.L., Roy, R. (1996). Fast polarization dynamics of an erbium-doped fiber ring laser. *Opt. Lett.* **21**, 1478–1480.

Winful, H.G., Rahman, L. (1990). Synchronized chaos and spatio-temporal chaos in arrays of coupled lasers. *Phys. Rev. Lett.* **65**, 1575–1578.

Yang, T.-H., Hunt, B.R., Ott, E. (2000). Optimal periodic orbits of continuous time chaotic systems. *Phys. Rev. E* **62**, 1950–1959.

Yu, Y.H., Kwak, K., Lim, T.K. (1995). Secure communication using small time continuous feedback. *Phys. Lett. A* **197**, 311–316.

Zibrov, S., Lukin, M.D., Scully, M.O. (1999). Nondegenerate parametric self-oscillation via multi-wave mixing in coherent atomic media. *Phys. Rev. Lett.* **83**, 4049–4052.

Zoldi, S., Greenside, H. (1998). Comment on ‘optimal periodic orbits of chaotic systems’. *Phys. Rev. Lett.* **80**, 1790.